


Summer 8-2017

Molecular and Pathological Analyses of Three New Mouse Mutations That Affect Ear Development and Function

Cong Tian

University of Maine, cong.tian@maine.edu

Follow this and additional works at: <http://digitalcommons.library.umaine.edu/etd>

 Part of the [Developmental Neuroscience Commons](#), and the [Genetics Commons](#)

Recommended Citation

Tian, Cong, "Molecular and Pathological Analyses of Three New Mouse Mutations That Affect Ear Development and Function" (2017). *Electronic Theses and Dissertations*. 2714.

<http://digitalcommons.library.umaine.edu/etd/2714>

This Open-Access Dissertation is brought to you for free and open access by DigitalCommons@UMaine. It has been accepted for inclusion in Electronic Theses and Dissertations by an authorized administrator of DigitalCommons@UMaine. For more information, please contact um.library.technical.services@maine.edu.

**MOLECULAR AND PATHOLOGICAL ANALYSES OF THREE NEW MOUSE MUTATIONS THAT AFFECT EAR
DEVELOPMENT AND FUNCTION**

By

Cong Tian

B.S., Ocean University of China, 2004

A DISSERTATION

Submitted in Partial Fulfillment of the

Requirements for the Degree of

Doctor of Philosophy

(in Biomedical Science)

The Graduate School

The University of Maine

August 2017

Advisory Committee:

Kenneth Johnson, Associate Professor, The Jackson Laboratory, Advisor

Robert Burgess, Professor, The Jackson Laboratory

Gregory Cox, Associate Professor, The Jackson Laboratory

Zhong-wei Zhang, Associate Professor, The Jackson Laboratory

Basile Tarchini, Assistant Professor, The Jackson Laboratory

Voot Yin, Assistant Professor, Mount Desert Island Biological Laboratory

**MOLECULAR AND PATHOLOGICAL ANALYSES OF THREE NEW MOUSE MUTATIONS THAT AFFECT EAR
DEVELOPMENT AND FUNCTION**

By Cong Tian

Dissertation Advisor: Dr. Kenneth Johnson

An Abstract of the Dissertation Presented in
Partial Fulfillment of the Requirements for the
Degree of Doctor of Philosophy
(in Biomedical Science)
August 2017

This dissertation presents three new mouse models that help to study the functions of *Enpp1*, *Atp6v1b1*, and *Tbx1* for ear development and function. *asj* (aging with stiffened joints) carries a missense mutation in the mouse *Enpp1* gene. *Enpp1* encodes the enzyme ENPP1 that regulate soft-tissue calcification and bone mineralization, and is associated with generalized arterial calcification of infancy and hypophosphatemic rickets in human patients. *asj* mutant mice show severe middle ear infection and tissue calcification, which provide a new mouse model to study otitis media and tympanosclerosis. *Atp6v1b1* encode a protein that is a subunit of the V-ATPase pump, which is the key regulator of pH homeostasis. *Atp6v1b1* mutation is associated with human distal renal tubular acidosis (dRTA) with hearing loss; however, *Atp6v1b1* knockout mice have mild kidney phenotype and normal hearing. *vtx* (vortex) mice carry a missense mutation in the mouse *Atp6v1b1* gene on a MRL.Mpj background, that shows severe hearing loss and vestibular dysfunction. Transfer the *vtx* mutation to a B6 background did not cause hearing loss, indicating genetic background effects underlie this variation. We performed linkage backcross to map the genetic loci that modify the degree of hearing loss on the two different background strains and found statistically significant linkage with a region on Chr13. Because MRL-*vtx* mice exhibit enlargements of the endolymphatic sac and duct in the inner ear but do not exhibit the overt metabolic acidosis characteristic of dRTA, they provide a new genetic model for

nonsyndromic deafness with enlarged vestibular aqueducts. *TBX1* haploinsufficiency is associated with human DiGeorge syndrome. *Tbx1* knockout mice are embryonic lethal and ear morphogenesis stops around E10 in the mutant mice. Study showed expression of TBX1 in the stria vascularis and vestibular dark cells, but because *Tbx1* KO mice don't have fully developed inner ear, new model is required to study *Tbx1* function at later development stage. *Tbx1*^{wdm1} (windmill) mice carry a missense mutation in the mouse *Tbx1* gene and have fully developed inner ear. Hearing loss and vestibular dysfunction correlate well with TBX1 expression in the stria vascularis and dark cells. This new *Tbx1* mouse model provides a valuable tool to study *Tbx1* function in the development of stria vascularis and semicircular canal.

DEDICATION

To Ye Zheng, the love of my life; to Kelly and Bowen, all the happy time with them; to my parents, You-he Tian, Zheng-mei Chen, and parent-in-laws, Qing-yu Zheng, Rong-zhi Zhang, for their love and support, and the sacrifices they have made so I can be where I am today.

ACKNOWLEDGEMENTS

Foremost, I would like to thank my advisor and mentor, Dr. Kenneth Johnson, for his support and training. Thanks, also, to the members of my dissertation committee, who steered me toward successful completion of research projects and my Doctorate. Thank you to Dr. Robert Burgess, Dr. Gregory Cox, Dr. Zhong-wei Zhang, Dr. Basile Tarchini, Dr. Voot Yin for your generous support, patience, and understanding. I thank Leona Gagnon, Chantal Longo-Guess, Sandra gray, and Abby Tadenev for their help in the lab. Thanks to Dr. Ron Korstanje, Belinda Harris, Dr. Kevin K. Ohlemiller for their help with my research projects. Thank you to the Graduate School of Biomedical Sciences and Engineering for accepting me into their program. Thanks, also, to my fellow GSBSE graduate students, past and present, for their friendship and camaraderie. A big thanks to the Jackson Laboratory for giving me the opportunity, support, and structure within which I could realize my potential and grow. Thanks to the many incredible science faculty, staff, and fellows of JAX who helped me in so many ways over the years.

I'm grateful to my family for their patience and sacrifice in helping me get to this point. Thank you to my wife Ye Zheng who showed me relentless support through the toughest hours. Thanks to my children, Kelly Tian and Bowen Tian, for all the happiness they bring to me. I thank my parents You-he Tian and Zheng-mei Chen, my sister Hui-min Tian, my parent-in-laws, Qing-Yu Zheng and Rong-zhi Zhang for their support.

TABLE OF CONTENTS

DEDICATION.....	ii
ACKNOWLEDGEMENTS.....	iii
LIST OF TABLES.....	viii
LIST OF FIGURES.....	ix
CHAPTER 1 ECTOPIC MINERALIZATION AND CONDUCTIVE HEARING LOSS IN <i>ENPP1</i> ^{ASJ} MUTANT MICE, A NEW MODEL FOR OTITIS MEDIA AND TYMPANOSCLEROSIS.....	1
1.1 Introduction	1
1.2 Materials and Methods	2
1.2.1 Mice.....	2
1.2.2 Genotyping the <i>Enpp1</i> ^{asj} mutation	2
1.2.3 Assessment of hearing by ABR	3
1.2.4 Histological analyses of middle and inner ears.....	3
1.2.5 Evaluation of pathology of middle ears.....	3
1.2.6 Scanning electron microscopy (SEM).....	4
1.3 Results.....	4
1.3.1 Hearing impairment in <i>Enpp1</i> ^{asj} mutant mice.....	4
1.3.2 Otitis media with effusion in <i>Enpp1</i> ^{asj/asj} mice	8
1.3.2.1 Middle ear effusion and epithelial proliferation in <i>Enpp1</i> mutant mice	8
1.3.2.2 Increased goblet cell density and mucin secretion in <i>Enpp1</i> ^{asj/asj} mice.....	12
1.3.2.3 Impaired Eustachian tube function due to epithelia proliferation.....	13
1.3.2.4 Impaired middle ear epithelial clearance function due to excess mucin and loss of microciliary function.....	14
1.3.3 Over-calcification of middle ear structures (tympansclerosis)	15

1.3.4 Bacterial infection does not play a role in the development of otitis media in <i>Enpp1^{asj/asj}</i> mice	17
1.4 Discussion.....	17
1.4.1 Otitis media-related ear pathology of <i>Enpp1^{asj}</i> mutant mice	17
1.4.2 Mineralization disorders and conductive hearing loss in <i>Enpp1^{asj/asj}</i> mice	18
1.5 Summary	20
CHAPTER 2 HEARING LOSS WITHOUT OVERT METABOLIC ACIDOSIS IN ATP6V1B1 DEFICIENT	
MRL MICE, A NEW GENETIC MODEL FOR NONSYNDROMIC DEAFNESS WITH	
ENLARGED VESTIBULAR AQUEDUCTS	
	21
2.1 Introduction	21
2.2 Materials and Methods	23
2.2.1 Mice.....	23
2.2.2 Genetic mapping and DNA analysis of the <i>vtx</i> mutation	24
2.2.3 Auditory brainstem response (ABR) measurements.....	25
2.2.4 Endocochlear potential (EP) recording	26
2.2.5 Tissue processing and imaging for histopathology	26
2.2.6 Inner ear paint fills and cleared whole mount preparations	27
2.2.7 Blood and urine analysis.....	27
2.2.8 Genetic mapping of modifier loci	27
2.2.9 Analyses of candidate modifier genes	28
2.3 Results.....	29
2.3.1 Genetic mapping of the <i>vtx</i> mutation.....	29
2.3.2 Gene identification and molecular characterization of the <i>vtx</i> mutation	30
2.3.3 Inner ear morphology and auditory function	32

2.3.4 Kidney-related phenotype.....	37
2.3.5 Genetic mapping of hearing loss modifiers	39
2.4 Discussion.....	43
2.5 Summary	47
CHAPTER 3 <i>TBX1</i> IS REQUIRED FOR SEMICIRCULAR CANAL FORMATION AND STRIA VASCULARIS	
MATURATION	49
3.1 Introduction	49
3.2 Materials and Methods	52
3.2.1 Mice.....	52
3.2.2 Genetic mapping of the <i>wdm1</i> mutation.....	52
3.2.3 Whole-exome sequencing.....	53
3.2.4 DNA sequence confirmation and genotyping of the <i>wdm1</i> mutation	53
3.2.5 Auditory brainstem response.	53
3.2.6 Histology.....	54
3.2.7 Immunofluorescence staining	54
3.2.8 Inner ear paint fills.....	55
3.2.9 RNA-seq.....	55
3.2.10 DIG-labeled riboprobes and mRNA in situ hybridization	56
3.3 Results.....	57
3.3.1 Genetic mapping of the <i>wdm1</i> mutation.....	58
3.3.2 Inner ear morphology.....	59
3.3.3 <i>TBX1</i> expression in postnatal mouse inner ear.....	61
3.3.4 Absence of marginal cell markers in the <i>Tbx1^{wdm1}</i> mutant mice	62
3.3.5 Gene expression differences caused by the <i>Tbx1^{wdm1}</i> mutation.....	63

3.4 Discussion.....	65
3.5 Summary	70
3.6 Future directions	70
CHAPTER 4 THESIS SUMMARY.....	72
BIBLIOGRAPHY	76
APPENDIX: CONTRIBUTIONS TO OTHER PROJECTS.....	85
BIOGRAPHY OF THE AUTHOR.....	87

LIST OF TABLES

Table 1.1	ABR thresholds of <i>asj/asj</i> mutant mice	6
Table 1.2	ABR thresholds of <i>+/+</i> or <i>+/asj</i> control mice	7
Table 1.3	Histological assessment of the middle ears of the <i>Enpp1</i> mutant and control mice.....	11
Table 2.1	Physiological parameters of <i>Atp6v1b1^{vtx/vtx}</i> (<i>vtx/vtx</i>) and <i>Atp6v1b1^{+/+}</i> (<i>+/+</i>) control mice on the MRL and B6 strain backgrounds.	38
Table 3.1	Primer sequence for in situ hybridization probes.....	56
Table 3.2	The top 10 upregulated, top 5 downregulated, and five other downregulated DE genes (FDR \leq 0.05) for <i>Tbx1^{wdml/wdml}</i> and <i>Tbx1^{wdml/+}</i> mice as ranked by fold-change.	64

LIST OF FIGURES

Figure 1.1	Progressive hearing loss in <i>Enpp1^{asj/asj}</i> mice	5
Figure 1.2	Otitis media in <i>Enpp1^{asj/asj}</i> mice	9
Figure 1.3	Development of otitis media in <i>Enpp1^{asj/asj}</i> mice.....	10
Figure 1.4	Increased density of goblet cells in <i>Enpp1^{asj/asj}</i> mice.	13
Figure 1.5	Scanning electron micrographs of epithelium lining the middle ear cavity.....	14
Figure 1.6	Calcification of middle ear structures (or tympanosclerosis) in <i>Enpp1^{asj/asj}</i> mice.....	16
Figure 2.1	ABR thresholds of MRL- <i>vtx/vtx</i> mutant mice and linkage backcross mice.....	29
Figure 2.2	Molecular characterization and consequences of the <i>Atp6v1b1^{vtx}</i> mutation.....	31
Figure 2.3	Paint fills and whole mounts of inner ears from MRL- <i>Atp6v1b1^{vtx/vtx}</i> mutant and control mice	33
Figure 2.4	Cross sections of cochleae from B6.MRL- <i>Atp6v1b1^{vtx/vtx}</i> and MRL- <i>Atp6v1b1^{vtx/vtx}</i> mice	34
Figure 2.5	Cross sections of vestibular organs from B6.MRL- <i>Atp6v1b1^{vtx/vtx}</i> and MRL- <i>Atp6v1b1^{vtx/vtx}</i> mice.....	35
Figure 2.6	ABR and EP measurements of auditory function in B6.MRL- <i>Atp6v1b1^{vtx/vtx}</i> and MRL- <i>Atp6v1b1^{vtx/vtx}</i> mice	36
Figure 2.7	Renal secretion in B6- and MRL- <i>Atp6v1b1^{vtx}</i> mutant mice at 17 weeks of age.....	38
Figure 2.8	ABR thresholds of parental strains, F1 hybrids, and N2 backcross mice.....	40
Figure 2.9	Mapping modifier loci that influence ABR thresholds of <i>Atp6v1b1^{vtx/vtx}</i> mice	41
Figure 3.1	Hearing loss in B6- <i>wddl/wddl</i> mutant mice	57
Figure 3.2	Molecular characterization and consequences of the <i>Tbx1^{wddl}</i> mutation	59
Figure 3.3	Cross sections of cochleae from <i>Tbx1^{wddl/wddl}</i> and <i>Tbx1^{wddl/+}</i> mice	60
Figure 3.4	Paint fills of inner ears from <i>Tbx1^{wddl/wddl}</i> mutant and control mice	61
Figure 3.5	The expression of TBX1 in the postnatal mouse inner ear.....	62

Figure 3.6 Immunodetection of KCNQ1, KCNJ10, and GLUT1 in P0 *Tbx1^{wdm/wdm}* and *Tbx1^{wdm/+}* mouse cochleas63

Figure 3.7 Examination of *Esrrb*, *Raldh2*, and *Dct* expression in the *Tbx1^{wdm}* mice and wild type mice with in situ hybridization65

CHAPTER 1 ECTOPIC MINERALIZATION AND CONDUCTIVE HEARING LOSS IN *ENPP1*^{ASJ} MUTANT MICE, A NEW MODEL FOR OTITIS MEDIA AND TYMPANOSCLEROSIS

1.1 Introduction

While many genes have been discovered that underlie Mendelian forms of sensorineural hearing loss (<http://hereditaryhearingloss.org/>), most cases of conductive hearing loss, often caused by otitis media and tympanosclerosis, have complex and poorly understood etiologies. Otitis media is an inflammation of the middle ear and is among the most common childhood illnesses. Heritability studies have shown that genetic factors can play an important role in otitis media susceptibility, but few contributing genes have been identified in human populations [1]. In contrast to human studies, a growing number of mouse mutations have been identified that manifest a high incidence of otitis media, including *Eya4*, *Tlr4*, *p73*, *MyD88*, *Fas*, *E2f4*, *Plg*, *Fbxo11*, *Evi1*[1, 2], *Sh3pxd2b*[3], *Rpl38*[4], *Isl1*[5], *Chd7*[6], *Lmna1*[7], *Phex*[8], *Oxgr1*[9], *Tgif1*[10], and *Mcp1*[11]. The wide diversity of these genes and their mutant pathologies, including craniofacial abnormalities with Eustachian tube malformations and innate immune response defects, underscores the complex nature of otitis media.

Here we report on the conductive hearing loss associated with a recessive ENU-induced missense mutation of the ectonucleotide pyrophosphatase/phosphodiesterase 1 gene (*Enpp1*) that was discovered at The Jackson Laboratory and named "ages with stiffened joints" (*asj*) because of the progressive ankylosis and osteoarthritis exhibited by mutant mice [12]. The *Enpp1* gene encodes an enzyme (ENPP1) that regulates soft-tissue calcification and bone mineralization by producing inorganic pyrophosphate, a major inhibitor of calcification. A previous analysis of *asj* mutant mice found that enzymatic activity of ENPP1 in the liver and inorganic pyrophosphate (PPi) levels in plasma were markedly reduced[13]. Other mouse mutations of *Enpp1* have been reported, including the naturally occurring "tiptoe walking" (*ttw*) nonsense mutation[14], an ENU-induced C397S missense mutation[15], and a genetically engineered knockout mutation[16]. The *Enpp1* mutant mice in these studies exhibited

extensive mineralization defects in a number of tissues, including spinal ligaments, long bones, articular cartilage, heart, aorta, arterial blood vessels, vibrissae, liver, kidneys, and retina. The effects of the *Enpp1* mutations on auditory function and middle and inner ear histology of mice, however, were not examined.

We show here that *Enpp1^{asj}* mutant mice exhibit a conductive hearing loss that is associated with middle and inner ear mineralization abnormalities. These mice provide a new animal model for studies of otitis media and tympanosclerosis and for the hearing loss recently shown to be associated with human ENPP1 mutations causing generalized arterial calcification of infancy and hypophosphatemic rickets[17, 18].

1.2 Materials and Methods

1.2.1 Mice

The recessive *asj* mutation was discovered at The Jackson Laboratory in 2004 in the C57BL/6J progeny of an ENU treated C57BL/6J male. The mutant strain name is C57BL/6J-*Enpp1^{asj}/GrsrJ* and is available from The Jackson Laboratory (Stock #012810). Experimental mice were housed in the Research Animal Facility of The Jackson Laboratory, and all procedures involving their use were approved by the Institutional Animal Care and Use Committee. The Jackson Laboratory is accredited by the American Association for the Accreditation of Laboratory Animal Care.

1.2.2 Genotyping the *Enpp1^{asj}* mutation

The *asj* mutation is a single nucleotide substitution of T to A in exon 7 of the *Enpp1* gene resulting in an amino acid substitution from valine to aspartic acid at residue 246 (p.V246D) of protein Reference Sequence NP_032839 . The T to A point mutation (nt 848 of mRNA Reference Sequence NM_008813) creates a new *TaqI* restriction site (TCGA), which is the basis of the genotyping method described by Harris and colleagues[12] and that was used in this study to distinguish wild-type from mutant alleles.

1.2.3 Assessment of hearing by ABR

Hearing was evaluated in anesthetized (Avertin, 0.4 mg/g mouse mass) wild-type, *Enpp1^{asj/+}*, and *Enpp1^{asj/asj}* mice by measuring auditory brainstem response (ABR). A computer-aided evoked potential system (Intelligent Hearing Systems) was used to measure mouse ABR thresholds as previously described [19].

1.2.4 Histological analyses of middle and inner ears

Histological analyses of the middle and inner ears were performed following the methods described previously[20]. Briefly, middle and inner ears from *Enpp1^{asj/asj}* mice and wild-type mice were dissected after transcardial perfusion with Bouin's fixative. Ear samples were immersed in Bouin's fixative (7 days for one-month-old mice and 30 days for mice older than 6 months) and embedded in paraffin. Sections (7 mm) were cut and mounted onto Fisher Superfrost Plus slides (Fisher Scientific, Pittsburgh, PA) and counterstained in hematoxylin/eosin (H&E). Goblet cells, whose sole function is to secrete mucus, were identified by Mayer's Mucicarmine staining method following the protocol provided by Electron Microscopy Sciences (Catalog #26320). The stepedial artery was dissected from 6-month-old control and mutant mice, sectioned without decalcification, and stained with Alizarin red following standard procedures[21].

1.2.5 Evaluation of pathology of middle ears

A scoring system of -/+/++/+++ was used to assess the severity of pathology in the middle ears following a previously described method with modifications[22]. Histological analysis of the middle ears of control and mutant mice was performed using an Olympus BX51 microscope. A '-' symbol was assigned when the pathology is absent in the middle ear. A '+' symbol was assigned when pathology was very scarce in the middle ear. A '++' symbol was assigned when pathology was more prevalent, but not to the point of spanning the entire middle ear. A '+++ symbol was assigned when pathology spanned the entire middle ear. The following pathologies were evaluated by this scoring system: middle ear

effusion, inflammatory cell infiltration, tissue proliferation (epithelial hyperplasia), abnormal tissue at the Eustachian tube opening in the middle ear cavity, ectopic mineralization, and clusters of goblet cells.

1.2.6 Scanning electron microscopy (SEM)

Middle ears from *Enpp1^{asj/asj}* and wild-type mice were dissected after transcatheter perfusion with 4% paraformaldehyde (PFA) and then immersed in 2.5% glutaraldehyde in 0.1 M cacodylate buffer (pH= 7.2) at 4°C overnight. Dissection was performed to expose the middle ear cavities. After three 15-minute washes with cacodylate buffer (pH= 7.2) at room temperature, samples were post-fixed with the osmium-thiocarbohydrazide-osmium-thiocarbohydrazide-osmium (OTOTO) method[23], and dehydrated in increasing concentrations of ethanol at 4°C. Samples were critical point dried with Hexamethyldisilazane (HMDS) and then air dried in fume hood. Samples were then coated with 15nm gold and analyzed in a Hitachi S-3000 scanning electron microscope (Hitachi, Tokyo, Japan) at 20 kV.

1.3 Results

1.3.1 Hearing impairment in *Enpp1^{asj}* mutant mice

Hearing in the *Enpp1* mutant mice and age-matched controls was evaluated by ABR threshold analysis. Initial ABR measurements of three-month-old mutant mice revealed a moderate to severe hearing loss with threshold increases of 25-35 decibels (dB) compared to the normal thresholds in the control mice for both click and all pure tone stimuli (8 kHz, 16 kHz, 32 kHz). To further characterize the hearing ability of *Enpp1^{asj/asj}* mice and to determine whether the hearing impairment is progressive with age, recurrent ABR measurements were performed in *Enpp1^{asj/asj}*, *Enpp1^{asj/+}*, and *Enpp1^{+/+}* littermates from 3 weeks to 30 weeks of age (Figure 1.1, Table 1.1, Table 1.2). *Enpp1^{asj/+}* and *Enpp1^{+/+}* mice (grouped as controls) showed normal ABR thresholds even at 30 weeks of age, whereas *Enpp1^{asj/asj}* mice exhibited elevated thresholds by 6 weeks of age. Hearing impairment is not congenital as mutant mice had normal

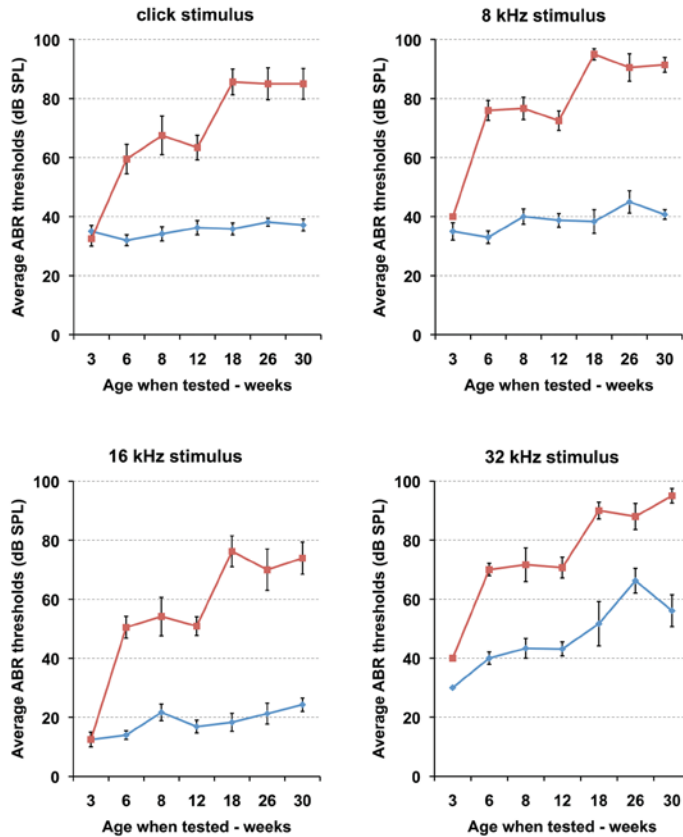


Figure 1.1 Progressive hearing loss in *Enpp1^{asj/asj}* mice

ABR threshold means are shown for *Enpp1^{asj/asj}* mice and littermate control mice, tested at the ages of 3 (n=6 mutant ears/8 control ears), 6 (n=10/10), 8 (n=6/6), 12 (n=22/16), 18 (n=8/6), 26 (n=10/8), and 30 (n=12/14) weeks. Starting from 6 weeks of age, the mutant mice exhibit significantly higher mean ABR threshold values at all the stimulus frequencies tested (click, 8 kHz, 16 kHz, 32 kHz) compared to those of the littermate controls. Thresholds of mutant mice continue to increase with age and by 18 weeks most of the *Enpp1^{asj/asj}* mice are profoundly hearing impaired. The increase in 32 kHz ABR thresholds of the control mice is due to the B6 background, a strain known to exhibit age-related hearing loss starting at high frequencies. Error bars indicate standard errors of the mean.

ABR thresholds at weaning age (3 weeks). Hearing loss in mutant mice progressed in two stages: average ABR thresholds increased by about 30-35 dB between 3 and 6 weeks of age, were relatively stable between 6 and 12 weeks, increased another 20-25 dB between 12 and 18 weeks, and remained stable between 18 and 30 weeks. At 12 weeks of age, only one out of 11 *Enpp1^{asj/asj}* mice tested showed normal thresholds in both ears (Table 1.1), giving a rough estimate of hearing loss penetrance of about 90%. No head bobbing or circling behaviors were observed in the mutant mice at all ages, indicating normal vestibular function.

Table 1.1 ABR thresholds of *asj/asj* mutant mice (* Highlighted ID numbers indicate ears were examined for pathology)

Mouse ID *	Age	Test Days	Sex	Right Ear thresholds (db SPL)			Left Ear thresholds (dB SPL)				
				Click	8	16	32	Click	8	16	32
5729	3 wk	23	F	30	30	10	35	40	45	15	35
5055 *	3 wk	22	M	30	40	10	40	35	40	15	40
5738	3 wk	25	M	30	20	10	40	30	30	10	35
4195 *	6 wk	38	M	35	70	50	80	75	80	60	70
5001	6 wk	39	F	70	80	40	70	45	50	30	60
5003	6 wk	39	M	60	80	40	80	60	90	50	70
4094 *	6 wk	41	F	70	80	70	70	75	80	55	70
4098	6 wk	41	M	35	70	50	60	70	80	60	70
3915	8 wk	50	F	75	80	50	85	70	75	40	80
3891 *	8 wk	55	F	35	60	35	45	75	75	55	75
3893 *	8 wk	55	M	75	85	75	70	75	85	70	75
3902	12 wk	75	F	45	50	30	40	40	50	30	40
3904	12 wk	75	M	65	75	40	70	40	40	40	50
3905 *	12 wk	75	M	30	50	20	40	80	85	60	90
3899 *	12 wk	75	F	60	65	50	70	70	85	50	65
4038	12 wk	89	F	100	90	60	90	80	80	50	70
4039	12 wk	89	F	65	80	40	70	80	80	50	80
4040	12 wk	89	M	70	80	60	90	70	85	50	90
4030	12 wk	101	F	90	90	80	90	90	90	80	90
4033	12 wk	101	M	60	80	70	70	40	60	60	70
4034	12 wk	101	M	40	70	50	70	70	80	50	80
4035	12 wk	101	M	70	80	50	70	40	50	50	60
5005	18 wk	123	F	95	100	95	100	100	100	95	100
5007	18 wk	125	F	90	100	70	90	60	90	50	90
5010	18 wk	136	F	90	100	70	85	80	90	80	75
5008	18 wk	144	F	80	90	70	90	90	90	80	90
3884 *	26 wk	172	M	100	100	90	90	75	100	60	100
3885 *	26 wk	172	F	90	100	70	80	100	100	100	100
3886	26 wk	172	M	100	100	90	90	70	85	70	60
3906	26 wk	188	F	100	100	80	100	95	90	70	100
3913	26 wk	188	M	60	70	40	90	60	60	30	70
3106	30 wk	202	F	100	100	100	100	90	90	70	100
3107	30 wk	202	F	100	100	90	100	100	100	90	100
3283	30 wk	204	F	100	100	90	100	100	100	90	100
3098	30 wk	206	F	80	90	80	90	50	80	40	70
3102	30 wk	206	M	70	80	70	90	90	90	60	90
3286	30 wk	223	M	80	90	50	100	50	80	50	100
3290	30 wk	223	M	100	100	90	100	80	80	65	90

Table 1.2 ABR thresholds of +/- or +/-asj control mice (* Highlighted ID numbers indicate ears were examined for pathology)

Mouse ID *	Age	Test Days	Sex	Right Ear thresholds (db SPL)				Left Ear thresholds (dB SPL)			
				Click	8	16	32	Click	8	16	32
5044	3 wk	21	F	35	30	20	40	40	40	20	40
5045	3 wk	21	M	35	30	20	35	30	30	20	30
5054	3 wk	22	F	35	40	10	30	30	30	10	30
5056	3 wk	22	M	33	30	10	30	40	40	20	30
4193 *	6 wk	38	M	30	30	10	40	35	30	20	40
5002	6 wk	39	F	20	20	10	30	40	30	15	40
5004	6 wk	39	M	30	40	10	40	30	40	10	40
4095 *	6 wk	41	F	30	40	20	50	35	40	20	50
4097	6 wk	41	M	30	30	10	40	40	30	15	30
3914	8 wk	50	F	30	40	25	50	35	40	30	50
3888	8 wk	55	F	25	30	20	40	35	40	20	40
3892 *	8 wk	55	M	40	50	25	50	40	40	10	30
3900 *	12 wk	75	F	30	35	10	40	30	35	20	40
3901	12 wk	75	F	30	40	25	50	60	60	35	60
3903	12 wk	75	F	25	30	20	40	35	30	20	40
4036	12 wk	89	F	35	30	10	30	50	35	15	40
4037	12 wk	89	F	50	55	35	70	35	40	20	40
4032	12 wk	101	M	25	30	10	40	35	30	10	40
4029	12 wk	101	F	35	40	10	40	40	40	10	40
4031	12 wk	101	M	30	40	10	40	35	50	10	40
5006	18 wk	123	F	35	30	10	30	35	40	20	40
5011	18 wk	136	F	30	50	10	60	35	50	20	40
5009	18 wk	144	F	35	30	30	60	45	30	20	80
3883 *	26 wk	172	F	40	40	20	80	40	50	20	60
3887 *	26 wk	172	M	40	60	30	70	40	60	40	50
3910	26 wk	188	M	35	30	10	70	40	40	10	80
3911	26 wk	188	F	30	40	20	50	40	40	20	70
3110	30 wk	202	F	30	40	20	40	30	40	20	40
3112	30 wk	202	M	30	40	20	50	30	40	20	50
3286	30 wk	204	M	30	30	20	45	40	40	20	50
3101	30 wk	206	M	35	40	20	40	45	40	30	40
3104	30 wk	206	M	30	30	10	40	40	40	20	45
5014	30 wk	231	F	40	50	30	80	50	40	30	90
5012	30 wk	234	F	40	50	40	85	50	50	40	90

1.3.2 Otitis media with effusion in *Enpp1*^{asj/asj} mice

To assess the causes of hearing impairment in the *Enpp1*^{asj/asj} mice, anatomical analysis of the middle and inner ears was performed after the completion of ABR measurements. We processed the whole bullae for histological studies, which allowed us to observe both middle and inner ear morphology. We did not observe any obvious inner ear defects in the *asj* mutant mice, such as hair cell and spiral ganglion cell loss, or stria vascularis degeneration (Figure 1.3H). However, we observed major histopathology in the middle and outer ear, with details described below.

1.3.2.1 Middle ear effusion and epithelial proliferation in *Enpp1* mutant mice.

All ears from *Enpp1*^{asj/asj} mice that had elevated ABR thresholds (n= 11) exhibited defects in the middle ear including retracted tympanic membranes and middle ear cavities filled with effusion (Figures 2, 3, Table 1.3) and a thickened epithelium with fibrous polyps (Figures 1.2B, 1.2D, 1.3C, Table 1.3). In addition, older *Enpp1*^{asj/asj} mice exhibited excessive accumulation of discharge in the external ear canal (Figure 2H). All the ears from the control *Enpp1*^{+/asj} and *Enpp1*^{+/+} mice examined (n =12) showed a transparent tympanic membrane, a clear middle ear cavity lined with a thin epithelium.

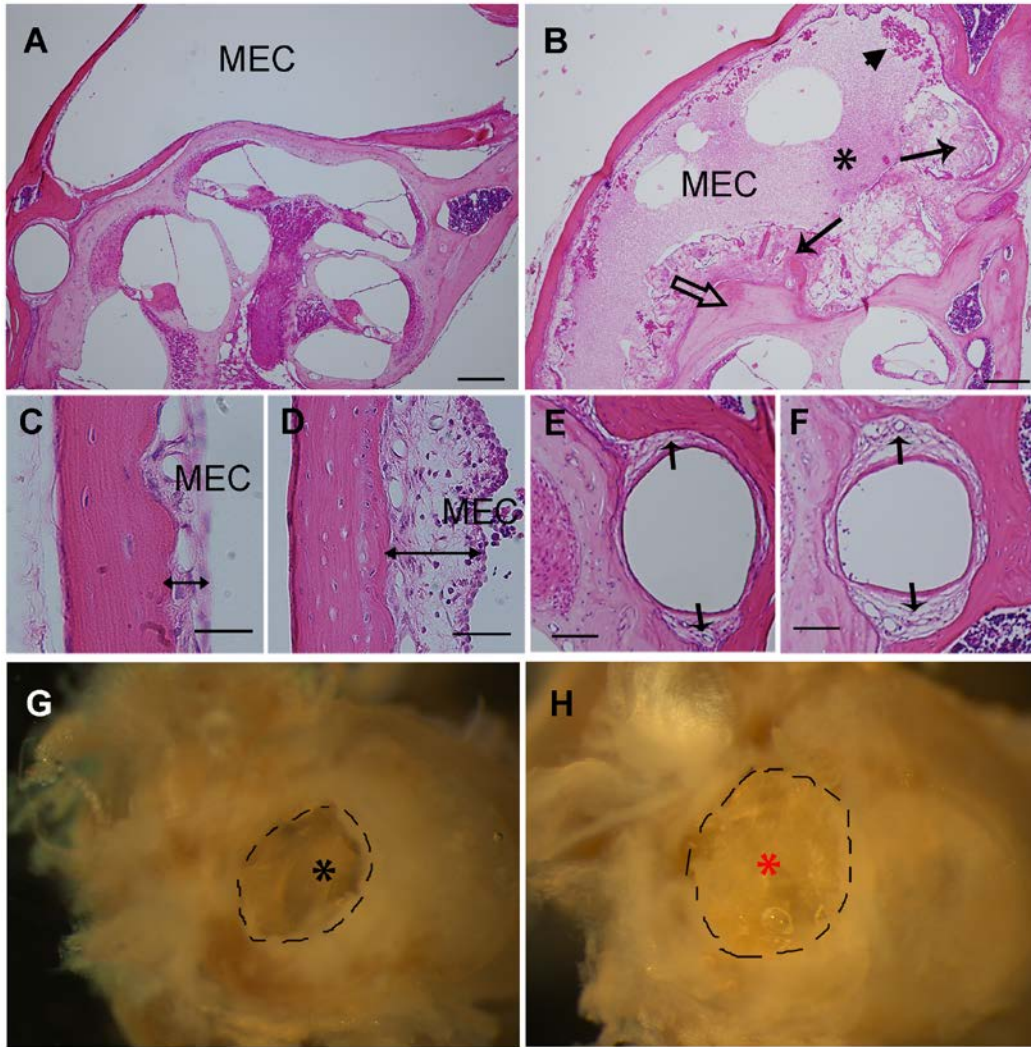


Figure 1.2 Otitis media in *Enpp1^{asj/asj}* mice

A, B: Representative images of pathological changes in the middle ears of *Enpp1^{asj}* mutant mice (B) compared with controls (A) at the age of 5 months. The middle ear cavity (MEC) of *Enpp1^{asj}* mutant mice is filled with effusions (black asterisk), fibroblastic and amorphous tissue masses (long arrows), and inflammatory cells (arrow head). Ectopic mineralization of the otic capsule is also evident in mutant mice (open arrow in B). Control mice show a clear middle ear cavity without fibroblastic proliferation (A). C, D: The thickness of the middle ear epithelium (double headed arrows) is greater in *Enpp1^{asj}* mutant mice (D) than controls (C). E, F: The stapedial artery wall (arrows) is thicker in *Enpp1^{asj}* mutant mice (F) than controls (E). G, H: Representative images of discharge in mutant mice (H) and littermate controls (G) at the age of 5 months. The external ear cavity of the mutant mice is filled with discharge (red asterisk), while control mice have a clear external ear canal and easily observable tympanic membrane (black asterisk). Scale bars: A, B = 200 μ m, C, D = 50 μ m, E, F = 80 μ m.

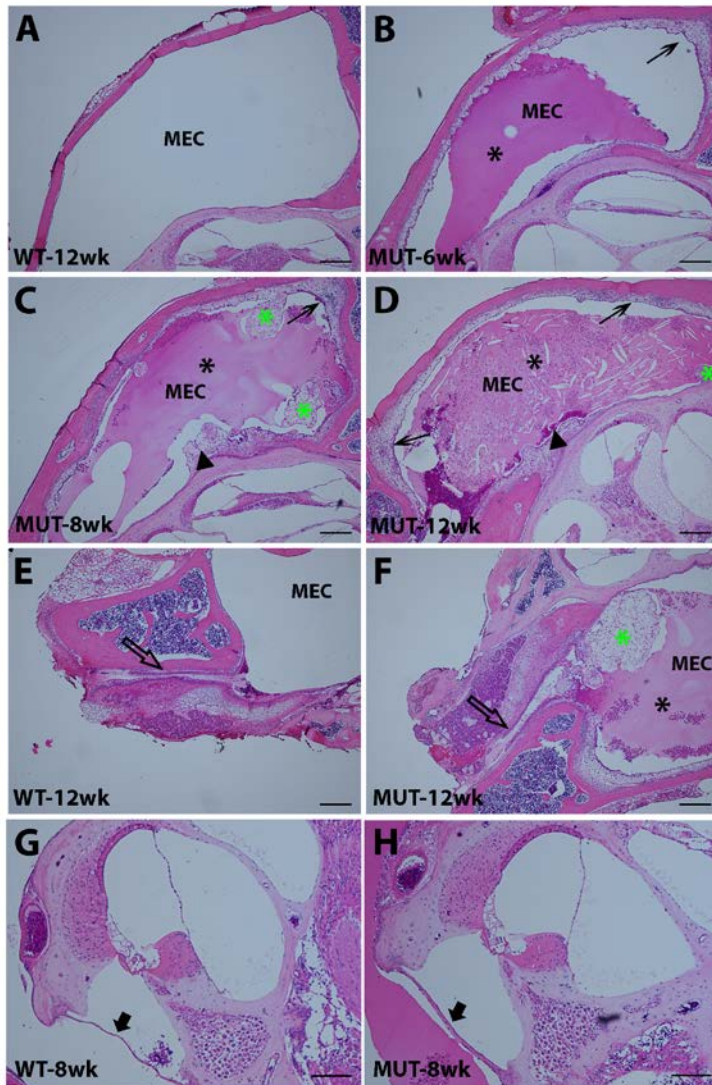


Figure 1.3 Development of otitis media in *Enpp1^{asj/asj}* mice.

A-D: 6-12 week time course of middle ear pathology of *Enpp1^{asj}* mutant mice (B, C, D) compared with a 12-week-old control (A). At 6 weeks of age (B), an aqueous effusion (black asterisk) and a slightly thickened epithelium (arrow) are observed in the middle ear cavity of the *Enpp1^{asj}* mutant mice. At 8 weeks (C), the middle ear cavity of the *Enpp1^{asj}* mutant mouse is filled with an aqueous effusion (black asterisk) and contains amorphous tissue masses (green asterisk). The middle ear epithelium is much thickened (arrow), and the otic capsule exhibits regions of ectopic mineralization (arrowhead) with adjacent fibroblastic proliferation. At 12 weeks (D), the middle ear cavity of mutant mice is filled with pus-like secretions (black asterisk), a thickened epithelium (arrows), and an amorphous tissue mass (green asterisk). E, F: Eustachian tube morphology of mutant (F) and control (E) mice at 12 weeks of age. In mutant mice, an amorphous tissue mass (green asterisk) is present near the orifice of the Eustachian tube (empty arrow), which may impede Eustachian tube function and lead to an accumulation of effusion in the middle ear cavity. G, H: Cochlear morphology and round window membranes of mutant (H) and control (G) mice. Cochlear morphology is grossly normal in *Enpp1^{asj}* mutant mice compared with controls; however, the round window membrane (black arrow) of mutant mice is thicker. MEC: middle ear cavity. Scale bars: A, B, C, D, E, F = 200 μ m, G, H = 100 μ m.

Table 1.3 Histological assessment of the middle ears of the Enpp1 mutant and control mice

Mouse ID	Age	Genotype	MEE	EH	IC	ETO	EM	CGC
4012L	1wk	Control	-	+	-	N/A	-	-
4017	1wk	Control	-	-	-	N/A	-	-
4015L	1wk	Control	-	-	-	N/A	-	-
4016L	1wk	Mutant	-	-	-	N/A	-	-
4016R	1wk	Mutant	-	-	-	N/A	-	-
4018L	1wk	Mutant	-	+	-	N/A	-	+
4022L	2wk	Control	-	-	-	N/A	-	-
4022R	2wk	Control	-	-	-	N/A	-	-
4019R	2wk	Control	-	-	-	N/A	-	-
4023L	2wk	Mutant	-	+	-	N/A	-	-
4023R	2wk	Mutant	-	+	-	N/A	-	-
4020L	2wk	Mutant	-	++	+	N/A	-	-
4008L	2wk	Mutant	-	+	-	N/A	-	-
4008R	2wk	Mutant	-	+	-	N/A	-	-
4007L	2wk	Mutant	-	+	-	N/A	-	+
4007R	2wk	Mutant	-	+	-	N/A	-	+
4002L	3wk	Control	-	-	-	N/A	-	-
4002R	3wk	Control	-	-	-	N/A	-	-
4001L	3wk	Control	-	-	-	N/A	-	+
4001R	3wk	Control	-	-	-	N/A	-	+
4004L	3wk	Mutant	-	-	-	N/A	-	-
4004R	3wk	Mutant	-	-	-	N/A	-	-
4000L	3wk	Mutant	-	-	-	N/A	-	-
4000R	3wk	Mutant	-	-	-	N/A	-	-
5055R*	3wk	Mutant	-	+	-	N/A	-	-
5055L*	3wk	Mutant	-	+	-	N/A	-	-
4193R*	6wk	Control	-	+	-	N/A	-	+
4195R*	6wk	Mutant	+	-	-	N/A	+	+
4094R*	6wk	Mutant	+++	+++	+	N/A	+	+++
3892L*	8wk	Control	-	-	-	-	-	-
3893R*	8wk	Mutant	+++	+++	+	+++	+	++
3891R*	8wk	Mutant	+	+	-	N/A	+	-
3900R*	12wk	Control	-	-	-	N/A	+	-
3905L*	12wk	Mutant	+++	+++	++	N/A	+	+++
3905R*	12wk	Mutant	+	+	+	+	+	-
3899L*	12wk	Mutant	+	+++	++	+++	+	+++
3899R*	12wk	Mutant	++	+++	++	N/A	+	++
3883L*	26wk	Control	-	-	-	N/A	-	-
3883R*	26wk	Control	-	-	-	-	-	-
3887L*	26wk	Control	-	-	-	N/A	-	+
3887R*	26wk	Control	-	-	-	-	-	-
3884L*	26wk	Mutant	+++	++	++	++	-	+++
3884R*	26wk	Mutant	+	++	+	++	+	+
3885L*	26wk	Mutant	-	-	+	-	-	+
3885R*	26wk	Mutant	++	++	+++	++	-	++
2094R	30wk	Mutant	++	++	++	+	+	++
2096R	30wk	Mutant	+++	+++	+++	++	+	++
2098R	30wk	Mutant	+++	+++	++	+++	+	++

MEE: Middle Ear Effusion; EH: Epithelial Hyperplasia; IC: Inflammatory Cells; ETO: Eustachian Tube Opening; EM: Ectopic Mineralization; CGC: Cluster of Goblet Cells. * Indicate ears with ABR data.

1.3.2.2 Increased goblet cell density and mucin secretion in *Enpp1^{asj/asj}* mice.

In the epithelium lining the middle ear cavity and the Eustachian tube, mucins secreted by goblet cells build the first line of defense in protecting the host from invading pathogens; movements of the cilia then help to get rid of the pathogens, with mucins serving as a lubricant [24]. However, when chronic inflammation is present, some of the epithelial cells transdifferentiate to mucin-secreting goblet cells [24]. These additional goblet cells secrete excessive mucins, which accumulate in the middle ear cavity and lead to conductive hearing loss (otitis media). We used Mayer's mucicarmine staining to detect the density of goblet cells in the *asj* mutant mice. Already at two weeks of age, an excess of goblet cells was observed around the opening of the Eustachian tube and in the Eustachian tube duct of mutant mice (Figure 1.4B).

In the control mice, scattered goblet cells were seen around the opening of the Eustachian tube, but very few were detected along the Eustachian tube duct (Figure 1.4A). Similar observations were made in two-month-old adult mice: more goblet cells were present in the epithelia lining the middle ear cavity and the Eustachian tube in mutants (Figure 1.4D) than in controls (Figure 1.4C).

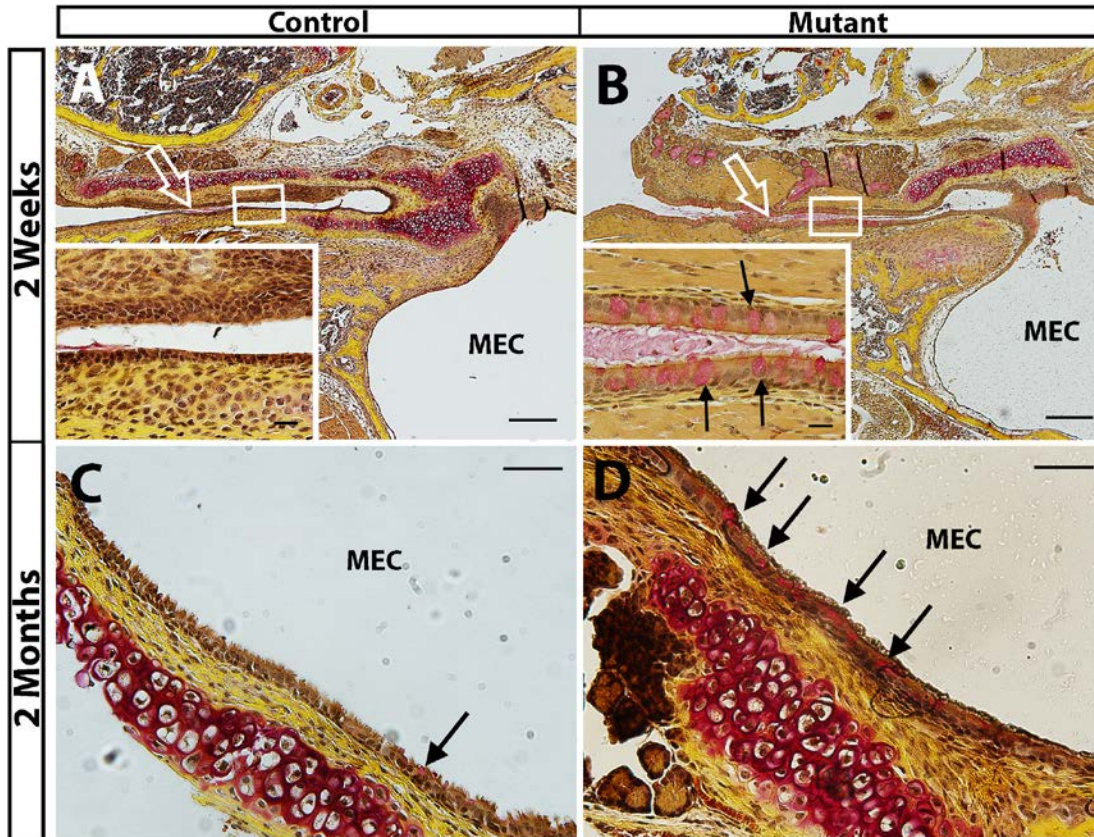


Figure 1.4 Increased density of goblet cells in *Enpp1^{asj/asj}* mice.

Mayer's mucincarmine method was used to visualize goblet cells (stained red) in the epithelia lining the Eustachian tube (A, B) and middle ear cavity (C, D) of mutant and control mice. A, B: Few goblet cells are seen in the epithelia lining the Eustachian tube of littermate control mice (A, empty arrow points to Eustachian tube, insert shows higher magnification of the Eustachian tube epithelia). By contrast, goblet cells are present at high density in the epithelium lining the Eustachian tube of *Enpp1^{asj}* mutant mice (B, empty arrow points to Eustachian tube, magnified inset shows goblet cells, marked by arrows, in the Eustachian tube epithelia). C, D: More goblet cells are present in the epithelia in the middle ear cavity (MEC) of the *asj* mutant mouse (arrows in D) than in the control (C). Scale bars: A, B = 200 μm , C, D = 50 μm , A and B inserts = 20 μm .

1.3.2.3 Impaired Eustachian tube function due to epithelia proliferation.

Out of 10 ear preparations (8-30 weeks) that allowed us to observe the opening of the Eustachian tube in the middle ear cavity, 7 had amorphous tissues that could potentially block the Eustachian tube (Table 1.3) thereby disrupting middle ear pressure regulation and ciliary clearance of secretions.

1.3.2.4 Impaired middle ear epithelial clearance function due to excess mucin and loss of microciliary function.

Using scanning electron microscopy (Fig. 1.5), we assessed the integrity of the mucociliary epithelium in 1-month-old and 6-month-old wild-type and *Enpp1^{asj/asj}* mice (n= 3 each genotype). The epithelium of one-month-old mutant mice had scattered areas with high densities of goblet cells (Figure 1.5B), which was confirmed by Mayer's mucincarmine staining. Goblet cell density in 6-month-old mutants could not be determined because of the obscuring layer of mucin (Figure 1.5D). These results indicate that excessive mucin secreted by increased numbers of goblet cells and the hindering effect of the mucin layer on ciliary function in the *asj* mutant mice are contributing factors to the occurrence of otitis media.

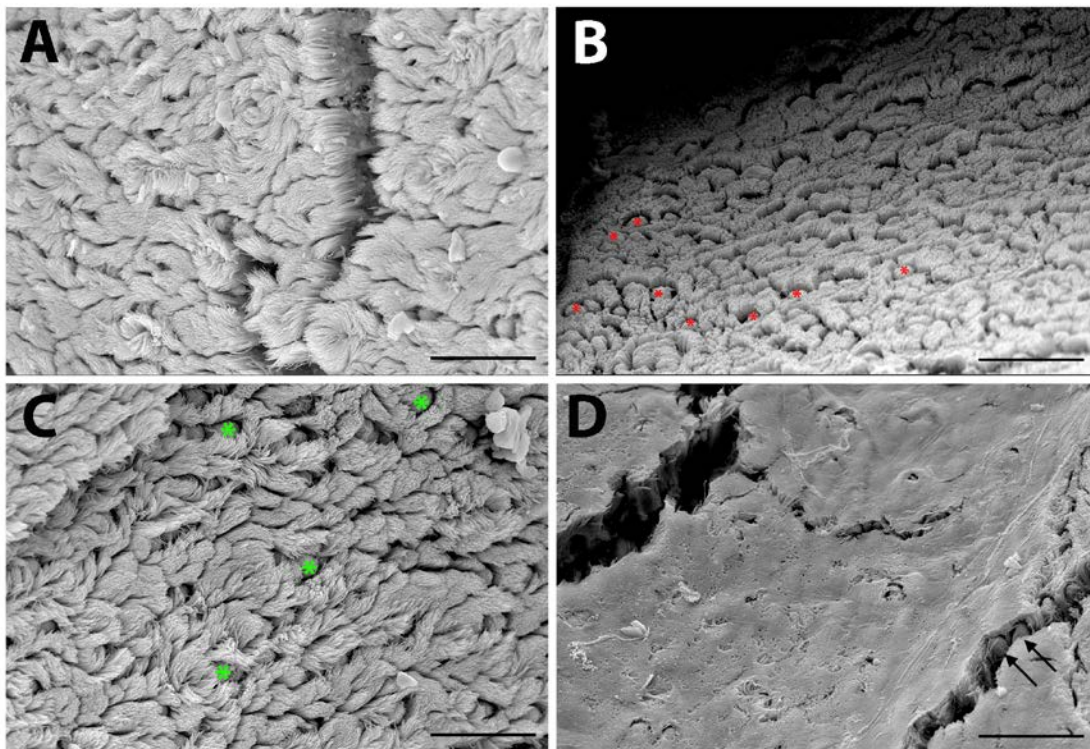


Figure 1.5 Scanning electron micrographs of epithelium lining the middle ear cavity

Compared with littermate controls (A), the middle ear epithelium in 1-month-old *Enpp1^{asj}* mutant mice (B) shows an increased number of goblet cells (red asterisks). Scattered goblet cells (green asterisks) and cilia are seen in the mucociliary epithelia of control mice at 6-months of age (C); however, a layer of mucin obscures most cilia and goblet cells (arrows) in age-matched *Enpp1^{asj}* mutant mice (D). Scale bars = 25 μ m.

1.3.3 Over-calcification of middle ear structures (tympanosclerosis)

6-month old control mice have transparent tympanic membrane (Figure 1.6A), mutant mice at the same age have retracted tympanic membrane due to the pressure of excessive discharge and white patch were observed at pars tensa of tympanic membrane in the mutant mice (Figure 1.6B). We dissected middle ear ossicles of 6-month-old *Enpp1^{asj/asj}* mice with littermate controls. Control mice have normal morphology of ossicles (Figure 1.6C). We found that stapes in the mutant mice have normal morphology and are freely removable from the round window (Figure 1.6D). Although malleus and incus has relative normal morphology, these two bones are fused (Figure 1.6D). The wall of the stapedia artery, which passes through the ring of the stapes, is thicker in *Enpp1^{asj}* mutant mice (Figure 1.2F) than controls (Figure 1.2E). Alarinate staining indicates excessive calcium deposition in the artery wall of the mutant mice (Figure 1.6F). Therefore, enlarged and stiffened stapedia artery could potentially impede the movement of the stapes and lead to impaired sound transmission to the inner ear. We observed overossification of round window ridge in the mutant mice (Fig. 1.2B, Table 1.3), which may indirectly contribute to otitis media and hearing loss. We observed that the round window membrane in *Enpp1^{asj}* mutant mice (Figure 1.3H) was thicker than in control mice (Figure 1.3G).

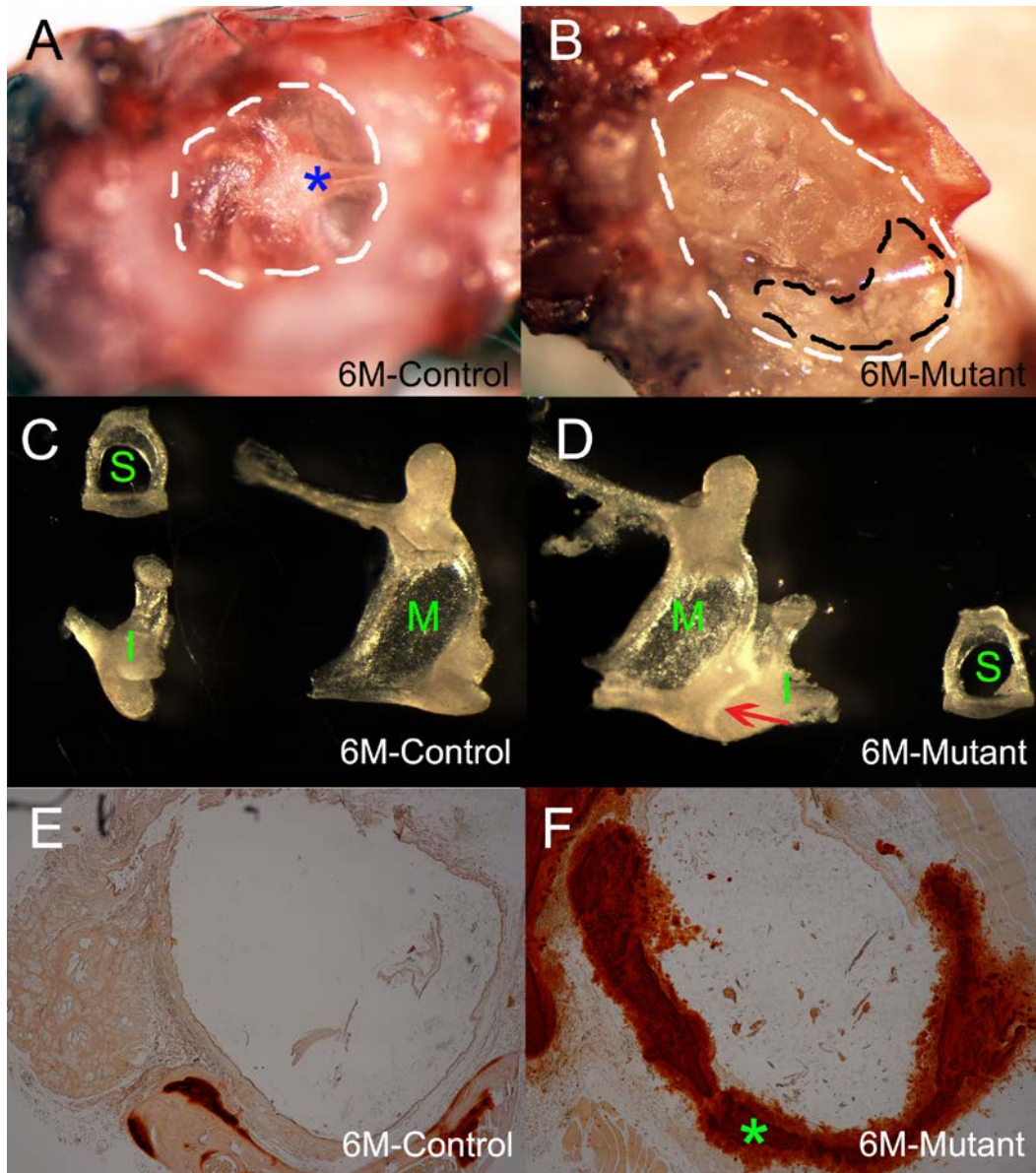


Figure 1.6 Calcification of middle ear structures (or tympanosclerosis) in *Enpp1^{asj/asj}* mice

In the control mice (A), the outer ear canal is clear without any discharge. The tympanic membrane appears to be transparent and malleus (blue asterisk) is clearly visible. In the age matched mutant mice (B), surrounding bone must be removed to expose the tympanic membrane, most of which is completely covered by discharge. White patches (inside black dashed lines) were observed on the tympanic membrane of the mutant mice (B). The ossicle bones of the age matched control and mutant mice appear to have similar morphology (C-D), but malleus and incus are fused in the mutant mice (D, red arrow). M: Malleus; I: Incus; S: Stapes. Alizarin red staining reveals extensive mineralization in the stapedial artery wall (green asterisk) in *Enpp1^{asj/asj}* mice (F), but not in the control mice (E).

1.3.4 Bacterial infection does not play a role in the development of otitis media in *Enpp1^{asj/asj}* mice

The effusion was confined within the middle ear cavity and did not appear to extend through the round window into the inner ear. To detect if otitis media in the *asj* mutant mice was caused by bacterial infection, we performed gram staining in the freshly prepared middle ear sections. We failed to detect any pathogens from the middle ear cavities of the *asj* mutant mice (data not shown), suggesting a non-infection origin of the otitis media in the *asj* mutant mice.

1.4 Discussion

1.4.1 Otitis media-related ear pathology of *Enpp1^{asj}* mutant mice

Beginning at 6 weeks of age, an effusion starts to appear in the middle ears of *asj* mutant mice, and moderate epithelial proliferation is observed lining the middle ear cavity. The degree of middle ear effusion and epithelial thickening in *asj* mutant mice correlates with ABR thresholds. At 12 weeks of age the content of the effusion changes from serous to suppurative, with a corresponding increase in ABR thresholds. These effusions in the middle ear cavity may interfere with the normal vibration of the tympanic membrane and movement of the ossicle chain; with suppurative effusion having a much stronger effect. We observed discharge in the outer ear cavity starting around 4 months of age. All of the ears examined from seven 6~7-month-old *asj* mutant mice showed complete blockage of the outer ear canal by discharge, which could explain the secondary increase in ABR thresholds that occurs in *asj* mutant mice between 12 and 18 weeks of age.

Mucins are secreted by goblet cells that lay scattered in the epithelium of digestive, respiratory, urinary, and reproductive tracts either at a basal level or at a high level upon stimulation [25]. Mucins, together with the cilia that line the epithelia, protect the host by cleaning invading pathogens. A similar mechanism is applied by the middle ear mucociliary system to clear middle ear effusions [24]. Disturbed phosphate homeostasis can cause systematic inflammation. Inflammation within the middle ear cavity triggers secretion of mucin into the middle ear cavity and transdifferentiation of more epithelial cells

into goblet cells, which lead to excessive effusion accumulation in the middle ear cavity. Continued chronic middle ear inflammation leads to tissue destruction and fibrosis. Thickened middle ear epithelia or fibrosis of epithelia, especially the epithelia around the opening of the Eustachian tube in the middle ear cavity can block the Eustachian tube and facilitate effusion accumulation. Although we don't have supporting evidence, excessive discharge in the outer ear canal might be caused by inflammation in the external ear. Defective action of the cilia lining the middle ear epithelia is often associated with development of otitis media, as seen in patients with primary ciliary dyskinesia (PCD) [26]. Impaired mucociliary function and increased number of goblet cells in the middle ear cavity of the *asj* mutant mice, confirmed by SEM and Mayer's mucicarmine staining, indicate that the middle ears of the *asj* mutant mice cannot maintain their ability to clear effusion, which therefore leads to conductive hearing loss. Overall, middle ear inflammation with effusion, amorphous tissue mass in the middle ear cavity, excessive discharge in the outer ear canal, and ectopic mineralization contribute to the conductive hearing loss in the *asj* mutant mice.

1.4.2 Mineralization disorders and conductive hearing loss in *Enpp1^{asj/asj}* mice

Mineralization disorders due to abnormal phosphate levels have been associated with inflammation in several different diseases, including chronic kidney disease [27, 28] and cardiovascular disease [29]. *Enpp1^{asj}* adds to a growing list of mouse mutations causing phosphate homeostasis disorders that have associated conductive hearing loss, including mutations of the *Ank*, *Phex*, *Rpl38*, and *Fgf23* genes. *Ank* (progressive ankylosis) encodes a multiple-pass transmembrane protein that regulates pyrophosphate levels, and *Ank* mutant mice were reported to have middle ear ossicle fusions and associated conductive hearing loss [30]. *ANK* mutations in human patients also have been reported with associated with conductive hearing loss [31]. *PHEX* (X-linked phosphate regulating endopeptidase) is an enzyme that is involved in regulating the balance of phosphate in the body. *PHEX* mutations are associated with X-linked hypophosphatemic rickets in human patients, with hearing loss as one of the

symptoms[32-34]. Mice with *Phex* mutations exhibit hypophosphatemia-related abnormalities and hearing impairment[35], which recently was shown to be associated with middle ear effusion and ciliary defects[8]. *Rpl38* (ribosomal protein L38) is not known to be directly involved in phosphate regulation; however, elevated organic phosphate levels in *Rpl38^{Ts}* mutant mice[4] suggest a potential but unknown function of *Rpl38* in phosphate homeostasis. *Rpl38^{Ts}* mutant mice have conductive hearing loss caused by ectopic ossification and cholesterol crystal deposition in the middle ear cavity, enlarged Eustachian tube, and chronic inflammation with effusion[4]. FGF23 (fibroblast growth factor 23) is a circulating hormone that controls phosphate and calcium homeostasis and bone mineralization. Abnormal serum levels of FGF23 lead to systemic pathologies in humans, including renal phosphate wasting diseases and hyperphosphatemia. FGF23-deficient mice show a mixed hearing loss and middle ear malformations[36], and changes in circulating FGF23 have been observed in humans and mice with ENPP1 and PHEX deficiencies[16, 37].

ENPP1 produces inorganic pyrophosphate (PPi), an inhibitor of mineralization. Because PPi levels are markedly reduced in *Enpp1^{asj/asj}* mice[13], it is not surprising to see ectopic mineralization and calcification of middle ear tissues, as was observed in other soft tissues of these mutant mice[13]. Calcification of soft tissues within the middle ear cavity could contribute in various ways to the conductive hearing loss of *Enpp1^{asj/asj}* mice. The stapedial artery is an embryonic artery that disappears at the early embryo stage in humans but is conserved in mice through adult ages [38]. We observed a thickened stapedial artery wall in *Enpp1^{asj}* mutant mice, which is likely due to calcification as has been observed in other soft tissues. The thicker arterial wall is not likely to affect transport function, but because the artery passes through the ring of the stapes, its thickened wall could potentially impede the vibration of the stapes and contribute to the conductive hearing loss of mutant mice.

Abnormal mineralization can also cause otosclerosis and tympanosclerosis, two conditions that commonly lead to hearing loss in human patients. Disruption of bone homeostasis of the otic capsule

can lead to otosclerosis [39], and the most common feature of otosclerosis is stapes fixation. Although we observed ectopic mineralization and bone deposition in the otic capsule of *asj* mutant mice starting from around 6 weeks of age, stapes fixation is absent from *Enpp1* mutant mice. Instead, we observed white patch on the tympanic membrane, malleus and incus fusion, which are typical symptoms of tympanosclerosis. We observed a thickened round window membrane in *Enpp1^{asj/asj}* mice at 8 weeks of age, which may increase the rigidity of the membrane and impede proper cochlear fluid movement and hair cell stimulation [40]. Therefore, *Enpp1^{asj}* mice can serve as a model for studying tympanosclerosis. Decreased PPI levels in *Enpp1^{asj/asj}* mice also lead to otitis media, perhaps the most important factor contributing to the hearing loss, but the underlying mechanism of pathology is uncertain. ENPP1 deficiency is known to cause elevated serum levels of FGF23 in *Enpp1* mutant mice[16], and excess FGF23 secreted in the middle ear may trigger mucoperiosteum proliferation, which may contribute to the development of otitis media. In support of this possibility, mucoperiosteum proliferation in *Enpp1^{asj/asj}* mice is remarkably enhanced around the regions of the otic capsule that exhibit ectopic mineralization. *Enpp1^{asj}* mice provide a tool to unravel the underlying mechanism of the development of otitis media that is associated with abnormal phosphate homeostasis.

1.5 Summary

This is the first report of hearing loss and ear pathology associated with a mutation of the mouse *Enpp1* gene. The conductive hearing loss of *Enpp1^{asj}* mutant mice provides a new animal model for studying otitis media and tympanosclerosis related to mineralization defects. It also provides a specific model for understanding the hearing loss recently reported to be a clinical feature associated with human *ENPP1* mutations[17, 18].

CHAPTER 2 HEARING LOSS WITHOUT OVERT METABOLIC ACIDOSIS IN ATP6V1B1 DEFICIENT MRL MICE, A NEW GENETIC MODEL FOR NONSYNDROMIC DEAFNESS WITH ENLARGED VESTIBULAR AQUEDUCTS

2.1 Introduction

Many of the transport proteins that are involved in acid secretion and bicarbonate reabsorption in the kidney have similar functions in the inner ear [41]. The vacuolar (v)H⁺-ATPase pump is one of the key membrane transporters for acid excretion in the α -intercalated cells of the distal nephron, and it is also expressed in the inner ear where it functions in endolymph pH homeostasis [42]. vH⁺-ATPase is a large multi-subunit complex consisting of both cytosolic (V₁) and transmembrane (V₀) domains. Distal renal tubular acidosis (dRTA) caused by vH⁺-ATPase mutations (OMIM 267300, 602722) is an autosomal recessive disorder of renal H⁺ transport causing a buildup of acid in the bloodstream (metabolic acidosis) with associated alkaline urine; it is frequently accompanied by sensorineural hearing loss. dRTA with hearing loss is caused by mutations in the *ATP6V1B1* gene [42, 43], which encodes the B1 subunit of the cytosolic domain of vH⁺-ATPase, and with mutations in the *ATP6VOA4* gene [43, 44], which encodes the α 4 subunit of the transmembrane domain. In contrast to the ubiquitous expression of most other vH⁺-ATPase subunits, expression of the B1 and α 4 subunits appears to be primarily restricted to the inner ear and kidney, in complexes that mediate H⁺ transport across the plasma membrane rather than across the membranes of intracellular organelles [45].

The *Atp6v0a4*^{-/-} knockout mouse recapitulates the systemic metabolic acidosis and hearing loss phenotype seen in human dRTA patients [46, 47]. In contrast, *Atp6v1b1*^{-/-} knockout mice exhibit a mild compensated acidosis (alkaline urine with impaired handling of an acid load) [48] and have normal hearing [49]. A compensatory membrane expression of the vH⁺-ATPase B2 subunit was proposed as a possible explanation for why *Atp6v1b1*^{-/-} knockout mice under baseline conditions are healthy and do not exhibit the overt metabolic acidosis and symptoms (growth retardation, failure to thrive) characteristic of dRTA patients with *ATP6V1B1* mutations [48]. In support of this hypothesis, B2-

containing H⁺-ATPase complexes, which normally localize to intracellular organelles, were shown to relocalize to the apical membranes of renal intercalated cells in B1-deficient *Atp6v1b1*^{-/-} knockout mice [50].

In the mouse inner ear, *Atp6v1b1* expression has been detected in the epithelial cells of the endolymphatic sac and duct and in the interdental cell layer of the cochlear spiral limbus [42, 49]. The inner ear expression pattern and the deafness that is associated with *ATP6V1B1* mutations in human dRTA patients suggest that ATP6V1B1 plays an important role in pH balance in the mouse inner ear. The surprising finding that *Atp6v1b1*^{-/-} knockout mice have normal hearing [49], however, implies that redundant mechanisms of pH regulation can compensate for the loss of the vH⁺-ATPase B1 subunit in the mouse inner ear. This compensation may come from relocalization of B2-containing vH⁺-ATPase complexes from intracellular to apical membranes as proposed for renal cells, or it may be accomplished by other acid-base transporting mechanisms or pH buffering systems in the inner ear.

Here, we describe the genetic and phenotypic characterization of a new spontaneous mouse mutation of the *Atp6v1b1* gene, named vortex (*vtx*) for the circling behavior that first identified mutant mice. Mice homozygous for this recessive mutation exhibit auditory and vestibular dysfunction associated with enlarged endolymphatic compartments of their inner ears, phenotypic features that were not observed in the previously reported *Atp6v1b1*^{-/-} knockout mouse [49] but that are similar to those of *Atp6v0a4*^{-/-} knockout mice [46]. Whereas the *Atp6v1b1*^{-/-} knockout mouse was characterized on a primarily C57BL/6 (B6) background with some admixture from 129S1-derived CJ7 ES cells [48], the spontaneous *Atp6v1b1*^{vtx} missense mutation arose on the genetically distinct MRL/MpJ (MRL) strain. We show by congenic strain analysis that the differences in inner ear phenotypes between MRL-*Atp6v1b1*^{vtx/vtx} and B6(129S1)-*Atp6v1b1*^{-/-} knockout mice are due to strain background differences and not to differences in the natures of their *Atp6v1b1* mutations. We exploited these strain-specific differences in a linkage backcross to map loci that modify the degree of hearing loss in *Atp6v1b1*^{vtx/vtx}

mice and found statistically significant linkage with Chromosome 13 markers. The results of our studies in mice provide insight into the hearing loss variability that is associated with human *ATP6V1B1* mutations and suggest that genetic background effects underlie this variation. Because MRL-*Atp6v1b1*^{vtx/vtx} mice exhibit enlargements of the endolymphatic sac and duct in the inner ear but do not exhibit the overt metabolic acidosis characteristic of dRTA, they provide a new genetic model for nonsyndromic deafness with enlarged vestibular aqueducts (EVA; OMIM 600791).

2.2 Materials and Methods

2.2.1 Mice

Experimental mice were bred and housed in the Research Animal Facility of the Jackson Laboratory in Bar Harbor, Maine. Mice were fed *ad libitum* with a 6% fat mouse diet. Water bottles were changed weekly and filled with acidified (pH 2.5-3.0) water. The light cycle was 12 hours light and 12 hours dark. Some post-weaning mice were shipped to Washington University in St. Louis, Missouri, for additional analyses. All procedures involving the use of experimental mice were approved by the Institutional Animal Care and Use Committees at The Jackson Laboratory and Washington University. All methods used in the study were performed in accordance with the guidelines and regulations of the U.S. National Institutes of Health (NIH) Office of Laboratory Animal Welfare (OLAW) and the Public Health Service (PHS) Policy on the Humane Care and Use of Laboratory Animals.

The vortex (*vtx*) mutation arose spontaneously on strain MRL/MpJ-*Fas*^{pr}/J (JAX Stock #485). The *Fas*^{pr} mutation was subsequently removed from the *vtx* colony by mating *vtx/vtx* mice with MRL/MpJ (Stock #486) mice and selecting progeny without the *Fas*^{pr} mutation as founders. The resulting strain is designated MRL/MpJ-*Atp6v1b1*^{vtx}/KjnJ (Stock #21771), here abbreviated MRL-*Atp6v1b1*^{vtx}. Mutant mice (*vtx/vtx*) can be identified without genotyping by their overt circling and head tilting behaviors, and the colony is maintained by mating +/*vtx* (unaffected) x *vtx/vtx* (affected) mice. Both female and male *vtx/vtx* mice are fertile and able to breed.

A C57BL/6J (B6) congenic strain carrying the *vtx* mutation was generated by first mating MRL-*Atp6v1b1*^{vtx/vtx} mice with B6 mice to produce F1 hybrids, followed by repeated backcrosses to B6 mice, at each generation selecting hybrids heterozygous for the MRL-derived *Atp6v1b1*^{vtx} mutation (inferred by the presence of MRL alleles at flanking markers *D6Mit144* and *D6Mit29*). N10 generation *Atp6v1b1*^{+/vtx} mice were then inbred, and the MRL-derived *Atp6v1b1*^{vtx/vtx} genotype was verified by DNA sequencing. The resulting homozygous congenic strain is designated B6.MRL-*Atp6v1b1*^{vtx}/KjNj (Stock #21772), here abbreviated B6.MRL-*Atp6v1b1*^{vtx}. To define the extent of the congenic region, 19 SNP markers along the length of Chromosome 6 were genotyped for B6 and MRL alleles, and the 74-84 Mb MRL-derived congenic region of B6.MRL-*Atp6v1b1*^{vtx} was determined to extend from a breakpoint between *rs13478686* (Chr6: 29,712,455; GRCm38) and *rs3023067* (Chr6: 36,019,022) to a breakpoint between *rs3024107* (Chr 6: 109,859,726) and *rs3693392* (Chr 6: 113,320,611).

2.2.2 Genetic mapping and DNA analysis of the *vtx* mutation

To genetically map the *vtx* mutation, individual DNA samples from linkage cross mice were typed for multiple MIT microsatellite markers located throughout the mouse genome. Previously described PCR methods [51] were used to genotype the chromosomal markers, which were then analyzed for co-segregation with the mutant phenotype. PCR primer pairs designed to amplify specific markers were purchased from Integrated DNA Technologies (Coralville, IA, USA).

PCR for comparative DNA analysis between *vtx/vtx* mutant and control mice was performed according to the same conditions as described above for genetic mapping. PCR primers used to identify the *vtx* mutation of the *Atp6v1b1* gene for genotyping were 5'- GATCCCCTTCTCCACATCAG -3' (forward) and 5'- AGCATGGTCTATGTGCTGGG -3' (reverse). The expected PCR product size (590 bp) was confirmed on a 3.5% agarose gel. PCR products then were purified with the QIAquick PCR Purification Kit (Qiagen Inc., Valencia, CA), and sequenced on an Applied Biosystems 3700 DNA Sequencer with an optimized Big

Dye Terminator Cycle Sequencing method. Typical DNA sequencing results for distinguishing *Atp6v1b1* wildtype and *vtx* mutant alleles are shown in Fig. 1.2A.

2.2.3 Auditory brainstem response (ABR) measurements

At the Jackson Laboratory, ABR thresholds were measured at 8, 16 and 32 kHz in a sound attenuating chamber using the SmartEP auditory evoked potential diagnostic system from Intelligent Hearing Systems (IHS, Miami, FL) as described previously [52]. Briefly, mice were anesthetized with tribromoethanol (0.2 ml of 20 mg/ml stock per 10 g of body weight, i.p.) and placed on a temperature controlled heating pad to maintain body temperature at 37°C. Three subdermal electrodes, placed at the vertex and behind each ear, were used to record brain stem responses to defined tone-bursts (3 ms duration, 1.5 ms cosine-gated rise/fall time). The responses were then amplified, filtered (100-3000 Hz) and averaged (25 kHz sampling rate, 10 ms analysis window). Stimulus intensity was initially decreased in 10 dB steps until the response began to disappear and then lowered in 5 dB steps; ABR threshold was defined as the lowest intensity at which an ABR response could be reliably obtained. With our testing system, average ABR thresholds for normal hearing mice are about 40, 20, and 45 dB SPL for 8, 16 and 32 kHz stimuli, respectively. Data from ABR tests at the Jackson Laboratory are shown in Figs. 1 and 8.

At Washington University School of Medicine (WUSM), ABR measurements were performed in a foam-lined, single-walled soundproof room (IAC). Animals were anesthetized (80 mg/kg ketamine, 15 mg/kg xylazine, IP) and positioned dorsally in a custom head holder. Core temperature was maintained at 37.5 ± 1.0 °C using a DC electric heating pad in conjunction with a rectal probe (FHC). Platinum needle electrodes (Grass) were inserted subcutaneously just behind the right ear (active), at the vertex (reference), and in the back (ground). Electrodes were connected to a Grass P15 differential amplifier (300-3,000 Hz, x100), then to a custom amplifier providing another 1,000X gain, then digitized at 30 kHz and visualized using Tucker Davis Technologies (TDT) System 2 hardware and software. Sine wave stimuli having 0.5 ms cos² rise/fall times and 5.0 ms total duration were also generated and calibrated

using TDT System2 hardware and software. Stimuli were presented free-field using TDT ES-1 speakers placed 7.0 cm from the right pinna and calibrated offline using an ACO Pacific 7016 ¼ inch microphone placed where the external auditory meatus would normally be. During ABR tests, tone burst stimuli at each frequency and level were presented up to 1,000 times at 20/sec. The minimum sound pressure level (SPL) required for visual detection of ABR Wave I was determined at 5, 10, 20, 28.3, 40 kHz and 56.6 kHz using a 5 dB minimum step size. Data from ABR tests at WUSM are shown in Fig. 2.6.

2.2.4 Endocochlear potential (EP) recording

EP recordings were performed at WUSM. Using a fine drill, a hole was made in the left cochlear capsule directly over scala media of the lower basal turn. Glass capillary pipettes (40-80 M Ω) filled with 0.15 M KCl were mounted on a hydraulic microdrive (Frederick Haer) and advanced until a stable positive potential was observed that did not change with increased electrode depth. The signal from the recording electrode was led to an AM Systems Model 1600 intracellular amplifier.

2.2.5 Tissue processing and imaging for histopathology

At the end of ABR and EP recordings at WUSM, animals were overdosed and perfused transcardially with cold 2.0% paraformaldehyde/2.0% glutaraldehyde in 0.1 M phosphate buffer (pH 7.4). Each cochlea was rapidly isolated, immersed in the same fixative, and the stapes was immediately removed. After decalcification in sodium EDTA for 72 hours, cochleae were post-fixed in buffered 1% osmium tetroxide, dehydrated in an ascending acetone series, and embedded in Epon. Cochleae were sectioned parallel to the modiolus at 4.0 μ m, then stained with toluidine blue for bright field viewing. All auditory and vestibular epithelia were examined qualitatively in at least three inner ears (three animals) per genotype. Bright field images used for illustration were obtained on a Zeiss LSM 700 laser scanning confocal microscope using ZENTM software.

2.2.6 Inner ear paint fills and cleared whole mount preparations

E15 embryos (MRL-*Atp6v1b1*^{vtx/+}, n= 5; MRL-*Atp6v1b1*^{vtx/vtx}, n=6) and P1 mice (MRL-*Atp6v1b1*^{vtx/+}, n=7 ; MRL-*Atp6v1b1*^{vtx/vtx}, n=5) were used for inner ear paint fills. E15 embryos were decapitated and whole heads were fixed in Bodian's fixative. P1 mice were decapitated and half-heads were fixed in Bodian's fixative after the brain was removed. Heads were fixed overnight and then dehydrated with 75% ethanol (2x 2 hours), 95% ethanol (2x 2 hours), and 100% ethanol (2x 2 hours). Heads were then rinsed once with methyl salicylate and cleared overnight by placing specimens in methyl salicylate. Inner ears were filled with 1% Wite-Out correction fluid in methyl salicylate using a Hamilton syringe, with a pulled glass capillary needle broken to a tip diameter of 20-40 μm . E15 inner ears were injected through the middle turn of the cochlea. Two injections were done for P1 inner ears with one injection to the cochlear middle turn and the second injection in the common crus (Kiernan, 2006). To observe otoconia, inner ears dissected from bisected heads of P1 mice were cleared with methyl salicylate as described above, sub-illuminated and photographed using a Leica dissecting microscope.

2.2.7 Blood and urine analysis

At 17 weeks of age spot urine and blood were collected from 5 males of each group. Immediately after collection, urine pH was measured by using a glass pH electrode (Thermo Orion Micro pH Probe). Sodium, potassium, and chloride were measured in urine and blood, calcium and creatinine were measured in urine on a Beckman AU680 Chemistry analyzer. Osmolality of blood and urine was measured using a 5004 micro-Osmette (Precision Systems).

2.2.8 Genetic mapping of modifier loci

For linkage backcross analysis to map modifier loci, tail-tip samples from individual N2 progeny mice were provided to the Jackson Laboratory's Genotyping Service, which outsources SNP genotyping to LGC Genomics (Beverly MA). Each mouse DNA sample was genotyped for 120 selected SNPs that

differ between the B6 and MRL strains. The ABR thresholds of the same backcross mice were evaluated as quantitative traits, and the MapManager QTXb20 program of least-squares linear regression [53] was used to analyze linkage and identify marker associations with ABR thresholds.

2.2.9 Analyses of candidate modifier genes

DNA and cDNA sequencing of candidate genes was performed on an Applied Biosystems 3700 DNA Sequencer with an optimized Big Dye Terminator Cycle Sequencing method, and the sequencing results were analyzed with Sequencher DNA Sequence Analysis Software (Gene Codes Corporation, Ann Arbor, MI, USA).

For qRT-PCR analysis of candidate gene expression, inner ears were dissected from two-week-old MRL-*Atp6v1b1*^{vtx/vtx}, MRL-*Atp6v1b1*^{vtx/+}, B6.MRL-*Atp6v1b1*^{vtx/vtx}, and B6 wild-type mice and snap frozen in liquid nitrogen. The two inner ears of each mouse were pooled together and homogenized in 1 ml TRIzol (Life Technologies) in GentleMACS M-tubes (Miltenyi Biotech) using a GentleMACS dissociator. Homogenates were briefly centrifuged to pellet and remove cell debris. Homogenates were phase separated in 1/5 volume of chloroform. RNAs were extracted using the MagMAX mirVana Total RNA Isolation Kit (Life Technologies) following the manufacturer's recommendations on the KingFisher Flex Purification System (Thermo Fisher Scientific). RNA quantity and quality were assessed using a Nanodrop 2000 (Thermo Scientific) and Bioanalyzer 2100 (Agilent) respectively. RNA was reverse-transcribed into cDNA using 500 ng total RNA and the Superscript IV First-Strand Synthesis System (Thermo Fisher Scientific) following the manufacturer's recommendations. cDNA was diluted 1:5 with RNase-free water, and 2 µl of was used for quantitative real-time PCR (qPCR) using a standard SYBR green comparative Ct template on a Life Technologies ViiA7 qPCR machine. Primer sequences were ATCCTTTTCCTGCGTCTGAC-forward and CTCATGGAGATGGCTGTCAG-reverse (110 bp product) for *Slc12a7* and AGGTGGTCACCTTCAAATGG-forward and ACCTTGTGGGACAGGTGAAA-reverse (106 bp product) for *Slc9a3*; both primer pairs produced robust single band products on agarose gels. The

double delta-Ct method was used to calculate fold changes in expression levels, and statistical analysis comparing mean delta Ct values was done with the two-tailed student test.

2.3 Results

2.3.1 Genetic mapping of the *vtx* mutation

The vortex (*vtx*) mutation arose spontaneously in a colony of MRL/MpJ (MRL) mice at The Jackson Laboratory. Mice homozygous for *vtx* are healthy and fertile with normal growth, but they exhibit vestibular dysfunction as evidenced by variable head tilting and circling behaviors, and they are profoundly hearing impaired as shown by ABR analysis (Fig. 2.1A).

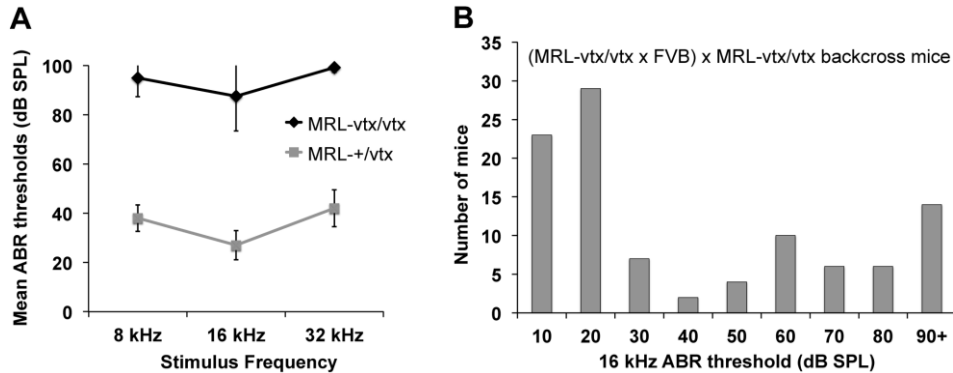


Figure 2.1 ABR thresholds of MRL-*vtx/vtx* mutant mice and linkage backcross mice

A. Average ABR thresholds of six (4 female, 2 male) MRL-*vtx/vtx* mutant mice and ten MRL-+/*vtx* control mice for 8, 16, and 32 kHz pure tone stimulus frequencies. All mice were tested between 4 and 6 weeks of age. Error bars represent standard deviations. Thresholds were assigned a value of 100 if no ABR was obtained at the maximum test stimulus of 100 dB SPL. **B.** Frequency distribution of 16 kHz ABR thresholds among 101 N2 mice of the (MRL-*vtx/vtx* x FVB) x MRL-*vtx/vtx* backcross. About half of the N2 mice are expected to be genotype +/*vtx* and half *vtx/vtx*.

We first attempted to genetically map *vtx* by generating an intercross of MRL-*vtx* mice with B6 mice; however, the cross was terminated because no abnormal vestibular-related behaviors were observed in multiple litters of F2 progeny from this cross. A second linkage intercross then was made with F1 hybrids between MRL-*vtx/vtx* mice and FVB/NJ (FVB) strain mice. Although the number of mutant (*vtx/vtx*) F2 progeny from this intercross, identified by their circling behavior and elevated ABR

thresholds, was less than expected, 18 were eventually produced and used for a genome-wide linkage screen with MIT microsatellite markers that differed in size between MRL and FVB. Results of this low-resolution screen indicated linkage of the *vtx* phenotype with markers *D6Mit15* (17% recombination) and *D6Mit366* (11% recombination) on Chr 6.

To verify and refine this linkage association, a backcross of (MRL-*vtx/vtx* x FVB) F1 hybrids to MRL-*vtx/vtx* mice was used to generate a total of 101 N2 progeny. Presumed genotypes (+/*vtx* or *vtx/vtx*) of the N2 mice were assigned according to their ABR thresholds. The distribution of ABR thresholds among N2 mice was strongly bimodal (Fig. 2.1B) as expected for a primarily monogenic trait. About half (59) of the 101 N2 backcross mice had 16 kHz thresholds equal to or less than 30 dB SPL (assigned +/*vtx* genotypes) and about half (42) had thresholds equal to or greater than 40 dB SPL (assigned *vtx/vtx* genotypes). Thresholds for 8 and 32 kHz stimuli were also analyzed to reinforce genotype assignments. The wide range of ABR thresholds among N2 mice in the *vtx/vtx* category (Fig. 2.1B) suggests the influence of strain-specific modifiers, which may explain why so few mutant phenotypes were observed in progeny from the (MRL x FVB)-+/*vtx* intercross. The N2 mice then were genotyped for multiple polymorphic SNP markers on Chr 6, and haplotype analysis refined the *vtx* candidate region to the interval between *rs13478778* (Chr6: 58,317,346 bp; GRCm38) and *rs3708822* (Chr6: 89,292,518 bp).

2.3.2 Gene identification and molecular characterization of the *vtx* mutation

The 31 Mb candidate region for the *vtx* mutation contains the *Atp6v1b1* gene (Chr6: 83,742,990 bp-83,758,855 bp), which encodes the B1 subunit of the vacuolar H⁺-ATPase. We considered *Atp6v1b1* a good candidate gene for the *vtx* mutation because (1) it is expressed in the inner ear, (2) mutations of the human *ATP6V1B1* and *ATP6VOA4* genes cause dRTA and deafness, and (3) the inner ear phenotype of *vtx/vtx* mutant mice is similar to that of *Atp6v0a4* knockout mice [46, 47]. The genomic DNA sequences of all 14 *Atp6v1b1* exons and their flanking splice sites in MRL-*vtx/vtx* mutant mice were

compared with those of MRL wildtype controls and revealed a single base pair mutation in exon 3 (c.233G>A) that changes the codon for glycine (GGC) to a codon for aspartic acid (GAC) at amino acid position 78 (p.G78D) of the mouse protein (Fig. 2.2). DNA sequence analysis of exon 3 in additional mutant and non-mutant mice confirmed this variant to be the recessive *Atp6v1b1*^{vtx} mutation. The *vtx* missense mutation occurs in the N-terminal domain of ATP6V1B1 (InterPro: IPR004100).

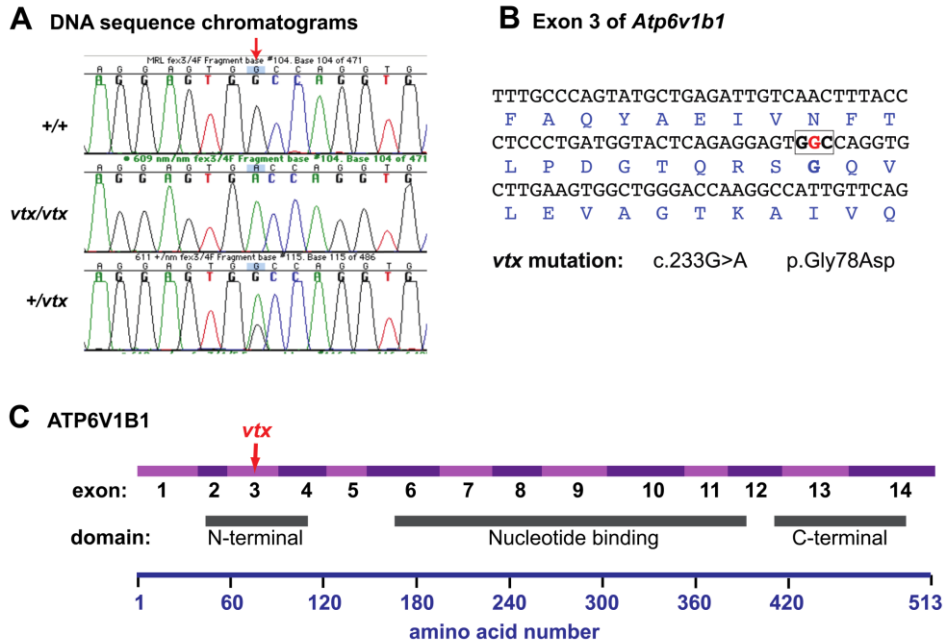


Figure 2.2 Molecular characterization and consequences of the *Atp6v1b1*^{vtx} mutation

A. DNA sequence chromatograms illustrating the G>A nucleotide change (indicated by red arrow) caused by the *vtx* mutation. **B.** DNA sequence of *Atp6v1b1* exon 3 with encoded amino acids shown below in blue font. The G nucleotide that is altered in the *vtx* mutation (shown in red) is part of the GGC codon (boldface, boxed) for glycine. The G>A nucleotide substitution at coding DNA position 233 (c.233G>A) causes a glycine to aspartic acid amino acid change at position 78 of the ATP6V1B1 protein (p.Gly78Asp). **C.** Schematic diagram of the ATP6V1B1 protein showing the regions encoded by exons 1-14 in alternating light and dark purple shades and locations of the three functional domains relative to the amino acid numbers shown below. The *vtx* mutation is in exon 3, which encodes part of the N-terminal domain of the protein.

The early onset, profound hearing impairment of *Atp6v1b1*^{vtx/vtx} mice on the MRL strain background (Fig.2.1A) is strikingly different from the previously reported normal auditory phenotype of *Atp6v1b1*^{-/-} knockout mice on a mixed B6/129S1 strain background [49]. To specifically test for MRL versus B6 strain background effects on the mutant phenotype, we generated B6.MRL-*Atp6v1b1*^{vtx/vtx}

congenic mice (described in Materials and Methods) and compared their inner ear and kidney phenotypes with those of MRL-*Atp6v1b1*^{vtx/vtx} mice.

2.3.3 Inner ear morphology and auditory function

Paintfills of the membranous labyrinths of inner ears from MRL-*Atp6v1b1*^{vtx/vtx} mutants and controls were examined in day 15 embryos (E15) and in newborn (P1) mice. Already at E15, the membranous labyrinth of MRL-*Atp6v1b1*^{vtx/vtx} embryos appeared dilated compared with inner ears of MRL-*Atp6v1b1*^{+ /vtx} littermate controls. The swelling was especially apparent in the endolymphatic sac and duct, but also noticeable in the utricle, saccule, and cochlear duct (Fig. 2.3A). The enlargement of the membranous labyrinth in inner ears of MRL-*Atp6v1b1*^{vtx/vtx} mutant mice became even more pronounced at P1 (Fig. 2.3B). Cleared whole-mount preparations of inner ears from newborn MRL-*Atp6v1b1*^{vtx/vtx} mice showed an obvious enlargement of the cochlear duct but also showed a conspicuous deficiency and dispersion of utricular and saccular otoconia compared with MRL-*Atp6v1b1*^{+ /vtx} littermate control mice (Fig. 2.3C). Whole mount preparations of inner ears from B6.MRL- *Atp6v1b1*^{vtx/vtx} mice showed normal morphology (not shown).

Cross-sections of plastic-embedded adult (2.5-4.5 months-of-age) cochleae (Fig. 2.4) revealed wholesale differences in the arrangement of cochlear fluid spaces in B6.MRL-*Atp6v1b1*^{vtx/vtx} and MRL-*Atp6v1b1*^{vtx/vtx} mutant mice. In the MRL-*Atp6v1b1*^{vtx/vtx} mutants, scala media appeared reduced in size in the lower basal turn, but expanded elsewhere. Scala vestibuli was generally expanded at the expense of scala tympani. The spiral limbus was widened laterally and contained few fibrocytes. Spiral ligament and stria vascularis were generally thinner, and strial layer structure was disorganized. In the ligament, type I and III fibrocytes were almost entirely missing behind the stria. Most noteworthy was an absence of the boney turn boundary between the lower cochlear base and lower apical turn. The boundary appeared fused with the osseous spiral lamina of the adjacent cochlear regions (not shown). Few hair cells were in evidence in any of the MRL-*Atp6v1b1*^{vtx/vtx} mutant cochleae examined. The abnormal

Figure 3

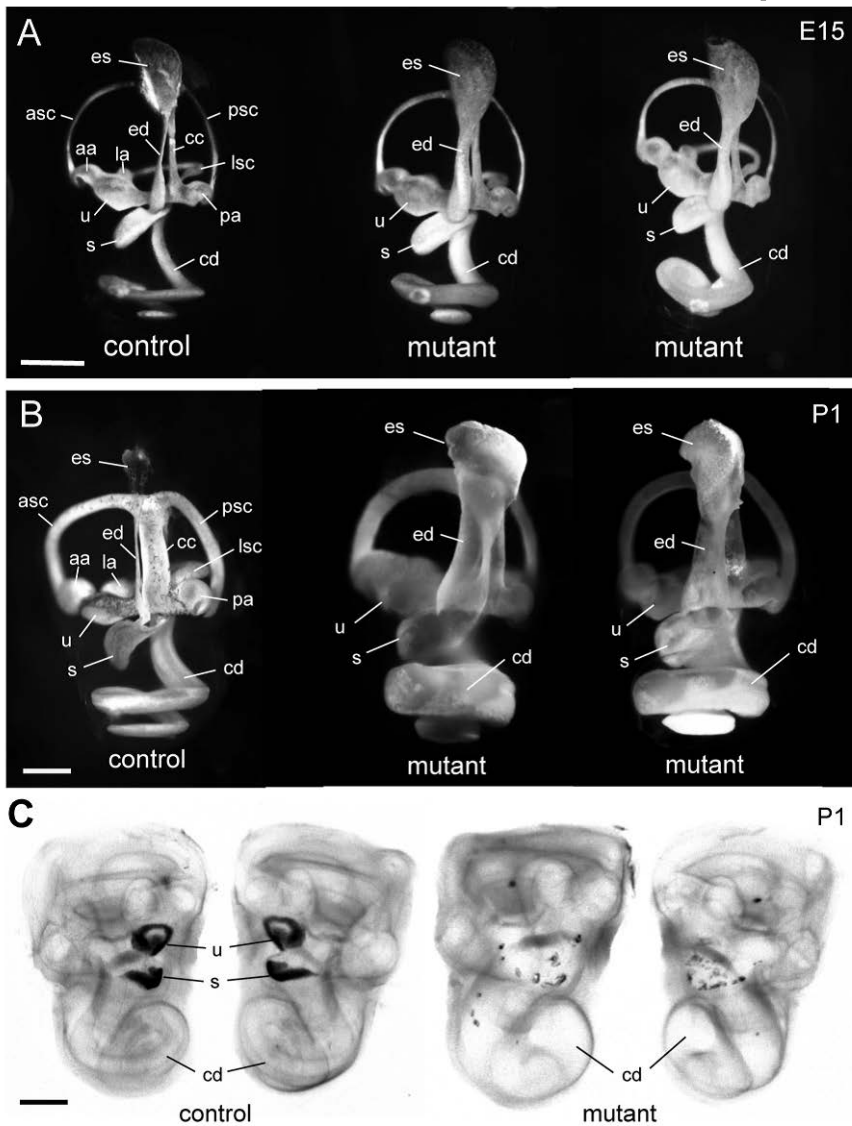


Figure 2.3 Paint fills and whole mounts of inner ears from *MRL-Atp6v1b1*^{vtx/vtx} mutant and control mice
A. Paint fills of the membranous labyrinths of inner ears from an E15-stage *MRL-Atp6v1b1*^{+/vtx} (control) embryo and two littermate *MRL-Atp6v1b1*^{vtx/vtx} (mutant) embryos. The endolymphatic sac (es), endolymphatic duct (ed), utricle (u), saccule (s), and cochlear duct (cd) appear enlarged in the two mutant inner ears compared with the control. **B.** Paint fills of the membranous labyrinths of inner ears from a newborn (P1) *MRL-Atp6v1b1*^{+/vtx} (control) mouse and two *MRL-Atp6v1b1*^{vtx/vtx} (mutant) littermates. The entire membranous labyrinth of the mutant inner ears appears swollen from an excess of endolymph. Other structures labeled in the control inner ears of A and B: anterior semicircular canal (asc), posterior semicircular canal (psc), lateral semicircular canal (lsc), anterior ampulla (aa), posterior ampulla (pa), lateral ampulla (la), common crus (cc). **C.** Cleared, whole-mount preparations of both inner ears from a P1 *Atp6v1b1*^{+/vtx} newborn mouse (control) and two *MRL-Atp6v1b1*^{vtx/vtx} (mutant) littermates, illuminated from below. Dark-appearing otoconia in the utricle (u) and saccule (s) are clearly visible in the control ear, but only a few widely dispersed otoconial crystals are seen in the mutant inner ears. The cochlear ducts (cd) of the mutant inner ears are enlarged compared with the control. Scale bars for A, B, C: 0.5 mm.

Figure 2.4 Cross sections of cochleae from B6.MRL-*Atp6v1b1*^{vtx/vtx} and MRL-*Atp6v1b1*^{vtx/vtx} mice

A,B. Whole cochlear profiles from B6.MRL-*Atp6v1b1*^{vtx/vtx} (A) and MRL-*Atp6v1b1*^{vtx/vtx} mice (B) imaged at the same magnification. B6.MRL-*Atp6v1b1*^{vtx/vtx} mutants appear normal while MRL-*Atp6v1b1*^{vtx/vtx} mutants feature greatly reduced scala tympani (compare areas marked with *), missing turn boundary between lower base and lower apex (compare areas marked with white arrows), and partial collapse of Reissner's membrane in the lower base (compare black arrows). **C,D.** Upper basal turn scala media profiles from different specimens of B6.MRL-*Atp6v1b1*^{vtx/vtx} (C) and MRL-*Atp6v1b1*^{vtx/vtx} mice (D) imaged at the same magnification. B6.MRL-*Atp6v1b1*^{vtx/vtx} mutants appear normal while MRL-*Atp6v1b1*^{vtx/vtx} mutants show widened profile, elongated and acellular spiral limbus, hair cell loss (see E,F), and lateral wall degeneration (see G). **E,F.** Enlarged views of organ of Corti from C,D show hair cell loss in MRL-*Atp6v1b1*^{vtx/vtx} mutants (black arrows). **G.** Enlarged view of MRL-*Atp6v1b1*^{vtx/vtx} mutant stria vascularis from D shows thin and disorganized stria and near absence of type I and III fibrocytes (white arrow). Scale bar in A applies to B. All other scale bars 20 μ m. LB: Lower base; UB: Upper base; LA: Lower apex; UA: Upper apex; RWM: Round window membrane; Sp Lim: Spiral Limbus; Sp Lig: Spiral ligament; RM: Reissner's membrane; StV: Stria vascularis; I, II, III, IV: Fibrocyte types by area; OC: Organ of Corti; IP: Inner pillar; OP: Outer pillar; DC: Deiters' cells; IHC: Inner hair cell; OHC: Outer hair cell.

Figure 2.5 Cross sections of vestibular organs from B6.MRL-*Atp6v1b1*^{vtx/vtx} and MRL-*Atp6v1b1*^{vtx/vtx} mice

A,B. Both B6.MRL-*Atp6v1b1*^{vtx/vtx} (A) and MRL-*Atp6v1b1*^{vtx/vtx} (B) mutant cristae appeared normal (posterior cristae is shown), including presence of cupula, hair cells, and dark cells. **C-F.** B6.MRL-*Atp6v1b1*^{vtx/vtx} maculae (sacculae shown in C) appeared normal. MRL-*Atp6v1b1*^{vtx/vtx} mutant maculae (sacculae is shown in D-F) showed normal complement of hair cells, but few, very large otoconia that tended toward triangular shapes. Macrophages (arrows in D) often lined the epithelial surface and surrounded abnormal otoconia. Scale bar in A applies to all panels. Cup: Cupula; HC: Hair cells; DC: Dark cells; Ot: Otoconia.

appearance of the lateral wall and absence of hair cells are consistent the complete absence of tone responses in these animals.

Comparison of the vestibular organs by genotype (Fig. 2.5) indicated little hair cell or neural loss in any group. MRL-*Atp6v1b1*^{vtx/vtx} mutant cristae were similar to those of the B6.MRL-*Atp6v1b1*^{vtx/vtx} mutants in normal appearance, including the presence of a cupula and complement of dark cells. The appearance of all maculae was likewise similar by genotype with respect to hair cells. What

distinguished MRL-*Atp6v1b1*^{vtx/vtx} mutant maculae was the frequent presence of macrophages lining the epithelium, contrasted with the complete absence of normal otoconia. Instead, the MRL-*Atp6v1b1*^{vtx/vtx} mutants featured very few, very large otoconia that tended toward triangular shapes. These also were often associated with macrophages. Based on appearance, it is possible that MRL-*Atp6v1b1*^{vtx/vtx} mutant cristae function normally if K⁺ levels are normal, since the endocochlear potential (EP) is normally low in the vestibular organs. The maculae, however, may be aberrantly responsive or unresponsive due to the lack of normal otoconia, despite little apparent hair cell loss.

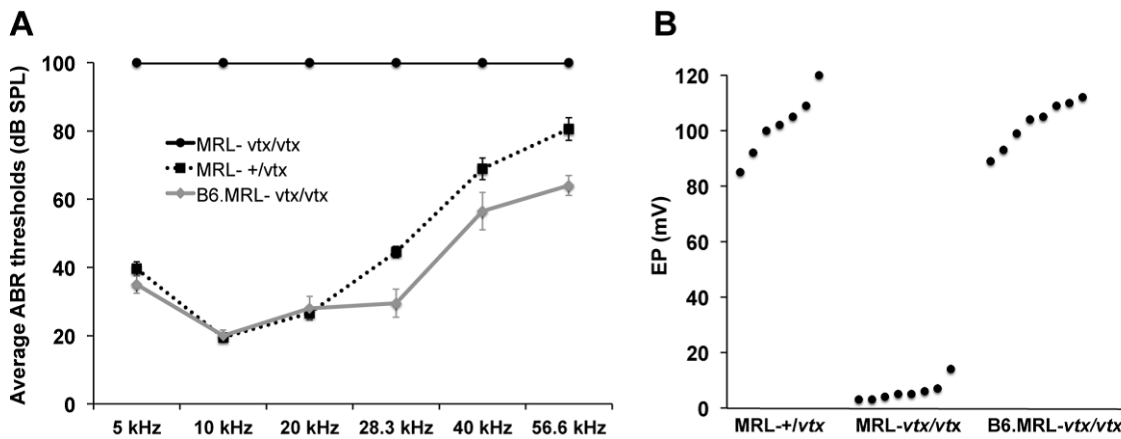


Figure 2.6 ABR and EP measurements of auditory function in B6.MRL-*Atp6v1b1*^{vtx/vtx} and MRL-*Atp6v1b1*^{vtx/vtx} mice

A. Average ABR thresholds of MRL-*Atp6v1b1*^{vtx/vtx} mice (MRL-vtx/vtx; 4 females, 6 males); MRL-*Atp6v1b1*^{+ /vtx} mice (MRL+/vtx; 3 females, 5 males); and B6.MRL-*Atp6v1b1*^{vtx/vtx} mice (B6.MRL-vtx/vtx; 5 females, 5 males). Thresholds were obtained from 5, 10, 20, 28.3, 40, and 56.6 kHz pure tone test frequencies. Thresholds were assigned a value of 100 if no ABR was obtained at the maximum test stimulus of 100 db SPL. Mice were tested between 2.5 and 4.5 months of age. Bars represent standard errors of the means. **B.** Endocochlear potential (EP) measurements (mV) of the same mice were obtained immediately after the ABR tests. EP values are shown for individual mice.

ABR thresholds of adult mice (2.5 and 4.5 months of age) were compared for 5, 10, 20, 28.3, 40, and 56.6 kHz test stimuli (Fig. 2.6A). Thresholds of B6.MRL-*Atp6v1b1*^{vtx/vtx} congenic strain mice and MRL-*Atp6v1b1*^{+ /vtx} control mice were similar and in the normal range for most inbred mouse strains. MRL-*Atp6v1b1*^{vtx/vtx} mice, however, failed to elicit an ABR even at the maximum test stimulus (100 dB SPL) for any of the test frequencies, indicating complete deafness. Likewise, EP measurements were normal in

B6.MRL-*Atp6v1b1*^{vtx/vtx} and MRL-*Atp6v1b1*^{+ /vtx} mice but nearly absent in MRL-*Atp6v1b1*^{vtx/vtx} mice (Fig. 2.6B). These results clearly demonstrate that the MRL strain background has a strong deleterious effect on the auditory phenotype of *Atp6v1b1*^{vtx/vtx} mutant mice.

2.3.4 Kidney-related phenotype

MRL-*Atp6v1b1*^{vtx/vtx} and B6.MRL-*Atp6v1b1*^{vtx/vtx} mice were healthy and showed no overt symptoms of metabolic acidosis. The previously reported B6(129S1)-*Atp6v1b1* knockout mice show increased urine pH, decreased calcium excretion, and decreased osmolality (9). We measured these characteristics in the MRL-*Atp6v1b1*^{vtx/vtx} and B6.MRL-*Atp6v1b1*^{vtx/vtx} mice and compared them with wildtype mice from the same genetic background. Similar to results reported for mice with the *Atp6v1b1* knockout mutation, mice homozygous for the *Atp6v1b1*^{vtx} mutation on the B6 background had a significantly higher urine pH (6.5 ± 0.1 vs 6.2 ± 0.1) compared to wildtype B6 mice (Figure 2.7A). We did not observe a difference between wildtype and *Atp6v1b1*^{vtx/vtx} mutant mice on the MRL background, but wildtype MRL mice had an unusually high urine pH (6.5 ± 0.2) compared to several other strains we tested: C57BL/6J (6.2 ± 0.1), A/J (6.1 ± 0.1), 129S1/SvImJ (5.8 ± 0.1), and NOD/LtJ (6.0 ± 0.2).

Decreased calcium excretion (urinary Ca^{2+}/Cr mg/g ratios) was observed in mice with the *Atp6v1b1*^{vtx} mutation in both genetic backgrounds (Figure 2.7B) although we saw a larger decrease (163.3 ± 17.4 vs. 45.9 ± 6.0 , approx. 70%) in the MRL background compared to the B6 background (139.2 ± 9.1 vs. 99.0 ± 9.6 , approx. 30%). We did not measure a significant effect of the *Atp6v1b1*^{vtx} mutation on osmolality on either background. In addition, we also measured potassium, sodium, and chloride concentrations in both blood and urine and did not find any significant differences between *Atp6v1b1*^{vtx/vtx} and wildtype mice on either strain background (Table 2.1).

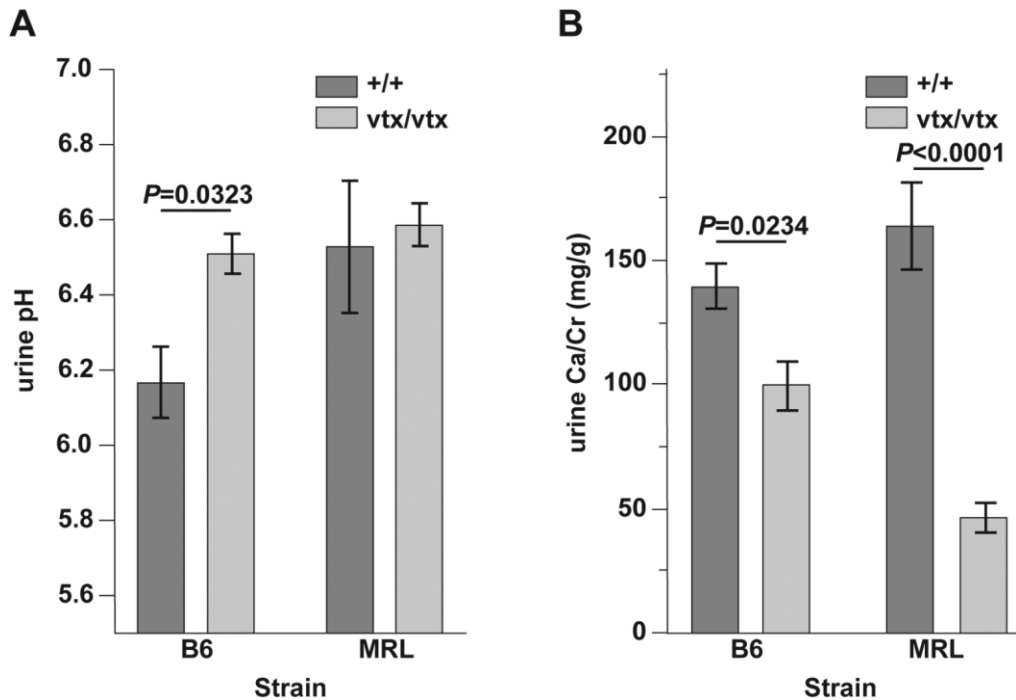


Figure 2.7 Renal secretion in B6- and MRL-*Atp6v1b1*^{vtx} mutant mice at 17 weeks of age

A. Urine pH is significantly increased in *vtx* mice compared to wildtype controls in the B6 background, but not in the MRL background. Urine pH of MRL^{+/+} mice is significantly higher than that of B6^{+/+} mice and similar to that of *vtx/vtx* mutant mice on either strain background. **B.** Calcium excretion is decreased in the mutant mice for both genetic backgrounds, but with a much larger decrease in MRL. Values are expressed as mean ± SE and each group contained 5 male mice.

Table 2.1 Physiological parameters of *Atp6v1b1*^{vtx/vtx} (*vtx/vtx*) and *Atp6v1b1*^{+/+} (*+/+*) control mice on the MRL and B6 strain backgrounds.

	MRL +/+	<i>vtx/vtx</i>	B6 +/+	<i>vtx/vtx</i>
Blood				
Na ⁺ , mM	156.4 ± 0.7	155.3 ± 1.0	151.5 ± 1.5	154.1 ± 0.9
K ⁺ , mM	5.6 ± 0.1	6.6 ± 0.7	5.2 ± 0.2	5.9 ± 0.4
Cl ⁻ , mM	104.4 ± 0.6	106.4 ± 1.2	110.1 ± 0.8	109.7 ± 0.7
Osm, mmol/kg	326 ± 3	323 ± 3	328 ± 2	320 ± 2
Urine				
Na ⁺ , mM	173.2 ± 42.1	142.8 ± 22.6	152.0 ± 15.8	154.6 ± 27.5
K ⁺ , mM	155.9 ± 27.7	136.4 ± 9.0	166.6 ± 16.5	157.4 ± 5.4
Cl ⁻ , mM	155.3 ± 34.6	134.5 ± 14.2	177.4 ± 19.6	167.4 ± 21.7
Osm, mmol/kg	993 ± 106	896 ± 139	1,026 ± 185	1,069 ± 254

There were no statistically significant differences between mutant and wildtype mice from the same genetic background. Values are mean ± SE. The number of male mice in each group is 5.

2.3.5 Genetic mapping of hearing loss modifiers

To genetically map loci that contribute to hearing loss differences between B6.MRL-*Atp6v1b1*^{vtx/vtx} and MRL-*Atp6v1b1*^{vtx/vtx} mutant mice, we first generated F1 hybrids between these two strains. The F1 hybrid mice are homozygous for the *vtx* mutation and for MRL alleles at linked loci within the congenic region of the B6.MRL-*Atp6v1b1*^{vtx/vtx} strain, and heterozygous for B6 and MRL alleles elsewhere in the genome. ABR thresholds of 6-week-old F1 hybrids are very similar to those of 8-week-old B6.MRL-*Atp6v1b1*^{vtx/vtx} congenic mice and much lower than those of 5-week-old MRL-*Atp6v1b1*^{vtx/vtx} mice (Fig 8A), indicating that B6-derived alleles at loci outside of the congenic region have a mostly dominant effect in preventing hearing loss. To reveal the phenotype of recessive MRL-derived, hearing loss-promoting alleles and reduce genetic complexity for mapping, the F1 hybrids were backcrossed to MRL-*Atp6v1b1*^{vtx/vtx} mice rather than intercrossed. We use the notation (MRL-*vtx/vtx* x B6.MRL-*vtx/vtx*) x MRL-*vtx/vtx* to represent this backcross. N2 progeny from this backcross are homozygous for the *Atp6v1b1*^{vtx} mutation and for MRL-derived alleles at linked loci within the congenic region, but are either homozygous for MRL alleles (M/M) or heterozygous for B6 and MRL alleles (B/M) at all other loci throughout the genome. ABR thresholds of the N2 backcross mice showed a broad, non-bimodal frequency distribution (Fig. 2.8B) suggesting that modifier effects on hearing loss are derived from multiple loci rather than a single locus with a large effect.

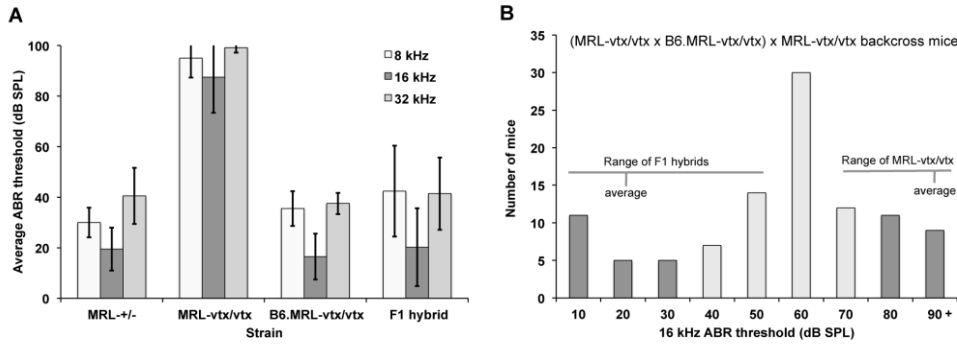


Figure 2.8 ABR thresholds of parental strains, F1 hybrids, and N2 backcross mice

A. Average ABR thresholds of MRL-*Atp6v1b1*+/*vtx* controls (MRL-+/*vtx*, N = 11, test age 5 wks); MRL-*Atp6v1b1**vtx*/*vtx* mutant mice (MRL-*vtx*/*vtx*; N = 6, test age 5 wks); B6.MRL-*Atp6v1b1**vtx*/*vtx* congenic mice (B6.MRL-*vtx*/*vtx*; N = 10, test age 8 wks); and MRL-*Atp6v1b1**vtx*/*vtx* x B6.MRL-*Atp6v1b1**vtx*/*vtx* F1 hybrid mice (N = 33, test age 6 wks). Error bars represent standard deviations of the means. Thresholds were assigned a value of 100 if no ABR was obtained at the maximum test stimulus of 100 db SPL. B. Frequency distribution of 16 kHz ABR thresholds among 102 backcross (N2) mice generated from matings of (MRL-*Atp6v1b1**vtx*/*vtx* x B6.MRL-*Atp6v1b1**vtx*/*vtx*) F1 hybrids with MRL-*Atp6v1b1**vtx*/*vtx* mice. All N2 mice (genotype *Atp6v1b1**vtx*/*vtx*) were tested for ABR thresholds at 4-6 weeks of age. The dark colored bars on the ends of the distribution indicate 40 N2 mice with the most extreme thresholds, which were used for whole-genome linkage analysis to map modifier loci.

We next performed a genome-wide linkage analysis of the N2 mice of the (MRL-*vtx*/*vtx* x B6.MRL-*vtx*/*vtx*) x MRL-*vtx*/*vtx* backcross. Out of a total of 102 N2 mice produced from this backcross (all having the *Atp6v1b1*^{*vtx*/*vtx*} genotype), 20 with the lowest and 20 with the highest thresholds were chosen for the initial linkage analysis. ABR thresholds were analyzed for their linkage with 120 segregating SNP markers strategically located on all chromosomes. ABR thresholds for 8-, 16-, and 32-kHz pure-tone auditory stimuli were evaluated as quantitative traits, and the MapManager QTXb20 program of least-squares linear regression [53] was used to analyze linkage associations of marker genotypes with ABR thresholds. Statistically significant linkage with ABR thresholds was found only for markers on Chr 13, with a maximum LOD score of 5.2 (Fig. 2.9A).

To verify and refine this linkage, we analyzed all 102 N2 mice for six SNP markers spanning Chr 13 using an interval mapping approach (Fig. 2.9B). The most likely candidate region for modifier gene(s) on this chromosome was found to be between *rs3719347* (39.5 Mb position, GRCm38) and *rs3023390* (96.7 Mb), with *rs3654821* (63.1 Mb) having the highest association (LOD 5.4 for 16 kHz thresholds).

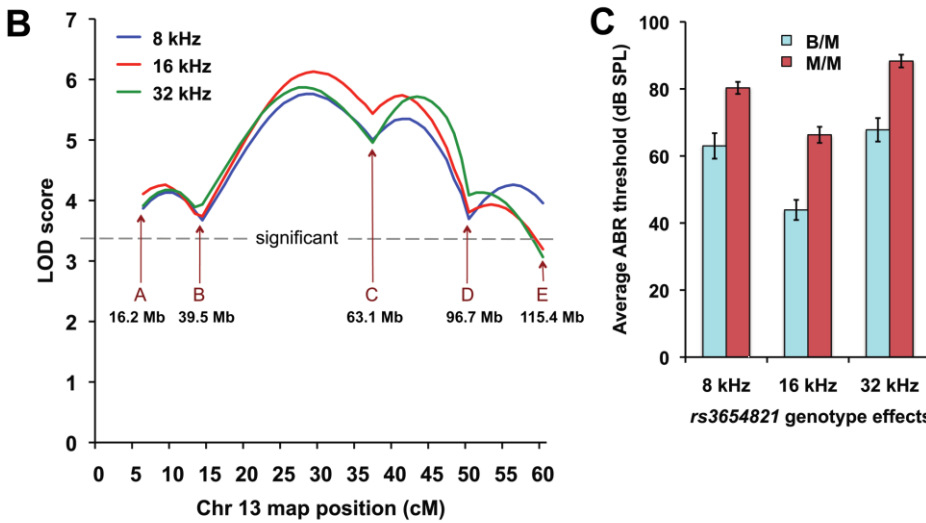
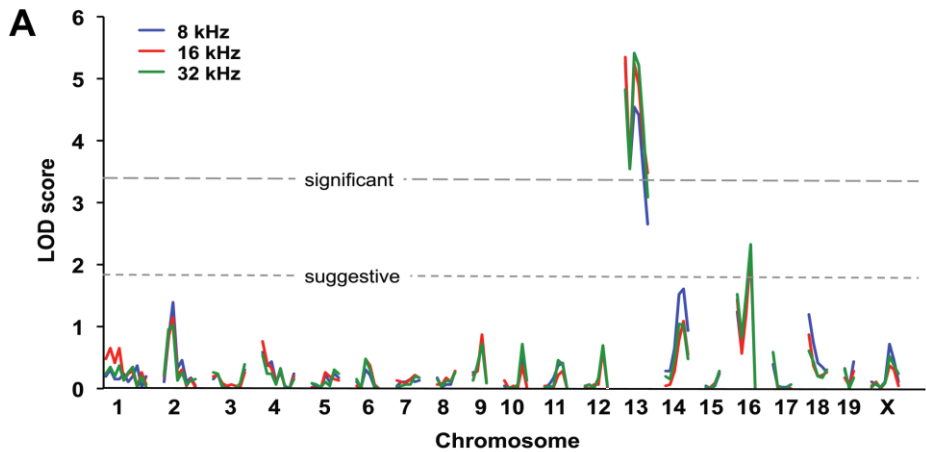


Figure 2.9 Mapping modifier loci that influence ABR thresholds of *Atp6v1b1vtx/vtx* mice

A. Genome-wide linkage associations of chromosomal markers with ABR thresholds. A subset of 40 N2 mice with extreme thresholds - 20 N2 mice with the lowest and 20 with the highest - were selected for the initial genome linkage screen. Different colors are used to indicate 8 kHz, 16 kHz, and 32 kHz threshold associations with marker loci. Horizontal dashed lines mark the minimum LOD score values for suggestive and significant linkage. Only markers on Chr 13 showed a significant association with ABR thresholds. B. Linkage associations of Chr 13 markers with ABR thresholds of all 102 N2 mice. The effects of a hypothetical QTL were analyzed at the position of each marker locus (A-E) and at 1 cM intervals between the marker loci. SNP marker loci and their Mb positions on Chr 13 are as follows: (A) *rs3701757*, 16.2 Mb; (B) *rs3719347*, 39.5 Mb; (C) *rs3654821*, 63.1 Mb; (D) *rs3023390*, 96.7 Mb; (E) *rs3724755*, 115.4 Mb. C. Genotype effects of the Chr 13 SNP marker *rs3654821* on the mean ABR thresholds (± SEM) of the 102 backcross mice. The *rs3654821* SNP was the marker with the highest linkage association, and variation at this locus can explain about 20% of the total ABR threshold variation observed among the 102 N2 mice. B/M, heterozygous for B6 and MRL alleles (N = 50); M/M, homozygous for MRL alleles (N = 52).

Segregation at this locus accounts for about 20% of the total threshold variation in the backcross mice. Interval mapping in 1 cM increments showed that slightly higher associations (max LOD 6.1) could be obtained for hypothetical loci about 8 cM on either side of *rs3654821* (Fig. 2.9B). ABR thresholds of backcross mice homozygous for MRL-derived alleles (genotype M/M) at the *rs3654821* locus were about 20 dB higher than those of mice heterozygous for B6 and MRL alleles (genotype B/M, Fig. 2.9C). Mean thresholds of mice with B/M (N=50) and M/M (N=52) *rs3654821* genotypes were statistically significantly different at all test frequencies (two-tailed Student's t-Test probabilities < 0.00001).

The most likely location for the Chr 13 modifier of hearing loss in the backcross mice is in the 39.5 - 96.7 Mb region (Fig. 2.9B). Within this large 57 Mb region, which contains about 400 protein-coding genes, we selected two candidates for further testing, *Slc9a3* and *Slc12a7*, because they are expressed in the inner ear and are known to be involved in ion homeostasis. Strong expression of the sodium hydrogen exchanger NHE3 (the protein encoded by *Slc9a3*) was demonstrated in the apical membrane of strial marginal cells [54], and H⁺ flux from this exchanger may play a role in controlling acid-base balance in cochlear endolymph [55]. A knockout mutation of *Slc12a7*, which encodes the KCC4 member of the K⁺-Cl⁻ cotransporter family, was shown to cause deafness and renal tubular acidosis; however, the endolymphatic compartments of *Slc12a7*^{-/-} inner ears were not enlarged [56]. We sequenced the 16 exons of *Slc9a3* and the 24 exons of *Slc12a7* along with their flanking splice sites in DNA from MRL mice and compared them to the reference sequence of the B6 strain, but found no differences except for two synonymous SNP variants detected in exons 11 and 13 of *Slc9a3*, which previously have been identified in other inbred strains. The two candidate genes also were examined by quantitative RT-PCR to evaluate and compare their mRNA expression levels in inner ear tissue of MRL and B6 mice at 2 weeks of age. We did not detect any differences in expression levels of these genes between MRL and B6 mice using the comparative delta-Ct method. The calculated fold changes (relative to the mean B6 value) in *Slc12a7* expression were 0.94 (range 0.78-1.13) for MRL and 1.00 (range 0.59-1.68) for B6, and the mean

delta Ct values were not significantly different (P=0.81). The calculated fold changes in *Slc9a3* expression were 1.04 (range 0.77-1.41) for MRL and 1.00, (range 0.82-1.22) for B6, and the mean delta Ct values were not significantly different (P=0.87).

2.4 Discussion

The glycine altered by the *Atp6v1b1*^{vtx} missense mutation is evolutionarily highly conserved, and both the SIFT (<http://sift.jcvi.org/>) and PolyPhen 2 (<http://genetics.bwh.harvard.edu/pph2/>) computer programs predict that the p.G78D substitution is probably damaging to protein function. Patients homozygous for a missense mutation of the corresponding amino acid (p.G78R) in the human ATP6V1B1 protein presented with dRTA and sensorineural hearing loss [57], further verifying the causative nature of the mouse *Atp6v1b1*^{vtx} missense mutation.

Evidence from rat kidney cell culture experiments suggests that point mutations in B1 subunits may cause dysfunction by inhibiting the normal trafficking of vH⁺-ATPase to the apical membrane [58]. If mutant B1 subunits cannot assemble into the native vH⁺-ATPase complex, they might compete for molecules necessary for trafficking of the compensatory B2 subunit to the apical membrane [50]. If so, the *vtx* missense mutation might be more damaging than the knockout mutation, and this may account for the phenotypic differences between *Atp6v1b1*^{-/-} and *Atp6v1b1*^{vtx/vtx} mutant mice. Alternatively, strain background differences may be responsible for their different phenotypes. The *Atp6v1b1*^{-/-} knockout mouse with normal hearing was characterized on a mixed B6/129S1 strain background [48], whereas the *Atp6v1b1*^{vtx/vtx} mutant mouse was initially characterized on an MRL strain background. To directly test the effect of strain background on the phenotype of *Atp6v1b1*^{vtx/vtx} mutant mice, we developed a congenic strain in which the MRL-*Atp6v1b1*^{vtx} mutation was transferred to the B6 background. ABR threshold measurements of the resulting B6.MRL-*Atp6v1b1*^{vtx/vtx} congenic strain mice demonstrated that they have normal hearing like B6(129S1)-*Atp6v1b1*^{-/-} knockout mice. We conclude from these results

that strain background differences are responsible for the different auditory phenotypes of MRL-*Atp6v1b1*^{vtx/vtx} mice and B6(129S1)-*Atp6v1b1*^{-/-} knockout mice.

The inner ear phenotype of MRL-*Atp6v1b1*^{vtx/vtx} mice (Figs. 3-5) is very similar to the inner ear phenotypes of *Atp6v0a4*^{-/-} [46], *Foxi1*^{-/-} [59], and *Slc26a4*^{-/-} [60] mice; all exhibit increased endolymph volume, loss of endocochlear potential, hearing impairment, deficient and abnormal otoconia, and vestibular dysfunction. *Foxi1* is a forkhead transcription factor that regulates expression of *Slc26a4* [59] and the *Atp6v1b1* and *Atp6v0a4* genes encoding vH⁺-ATPase subunits in the endolymphatic sac (ES) epithelia [61]. Mutations of these genes impede fluid absorption in the ES causing endolymph build up and dilatation of the membranous labyrinth [62, 63]; however, the molecular mechanisms underlying these effects are not fully understood. According to one proposed mechanism [62], mutations of these genes reduce the ES epithelium-generated H⁺ current that normally forces Na⁺ transport and fluid movement out of the ES lumen. The hearing loss, vestibular dysfunction, and other inner ear abnormalities of these mutant mice are thought to be consequences of this disrupted fluid homeostasis in the ES during embryonic development [63].

Paintfills of the membranous labyrinths of P1 inner ears of MRL-*Atp6v1b1*^{vtx/vtx} mice (Fig. 2.3B) and P0 inner ears of *Atp6v0a4*^{-/-} mice [46] show a similar morphology with greatly expanded endolymphatic sac and cochlear duct. While cochlear cross sections of P0 *Atp6v0a4*^{-/-} mice show expansion of scala media, reduced scala vestibuli, and distended Reissner's membrane consistent with increased endolymph volume, cochlear cross sections of adult (2.5-4.5 month-old) MRL-*Atp6v1b1*^{vtx/vtx} mice (Fig. 2.4) do not show these features, although they do show an overall increase in the dimensions of the cochlear capsule. We interpret these differences as a reflection of enlarged capsule formation during the period when the membranous labyrinth is in an expanded state (Fig. 2.3B), followed by a subsequent reduction in endolymph volume at older ages (after loss of stria vascularis function), resulting in reduced size of the scala media and non-distended Reissner's membrane (Fig. 2.4).

Although MRL-*Atp6v1b1*^{vtx/vtx} mice have malformed and dysfunctional inner ears, kidney dysfunction is minimal (Fig. 2.7; Table 2.1). The mild renal phenotype (compensated acidosis) of MRL-*Atp6v1b1*^{vtx/vtx} and B6.MRL-*Atp6v1b1*^{vtx/vtx} mice is similar to that reported for B6-*Atp6v1b1*^{-/-} mice [48]. A compensatory membrane expression of the B2 subunit of the vH⁺-ATPase complex was proposed to explain why B6-*Atp6v1b1*^{-/-} mice are healthy and do not exhibit the overt metabolic acidosis characteristic of dRTA patients with *ATP6V1B1* mutations [48], and this explanation may also apply to MRL-*Atp6v1b1*^{vtx/vtx} and B6.MRL-*Atp6v1b1*^{vtx/vtx} mice. In contrast, the severe metabolic acidosis reported for *Atp6v0a4*^{-/-} mice [46] may be a consequence of the inability of other vH⁺-ATPase subunits to compensate for the a4 subunit deficiency.

Although similar, the urine pH measurements for both the *Atp6v1b1*^{vtx/vtx} and wildtype mice were lower compared to the previously described values by Finberg *et al* (8). It is important to point out that the standard of care at The Jackson Laboratory is to provide mice with acidified (pH 2.5-3.0) water, and mice are therefore under an acid load, which might explain the urine pH difference. As previously reported for *Atp6v1b1* [48] and *Atp6v0a4* [47] knockout mice, *Atp6v1b1*^{vtx/vtx} mice on both the B6 and MRL genetic backgrounds are hypocalciuric, which is opposite to the hypercalciuria reported for human patients with mutations in these genes [64].

There was no significant difference in urine pH between *Atp6v1b1*^{vtx/vtx} and wildtype mice on the MRL background, but compared to all other strains we measured, MRL wildtype mice have a higher urine pH that is comparable to that of *Atp6v1b1*^{vtx/vtx} mutant mice on either the B6 or MRL background. A possible explanation is that the MRL strain has a mutation in a gene involved in the regulation of urine pH and that this is epistatic to the *Atp6v1b1*^{vtx} mutation. If this is indeed the case, then the much larger effect of the *Atp6v1b1*^{vtx} mutation on calcium excretion in the MRL background (70% decrease) compared to the B6 background (20% decrease) suggests a synergistic interaction of the mutations on this phenotype.

Levels of K^+ and Cl^- in the blood did not differ between *Atp6v1b1*^{vtx/vtx} and wildtype mice on either the MRL or B6 strain background (Table 2.1), which agrees with the findings for the *Atp6v1b1*^{-/-} knockout mouse with compensated acidosis [48]. In contrast, the *Atp6v0a4*^{-/-} mouse with severe metabolic acidosis has significantly lower concentrations of K^+ and Cl^- in the blood than controls [47]. Although the mild renal phenotype of MRL-*Atp6v1b1*^{vtx/vtx} mice is similar to that of *Atp6v1b1*^{-/-} mice, its severe inner ear phenotype is similar to that of *Atp6v0a4*^{-/-} mice. The difference in severity between the inner ear and kidney phenotypes of MRL-*Atp6v1b1*^{vtx/vtx} mice may be due to modifying genetic factors that have stronger effects on H^+ transport and ion homeostasis in the inner ear than in the kidney tubule. Not all cases of dRTA caused by *ATP6V1B1* mutations have associated hearing loss [44], which lends support to the idea that inner ear and kidney-related pathologies are not always coupled.

In an attempt to identify genetic factors that contribute to the different inner ear phenotypes of MRL-*Atp6v1b1*^{vtx/vtx} and B6.MRL-*Atp6v1b1*^{vtx/vtx} mice, we analyzed ABR threshold associations in a linkage backcross involving these two strains. Thresholds of *Atp6v1b1*^{vtx/vtx} progeny from the backcross showed a broad frequency distribution with mostly intermediate values rather than a bimodal distribution with two discrete groupings of more extreme values (Fig. 2.8B), indicating contributions from multiple genes. A genome-wide linkage screen detected statistically significant associations only with Chr 13 markers (Fig. 2.9A), but even the highest association at this locus could account for only about 20% of the total ABR threshold variation in the backcross mice. Together, these results suggest a complex genetic basis for the difference in MRL and B6 strain background effects on hearing thresholds of *Atp6v1b1*^{vtx/vtx} mice, with multiple contributing genes each having relatively small effects.

We examined two interesting candidate modifier genes with known roles in inner ear fluid homeostasis (*Slc9a3* and *Slc12a7*) that lie within the candidate region of Chr 13 (39.5 – 96.7 Mb; Fig. 2.9B), but did not find any differences in the DNA sequences of their exons or in their mRNA expression levels in P14 inner ear tissue. Our results, however, do not rule out the possibility that non-coding

sequence differences in these genes might cause subtle expression differences during inner ear development that we did not detect in two-week-old mice. Of course, one or more of the many other genes in the candidate region could also be responsible for the Chr 13 modifier effect. Urine pH and calcium excretion were not measured in the linkage backcross mice although they showed significant differences between strains and genotypes (Fig. 2.7), and it is possible these differences may co-vary with ABR thresholds. If so, then genes located in the Chr 13 candidate region that are not known to affect inner ear function but are known to play a role in kidney function, such as *Slc34a1*, may also be considered as candidate modifiers of the *Atp6v1b1* phenotype.

Our results clearly establish that genetic background differences can have a profound effect on the auditory phenotypes associated with *Atp6v1b1* mutations in mice and suggest that similar genetic background effects could contribute to the phenotypic variability associated with human *ATP6V1B1* mutations. Human cases of dRTA are reported to have variable degrees of inner ear abnormalities [65] and hearing loss [44]. Determining the genetic causes underlying the phenotypic differences among mouse *Atp6v1b1* mutations on different strain backgrounds may shed light on the underlying causes of this clinical heterogeneity.

2.5 Summary

Enlargement of the vestibular aqueduct (EVA, OMIM 600791), the bony canal that encloses the endolymphatic duct, is a common inner ear malformation diagnosed in children with hearing loss (<https://www.nidcd.nih.gov/health/enlarged-vestibular-aqueducts-and-childhood-hearing-loss>). High resolution computed tomography studies have detected bilaterally enlarged vestibular aqueducts in patients with autosomal recessive dRTA and deafness [65, 66]. The combination of EVA and hearing loss is also characteristic of several other syndromes, including Pendred, branchio-oto-renal, CHARGE, and Waardenburg syndromes [67]. Pendred syndrome, caused by mutations of *SLC26A4*, does not always present with thyroid goiter, and these cases constitute the major known underlying cause of

nonsyndromic EVA and hearing loss. Because 50% of European or North American Caucasian individuals with EVA-associated hearing loss have no obvious *SLC26A4* mutations [68], mutations of other as yet unidentified genes are thought to be responsible for some of the remaining unknown cases. Variants of *KCNJ10* and *FOXI1* have been proposed to underlie some of these cases [69, 70], but contradictory results have been reported in other studies [71-73]. MRL-*Atp6v1b1*^{vtx/vtx} mutant mice are deaf with enlarged endolymphatic compartments of the inner ear but do not recapitulate the overt metabolic acidosis characteristic of dRTA. They thus provide a new genetic model for nonsyndromic deafness with EVA and suggest that mutations in the human *ATP6V1B1* gene might account for some of the unknown genetic cases of this disorder that are not associated with *SLC26A4* mutations.

CHAPTER 3 TBX1 IS REQUIRED FOR SEMICIRCULAR CANAL FORMATION AND STRIA VASCULARIS

MATURATION

3.1 Introduction

The mammalian inner ear derives from the otic placode, an ectodermal thickening adjacent to the hindbrain, formed around embryonic day (E) 8.0. The placode invaginates and forms the otic vesicle (otocyst) around E9.5. Starting from E10.5, morphogenesis of the vesicle initiates with endolymphatic sac and duct formation from an outgrowth in the dorsal part of the vesicle and cochlear formation from an outgrowth in the ventral direction. Vestibular organ formation starts around E11.5, with dorsolateral evagination of the otic epithelium to form the ventral canal plate, the precursor of the anterior and posterior semicircular canals. Slightly later, the otic epithelium evaginates laterally to form the lateral canal plate, the precursor of the lateral semicircular canal. The canals are formed at E12.5 by fusion of cells in the vertical plate and the lateral canal plate, followed at E13.5 by resorption of the fused cells into the epithelium. During this period, additional evaginations of the central region form the utricle and saccule. By E14.5, the inner ear epithelium has acquired its mature morphology[74]. Fully developed vestibular organs consist of three semicircular canals, saccule, and utricle, which are important for maintaining body balance and sense angular and linear movement. Sensory hair cells in the cristae ampullaris of the semicircular canals and maculae of the saccule and utricle detect liquid movement within the vestibular portion of the inner ear. Cochlea development occurs slightly later than vestibular organ development. Cochlea formation starts from a ventral outgrowth of otic epithelium around E10.5. The cochlear duct continues to grow and reaches full length around E18. Tissues and cells within the cochlea undergo differentiation and proliferation during this time period and give rise to structures such as the organ of Corti, stria vascularis, and spiral ligament. Some tissues continue to develop postnatally. For example, hair cell bundles continue to refine their shape and reach the adult-like morphology around P15 [75], and interdigitation of intermediate and marginal cells of the stria vascularis fully

mature at around P6 [76]. The cochlea within the adult mammalian inner ear is the organ responsible for sound perception. Transmission of acoustic waves from middle ear to the cochlea through the oval window lead to vibrations of the basilar membrane, and subsequent hair cell depolarization converts this mechanical force to a neural impulse that is transmitted to the brain through the acoustic nerve.

Endolymph, the liquid within the membranous labyrinth of the inner ear, is critical for normal hair cell function. Endolymph is unique in that it contains a very high concentration of K^+ and a low concentration of Na^+ , which creates a positive potential of 80-100 mV in the scala media called the endocochlear potential (EP). Endocochlear potential provides the major driving force for K^+ influx, which contributes to the high sensitivity of hair cells to mechanical stimulation. Hair cells, supporting cells beneath the hair cells, other epithelial cells on the basilar membrane, and cells of the stria vascularis and spiral ligament work together to mediate cochlear K^+ circulation. The stria vascularis is essential for generating the EP. Genes encoding ion channel and transporter proteins, including *KCNJ10*, *NKCC1*, *CIC-K/barttin*, and *KCNQ1/KCNE1*, are expressed in the stria vascularis and mutations in these genes lead to reduced or absent EP and hearing impairment in the animal models [77-85].

Three layers of cells are found in the stria vascularis (SV). Lining the scala media are the marginal cells derived from the otic epithelium; the intermediate cells are specialized melanocyte-like cells derived from migratory neural crest cells; and the basal cells are adjacent to the fibrocytes of the spiral ligament and are derived from otic mesenchyme. Endodermally derived blood vessels are interspersed between these cell layers throughout the SV. The SV continues to develop after birth and reaches maturation around P6. This process is majorly completely by interdigitation of marginal cells with intermediate cells [76]. The vestibular labyrinth also contains endolymph, although its potential relative to body fluid is ~ 0 mV compared with the 80-100mV EP of the scala media in the cochlea. Ion concentrations in the vestibular endolymph are thought to be maintained by “dark cells” in the epithelia of semicircular canal ampullae. Dark cells harbor $Na^+-K^+-ATPase$, *NKCC1*, and *CIC-K/barttin* at their

infolded basolateral membrane and express KCNQ1/KCNE1 at the apical membrane. *Kcne1*, *Kcnq1*, and *Slc12a2* knockout mice exhibit a collapse of vestibular endolymphatic space and balance defects in addition to cochlear dysfunctions [78-80, 83, 86, 87].

Tbx1 belongs to the t-box protein family. T-box proteins are transcription factors that play important roles in tissue and organ formation during embryonic development. *TBX1* haploinsufficiency is associated with human DiGeorge syndrome (DGS = Del22q11.2), which is characterized by cardiovascular malformations, hypoplasia or aplasia of the thymus and parathyroid gland, craniofacial defects, and hearing impairment. Previous studies have shown that *Tbx1* is required for cardiac outflow tract morphogenesis [88, 89], pharyngeal apparatus morphogenesis [90, 91], skeletal development [92, 93], cerebral cortex development [94, 95], and inner ear morphogenesis [96]. *Tbx1* null mice are embryonic lethal, and inner ear development is stopped at the otocyst stage around E10 [96]. Although *Tbx1* conditional knockout mice are viable, inner ear development in these mice is also arrested at the otocyst stage [97]. Additional studies showed that *Tbx1* contributes to inner ear morphogenesis possibly through its regulation of cell fate determination [98, 99], cell proliferation [99] and survival [100], neural crest migration, and spatial pattern stabilization [101]. Interestingly, a reporter gene study showed that *Tbx1* is expressed in the stria vascularis and vestibular dark cells at E18.5 [100], suggesting that *Tbx1* has specific functions in these tissue types. However, because the inner ear does not develop beyond the otocyst stage in the null and conditional knockout mice, a new *Tbx1* model is required to study *Tbx1* function in the stria vascularis and vestibular organs at later development stages.

In this study, we report on a recessive ENU-induced mutation named windmill (*wdm1*) because of the circling behavior of homozygous mutant mice. We show that mutant mice are deaf and that *wdm1* is a missense mutation of *Tbx1*. In contrast to previously reported *Tbx1* knockout mouse models, *Tbx1^{wdm1}* mutant mice are viable with fully formed but abnormal inner ears. They thus provide the first model to study the roles of *Tbx1* in inner ear development beyond the early otocyst stage. We show that

the deafness and vestibular dysfunction in *Tbx1^{wdml}* mutant mice is due to stria vascularis and semicircular canal defects, demonstrating the importance of TBX1 function in the development of these inner ear structures.

3.2 Methods and Materials

3.2.1 Mice

Experimental mice were bred and housed in the Research Animal Facility of the Jackson Laboratory in Bar Harbor, Maine. Mice were fed *ad libitum* with a 6% fat mouse diet. Water bottles were changed weekly and filled with acidified (pH 2.5-3.0) water. The light cycle was 12 hours light and 12 hours dark. All procedures involving the use of experimental mice were approved by the Institutional Animal Care and Use Committees at The Jackson Laboratory. All methods used in the study were performed in accordance with the guidelines and regulations of the U.S. National Institutes of Health (NIH) Office of Laboratory Animal Welfare (OLAW) and the Public Health Service (PHS) Policy on the Humane Care and Use of Laboratory Animals.

The windmill (*wdml*) mutation is an ENU induced mutation generated by the Neuroscience Mutagenesis Facility at The Jackson Laboratory (JAX) and originally designated nmf219 (Stock #4831). The mutant strain is designated C57BL/6J-*Tbx1^{wdml}*/KjNj, here abbreviated B6-*Tbx1^{wdml}*. Mutant mice (*wdml/wdml*) can be identified without genotyping by their overt circling and head tilting behaviors, and the colony is maintained by mating *+/wdml* (female) x *wdml/wdml* (male) mice.

3.2.2 Genetic mapping of the *wdml* mutation

The *nmf219* (*wdml*) mutation was originally mapped to the 15913052-32312179 bp position of Chr 6 (GRCm38) by the JAX Neuroscience Mutagenesis Facility. To refine this map position, B6-*wdml/wdml* mice were crossed to CAST mice, and F1s were intercrossed to produce F2 progeny for linkage cross analysis. Individual DNA samples from linkage cross mice were typed for multiple MIT microsatellite markers located on Chr 16. Previously described PCR methods (Johnson et al. 2012) were

used to genotype the chromosomal markers, which were then analyzed for co-segregation with the mutant phenotype. PCR primer pairs designed to amplify specific markers were purchased from Integrated DNA Technologies (Coralville, IA, USA).

3.2.3 Whole-exome sequencing

DNA purification, library construction, deep sequencing, and data quality control were performed by the Jackson Laboratory's Next Generation Sequencing service, and data analysis and annotation were performed by the Computational Sciences Biostatistics service. Purified genomic DNA from *wdm1/wdm1* mice and C57BL/6J controls were used to create libraries for whole-exome sequence capture.

3.2.4 DNA sequence confirmation and genotyping of the *wdm1* mutation

PCR for comparative DNA analysis between *wdm1* mutant and control mice was performed according to the same conditions as described above for genetic mapping. PCR primers used to genotype the *wdm1* mutation of the *Tbx1* gene were 5'-CGATGTTGCCCTAGGTATGC-3' (forward) and 5'-GGCCTACAACAGGAGACAGC-3' (reverse). PCR products digested with TaqI restriction enzyme (140 bp and 92 bp for the wild-type allele and 232 bp for the *wdm1* allele) were separated on a 3.5 % agarose gel. For DNA sequence confirmation of genotypes, PCR products were purified with the QIAquick PCR Purification Kit (Qiagen Inc., Valencia, CA), and sequencing was performed using the same primers as for DNA amplification, then run on an applied biosystems 3700 DNA Sequencer with an optimized Big Dye Terminator Cycle Sequencing method.

3.2.5 Auditory brainstem response

ABR thresholds were measured at 8, 16 and 32 kHz in a sound attenuating chamber using the SmartEP auditory evoked potential diagnostic system from Intelligent Hearing Systems (IHS, Miami, FL) as described previously [52]. Briefly, mice were anesthetized with tribromoethanol (0.2 ml of 20 mg/ml stock per 10 g of body weight, i.p.) and placed on a temperature controlled heating pad to maintain

body temperature at 37°C. Three subdermal electrodes, placed at the vertex and behind each ear, were used to record brain stem responses to defined tone-bursts (3 ms duration, 1.5 ms cosine-gated rise/fall time). The responses were then amplified, filtered (100-3000 Hz) and averaged (25 kHz sampling rate, 10 ms analysis window). Stimulus intensity was initially decreased in 10 dB steps until the response began to disappear and then lowered in 5 dB steps; ABR threshold was defined as the lowest intensity at which an ABR response could be reliably obtained. With our testing system, average ABR thresholds for normal hearing mice are about 40, 20, and 45 dB SPL for 8, 16 and 32 kHz stimuli, respectively.

3.2.6 Histology

Histological analyses of the middle and inner ears were performed following the methods described previously[20]. Briefly, inner ears from *Tbx1^{wdm/wdm}* mice and wild-type mice were dissected and immersed in Bouin's fixative and embedded in paraffin. Sections (7 μm) were cut and mounted onto Fisher Superfrost Plus slides (Fisher Scientific, Pittsburgh, PA) and counterstained in hematoxylin/eosin (H&E).

3.2.7 Immunofluorescence staining

Postnatal mouse inner ears were dissected and fixed in 4% formaldehyde/PBS overnight. Tissues were then washed with PBS 3x 5min, rinsed with 10%, 20%, and 30% glucose/PBS solution, frozen in Tissue-TekVR O.C.T. compound (Sakura Finetek USA Inc, Torrance, CA, USA) and sectioned at 10 μm. Sections were fixed in 4% formaldehyde/PBS for 10 min and permeabilized in 0.2% Triton X-100/PBS for 5 min. Inner ear sections were subsequently blocked in 3% goat or donkey serum plus 2% BSA in PBS for 1h, incubated with primary antibodies in the blocking solution at specific dilution ratio at 4°C overnight, washed several times with PBS and incubated with secondary antibody in blocking solution for 1h. After extensive washes with PBS, the stained inner ear sections were mounted on glass slides using Shandon™ Immu-Mount™ aqueous non-fluorescing mounting medium (Thermo Electron Corporation, Pittsburgh, PA, USA) and imaged using an Olympus FV1000 confocal laser scanning

microscope. Primary antibodies used were: KCNQ1 (Santa cruz, cat#: sc-10646, 1:200), KCNJ10 (Alomone labs, cat#: apc-035, 1:400), GLUT1 (Santa cruz, cat#: sc-1605, 1:100), secondary antibodies used were donkey anti goat cy3 (Abcam, cat#: ab6949, 1:500) and goat anti rabbit Alexa 488 (Invitrogen, cat#: A11008, 1:500).

3.2.8 Inner ear paint fills

E14.5 embryos (B6-Tbx1^{wdml/+}, n= 5; B6-Tbx1^{wdml/wdml}, n=6) were used for inner ear paint fills. E14.5 embryos were decapitated and whole heads were fixed in Bodian's fixative. Heads were fixed overnight and then dehydrated with 75% ethanol (2x 2 hours), 95% ethanol (2x 2 hours), and 100% ethanol (2x 2 hours). Heads were then rinsed once with methyl salicylate and cleared overnight by placing specimens in methyl salicylate. A micromanipulator was used to fill inner ears were filled with 1% Wite-Out correction fluid in methyl salicylate using a Hamilton syringe, with a pulled glass capillary needle broken to a tip diameter of 20-40 μm . Inner ears were injected through the middle turn of the cochlea.

3.2.9 RNA-seq

Five E16.5 mutant mice and 5 littermate controls were used for the analysis. For each sample, RNA was isolated from 2 inner ears using the MagMAX mirVana Total RNA Isolation Kit (ThermoFisher) and the KingFisher Flex purification system (ThermoFisher). Tissues were lysed and homogenized in TRIzol Reagent (ThermoFisher). After the addition of chloroform, the RNA-containing aqueous layer was removed for RNA isolation according to the manufacturer's protocol, beginning with the RNA bead binding step. RNA concentration and quality were assessed using the Nanodrop 2000 spectrophotometer (Thermo Scientific) and the RNA Total RNA Nano assay (Agilent Technologies). Libraries were prepared by the Genome Technologies core facility at The Jackson Laboratory using the KAPA mRNA HyperPrep Kit (KAPA Biosystems), according to the manufacturer's instructions. Briefly, the protocol entails isolation of polyA containing mRNA using oligo-dT magnetic beads, RNA fragmentation,

first and second strand cDNA synthesis, ligation of Illumina-specific adapters containing a unique barcode sequence for each library, and PCR amplification. Libraries were checked for quality and concentration using the DNA 1000 assay (Agilent Technologies) and quantitative PCR (KAPA Biosystems), according to the manufacturers' instructions. Libraries were pooled and sequenced by the Genome Technologies core facility at The Jackson Laboratory, 75 bp single-end on the NextSeq 500 (Illumina) using NextSeq High Output Kit v2 reagents (Illumina).

3.2.10 DIG-labeled riboprobes and mRNA *in situ* hybridization

DNA sequences of primers for amplifying *Raldh2*, *Esrrb*, *Dct* are listed in Table 3.1. The sequence for the SP6 promoter was added as a 5' overhang to the reverse primer so that the antisense probe could be generated directly from the PCR product. A digoxigenin-11-UTP (DIG) labeled antisense riboprobe was produced from the purified PCR product by *in vitro* transcription according to the manufacturer's instructions (Roche Applied Science, Indianapolis, IN).

Table 3.1 Primer sequence for *in situ* hybridization probes

<u>Gene</u>	<u>Primer Sequence</u>	<u>Reference</u>
<u><i>Raldh2</i></u>	TAACAATGAATGGCAGAACTCAG	<u>[102]</u>
	GCGATTTAGGTGACACTATAGGCAATTTCCAGGTGAACATC	
<u><i>Esrrb</i></u>	TTTGCTGCTGTTTCTCCTT	<u>www.eurexpress.org</u>
	GCGATTTAGGTGACACTATAGTGTGTTGTCCAACCTTGCT	
<u><i>Dct</i></u>	AATTCTTCAACCGGACATGC	<u>Self-designed</u>
	GCGATTTAGGTGACACTATAGGCATCTGTGGAAGGGTTGTT	

In situ hybridization was performed as described with the following modifications. Tissue was fixed overnight at 4°C in 4% paraformaldehyde. Sections were mounted on Superfrost plus slides (Fisher Scientific, Suwanee, GA). Slides were air dried at room temperature for 1–2 hours, followed by fixation in 4% paraformaldehyde for 10 minutes. Digestion was carried out for 10 min at room temperature in buffer consisting of 50 mM Tris, pH 7.5, 5 mM EDTA, and 1 µg/ml proteinase K followed by fixation in 4%

paraformaldehyde for 5 min. Hybridization was performed at 65° C overnight in buffer consisting of 50% deionized formamide, 0.3 M NaCl, 20 mM Tris, pH 8.0, 5 mM EDTA, pH 8.0, 10% dextran sulfate, 1× Denhardt's solution, 0.5 mg/ml tRNA from baker's yeast (Sigma, St. Louis, MO), and 500 ng/ml of the denatured DIG labeled probe. Washes were also carried out at 65° C. Following immunological detection, slides were mounted with VECTASHIELD mounting medium (Vector Laboratories, Burlingame, CA).

3.3 Results

In contrast to previously reported *Tbx1* knockout and conditional knockout mice, mice homozygous for the *Tbx1*^{wdml} mutation are healthy and fertile with normal growth. Outer, middle, and inner ears of *Tbx1*^{wdml} mutant mice have normal gross morphology at weaning age, but they exhibit vestibular dysfunction as evidenced by variable head tilting and circling behaviors, and all mutant mice showed profound hearing loss at weaning age (Figure 3.1).

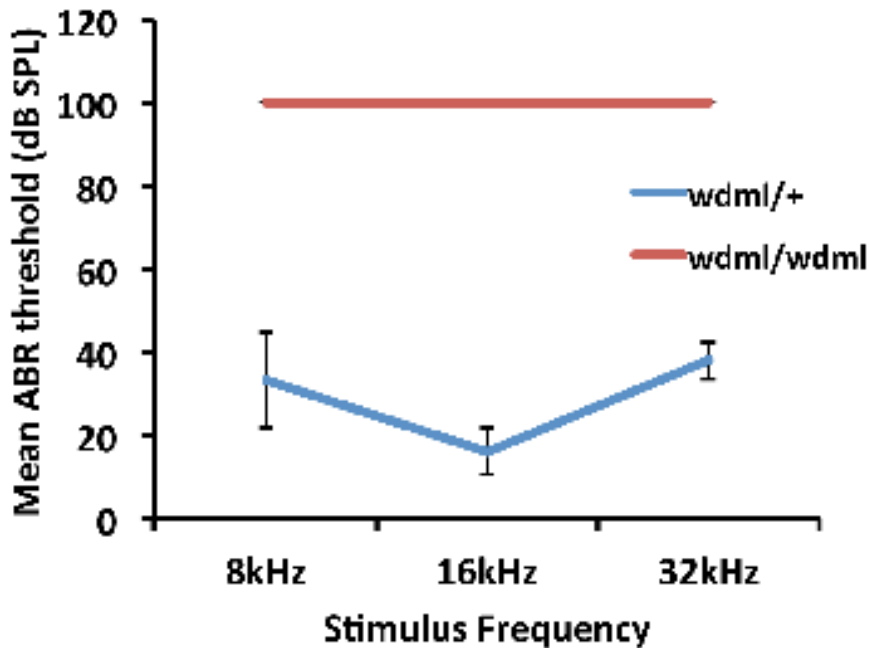


Figure 3.1 Hearing loss in B6-*wdml/wdm1* mutant mice

Average ABR thresholds of seven B6-*wdml/wdm1* mutant mice and five B6-*wdml/+* control mice for 8, 16, and 32 kHz pure tone stimulus frequencies. All mice were tested between 4 and 6 weeks of age. Error bars represent standard deviations. Thresholds were assigned a value of 100 if no ABR was obtained at the maximum test stimulus of 100 dB SPL.

3.3.1 Genetic mapping of the *wdml* mutation

To refine the map position of the *wdml* mutation on Chr 16, an intercross of (B6-*wdml/wdml* x CAST/EiJ) F1 hybrids was used to generate a total of 263 mutant (*wdml/wdml*) F2 progeny. Presumed genotypes of the F2 mice were assigned according to their vestibular phenotype (head tilting/circling). The F2 mice were then genotyped for Chr 16 MIT microsatellite markers that differed in size between B6 and CAST, and haplotype analysis narrowed the candidate gene interval to a 2.7 MB region of Chr 16 (*D16Mit143*, 18.1 Mb, and *D16Mit145*, 20.8Mb) containing 54 protein-coding genes. Using high-throughput, next generation exome sequencing, 15 putative sequence differences in exons were identified between B6-*wdml/wdml* and B6 +/+ control DNA in the 2.7 Mb candidate gene interval. Only three of these putative variants had mismatch ratios greater than 0.6, and of these only the *Tbx1* variant was predicted to have a negative effect on protein function. The mutation discovered in the *Tbx1* gene is a single base pair change in exon 3 (c.665A>G) that change the codon for aspartic acid (GAC) to a codon for glycine (GGC) at amino acid position 212 (p.D212G) of the mouse protein (Figure 3.2).

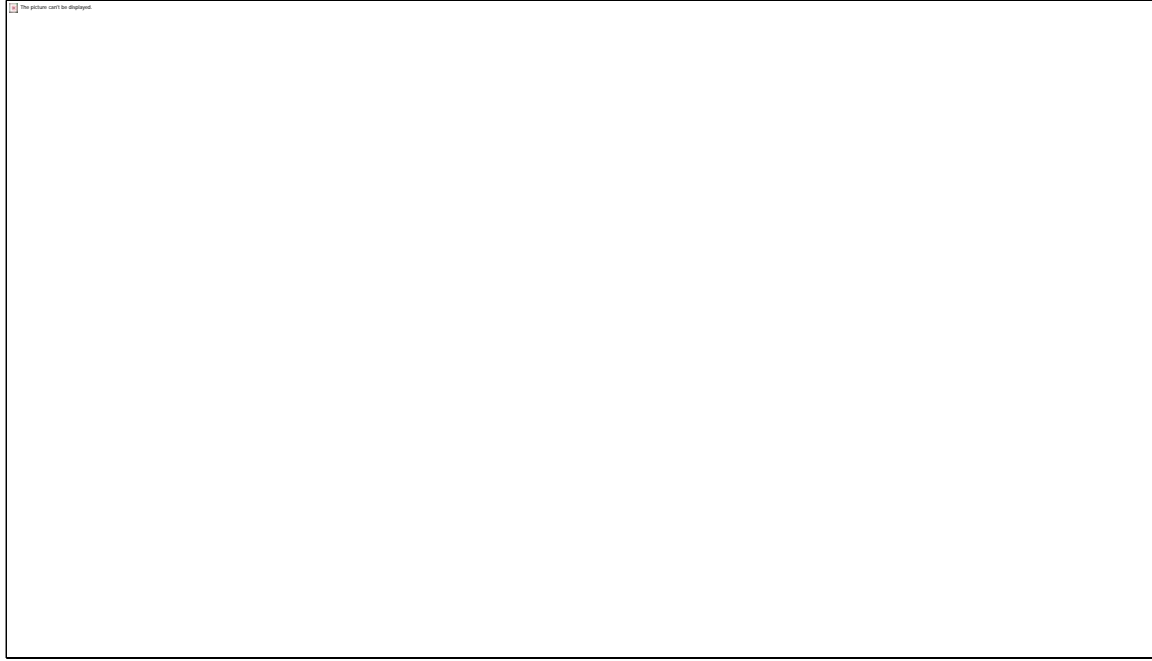


Figure 3.2 Molecular characterization and consequences of the *Tbx1*^{w^{dml}} mutation

A. DNA sequence chromatograms illustrating the A>G nucleotide change (indicated by red arrow) caused by the *w^{dml}* mutation. B. DNA sequence of *Tbx1* exon 3 with encoded amino acids shown below in blue font. The A nucleotide that is altered in the *w^{dml}* mutation (shown in red) is part of the GAC codon (boldface, boxed) for aspartic acid, and also part of a *TaqI* restriction enzyme digestion site (TCGA, highlighted in green). The A>G nucleotide substitution at coding DNA position 635 (c.635A>G) causes an aspartic acid to glycine amino acid change at position 212 of the TBX1 protein (p.Asp212Gly). C. Schematic diagram of the TBX1 protein showing the regions encoded by exons 1-7 in alternating purple and orange and locations of the T-box DNA binding domain relative to the amino acid numbers shown below. The *w^{dml}* mutation is in exon 3, which encodes part of the T-box DNA binding domain of the protein

3.3.2 Inner ear morphology

Cross-sections of paraffin-embedded postnatal cochleae were created to observe cochlear structure in the *Tbx1* mutant ear and age-matched controls. At P3, mutant *Tbx1*^{w^{dml}/w^{dml}} cochleae have normal-looking endolymph and perilymph compartments; organ of Corti, stria vascularis, and spiral ligament appear to be at the right development stage with normal morphology and Reissner's membrane appears at the right location (Figure 3.3). By P7, mutant mice showed collapsed Reissner's membrane, reduced endolymph volume, and undeveloped stria vascularis. At 5 months of age, mutant mice showed a completely collapsed Reissner's membrane, extremely reduced endolymph volume, and

a still undeveloped stria vascularis, as well as severe organ of Corti degeneration, which is likely a secondary effect of stria vascularis dysfunction.

Paintfills of the membranous labyrinths of inner ears from B6-*Tbx1*^{wdml/wdml} mutants and controls were examined in day 14.5 embryos (E14.5). The cochlea of E14.5 mutant mice has an overall normal gross morphology; however, there is an obvious malformation of the vestibular apparatus, especially the posterior semicircular canal (Figure 3.4). Mutant mice have normal saccule, utricle, and anterior and lateral semicircular canals. The posterior semicircular canal and common crus of mutant mice, however, are fused into one plate, indicating failure of fusion plate resorption. In addition, the anterior and lateral ampullae are not fully separated in the mutant inner ear.

Figure 3.3 Cross-sections of cochleae from *Tbx1*^{wdml/wdml} and *Tbx1*^{wdml/+} mice

A,B. Whole cochlear profiles from P3 *Tbx1*^{wdml/+} (A) and *Tbx1*^{wdml/wdml} mice (B) imaged at the same magnification. *Tbx1*^{wdml/wdml} mutants appear normal compared to the age-matched *Tbx1*^{wdml/+} control mice. **C,D.** Whole cochlear profiles from P7 *Tbx1*^{wdml/+} (C) and *Tbx1*^{wdml/wdml} mice (D) imaged at the same magnification. *Tbx1*^{wdml/wdml} mutants show collapsed Reissner's membrane (yellow arrowhead), reduced endolymph volume (green asterisk) and smaller stria vascularis region (red arrow). **E,F.** Enlarged views of organ of Corti in *Tbx1*^{wdml/wdml} mutants at 5 months old show reduced endolymph volume (red asterisk), collapsed Reissner's membrane (black arrow), and no stria vascularis (white arrow) in comparison to the controls.

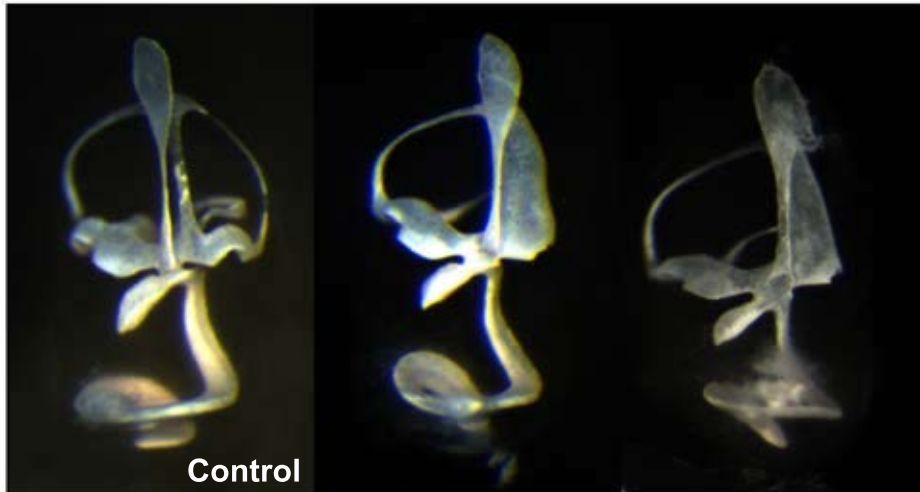


Figure 3.4 Paint fills of inner ears from *Tbx1*^{wdml/wdml} mutant and control mice

Paint fills of the membranous labyrinths of inner ears from an E14.5-stage *Tbx1*^{wdml/+} (control) embryo and two littermate *Tbx1*^{wdml/wdml} (mutant) embryos. The endolymphatic sac (es), endolymphatic duct (ed), utricle (u), saccule (s), and cochlear duct (cd) in the two mutant inner ears appear to be normal compared with the control. Posterior semicircular canal (psc) is fused with common crus as show by the white arrow in two of the mutant ears.

3.3.3 TBX1 expression in postnatal mouse inner ear

Tbx1 expression previously has been studied in embryos; however, there is no report of *Tbx1* expression during early postnatal stages. We used TBX1 antibody to detect and localize TBX1 expression in the inner ear of *Tbx1*^{wdml} mutant mice and littermate controls at P3 and P15 (Figure 3.5). TBX1 expression is observed in marginal cells of the stria vascularis in the cochlea and in the dark cells of the crista ampullaris in the vestibular system of mutant and control inner ears at P3; however, this expression disappears by P15. TBX1 expression also was observed in hair cells and supporting cells of the crista ampullaris of mutant and control mice at both P3 and P15. TBX1 immunostaining intensity and localization in *Tbx1*^{wdml} mutant mice was the same as that seen in the control mice, indicating that the p.D212G missense mutation does not affect the stability or localization of the TBX1 protein.

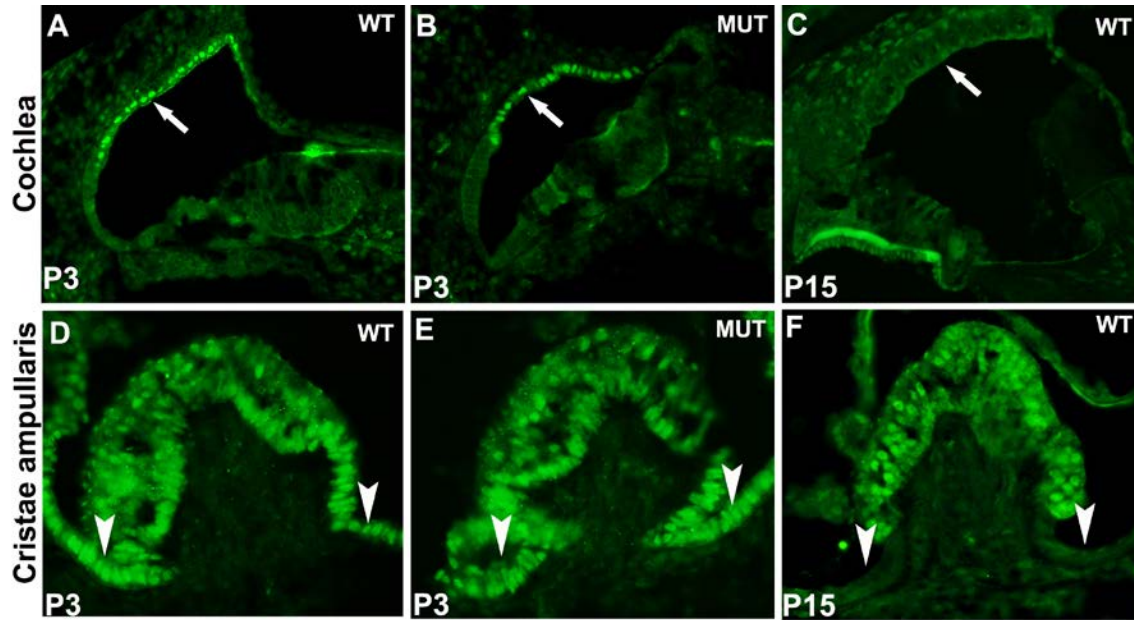


Figure 3.5 The expression of TBX1 in the postnatal mouse inner ear

(A-C) Immunolabeling on transverse sections through the cochlea reveals that TBX1 is expressed in the stria vascularis (white arrow) in both mutant and control mice (A-B) and in the vestibular dark cells (white arrowhead) of both mutant and control mice (D-E). No expression of TBX1 is detected in the stria vascularis (C, white arrow) and dark cells (F, white arrowhead) at P15 in the wild type mice.

3.3.4 Absence of marginal cell markers in the *Tbx1*^{w^{dml}/w^{dml}} mutant mice

Because the stria vascularis appeared abnormal in mutant mice, markers for stria vascularis marginal cells (*Kcnq1*), intermediate cells (*Kcnj10/Dct*), and basal cells (*Glut1/Cldn11*) were used to examine the effects of the *Tbx1*^{w^{dml}} mutation on the cellular structure of the stria vascularis. Because the stria vascularis was undeveloped at P7, we chose to examine these cell types in P0 and P3 mice. Immunohistochemical results showed that the marginal cell marker KCNQ1 is absent from the *w^{dml}* mutant mice and expression of the capillary endothelial cell marker (GLUT1) appears to be weaker and within a slightly reduced region (Figure 3.6). Results from mRNA *in situ* hybridization experiments showed *Esrrb* expression in marginal cells of E16.5 and P3 wild type mice but a lack of expression in age-matched mutant mice. Expression of *Dct*, (an intermediate cell marker) was reduced in the stria vascularis of *w^{dml}* mutant mice (Figure 3.6).

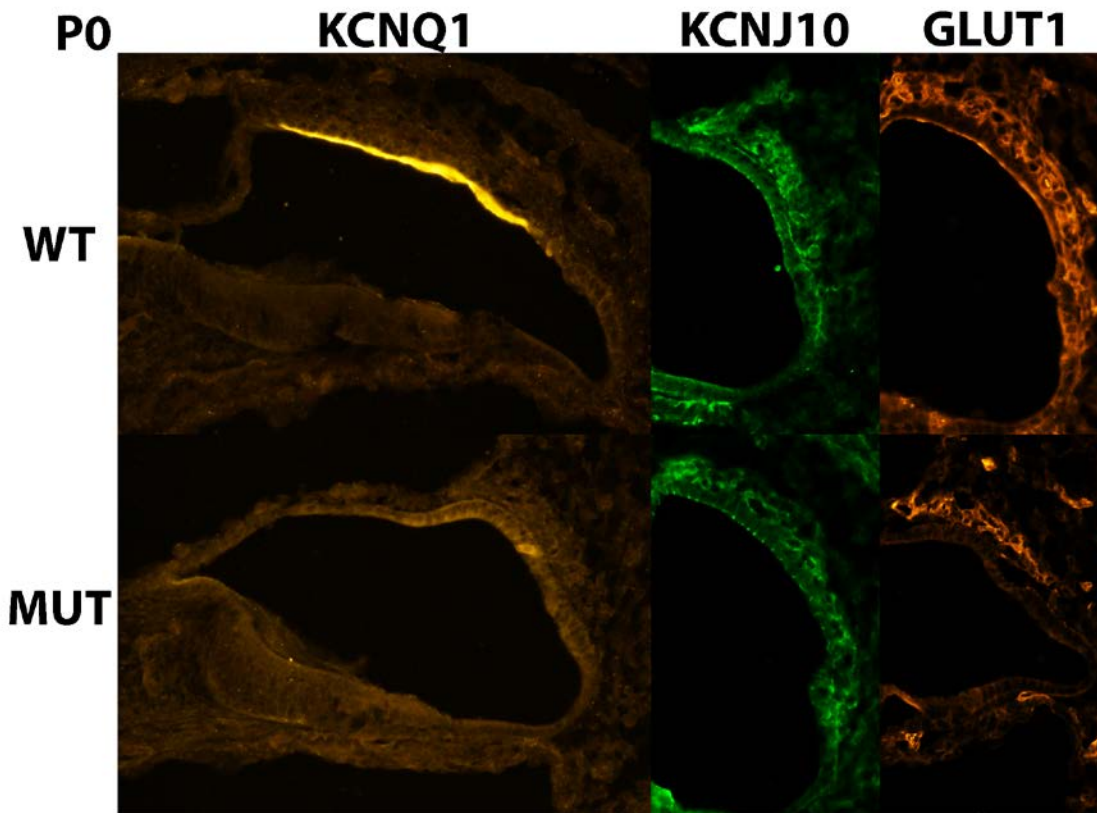


Figure 3.6 Immunodetection of KCNQ1, KCNJ10, and GLUT1 in P0 $Tbx1^{wdml/wdml}$ and $Tbx1^{wdml/+}$ mouse cochlea

KCNQ1, KCNJ10, and GLUT1 expression are detected in the marginal cells (A), intermediate cells (B), and basal cells (C), respectively, in the wild type mice. Reduced KCNQ1 expression is detected in the $Tbx1^{wdml/wdml}$ mice (D), while KCNJ10 and GLUT1 showed reduced expression in the $Tbx1^{wdml/wdml}$ mice (E-F).

3.3.5 Gene expression differences caused by the $Tbx1^{wdml}$ mutation

As $Tbx1$ is a transcription factor, we wanted to know whether the $Tbx1^{wdml}$ mutation leads to a different gene expression profile in mutant mice. We applied RNA-seq to identify genes that showed inner ear expression differences between $Tbx1^{wdml}$ mutant and control E16.5 embryos and identified 379 that are up regulated and 87 that are down regulated. The genes whose expression levels were most affected by the $Tbx1^{wdml}$ mutation are listed in Table 3.2 (A full list of up regulated and down regulated genes can be found in the Appendix A). Down regulation of *Esrrb*, and *Dct* were consistent with our *in situ* hybridization results (Figure 3.7) and provided evidence for the reliability of the RNA-seq results.

Table 3.2 The top 10 upregulated, top 5 downregulated, and five other downregulated DE genes (FDR ≤ 0.05) for *Tbx1*^{wdml/wdml} and *Tbx1*^{wdml/+} mice as ranked by fold-change

Gene Symbol	Ensembl ID	Log ₂ fold-change	P Value	FDR-Adjusted P value
Myh2	ENSMUSG00000033196	4.223735601	2.44E-26	9.67E-24
Myoz1	ENSMUSG00000068697	4.219894733	2.97E-51	4.59E-48
Smtnl1	ENSMUSG00000027077	3.62677157	7.26E-19	1.58E-16
Mylk2	ENSMUSG00000027470	3.315103192	4.84E-19	1.10E-16
Ckm	ENSMUSG00000030399	3.258077476	7.67E-55	1.48E-51
Myh8	ENSMUSG00000055775	3.118427271	3.72E-53	6.40E-50
Hspb3	ENSMUSG00000051456	3.05773731	1.00E-12	1.28E-10
Col6a4	ENSMUSG00000032572	2.968700531	2.13E-22	6.59E-20
Trim54	ENSMUSG00000062077	2.914416126	3.17E-14	4.67E-12
Tnnt3	ENSMUSG00000061723	2.91225841	9.75E-46	1.26E-42
Dlx3	ENSMUSG00000001510	-1.30775381	0.001061858	0.035029985
Aldh1a2	ENSMUSG00000013584	-1.38788924	1.68E-05	0.000890633
Dct	ENSMUSG00000022129	-1.470836677	3.56E-07	2.54E-05
Otx2	ENSMUSG00000021848	-1.852520264	6.51E-14	9.24E-12
Esrrb	ENSMUSG00000021255	-2.585855096	3.19E-35	2.06E-32
Bsnd	ENSMUSG00000025418	-4.12050993	5.75E-22	1.65E-19
Pomc	ENSMUSG00000020660	-4.227201537	1.93E-42	1.87E-39
Kcne2	ENSMUSG00000039672	-5.820402262	1.26E-35	8.45E-33
Ttr	ENSMUSG00000061808	-9.422410447	4.39E-170	1.13E-166

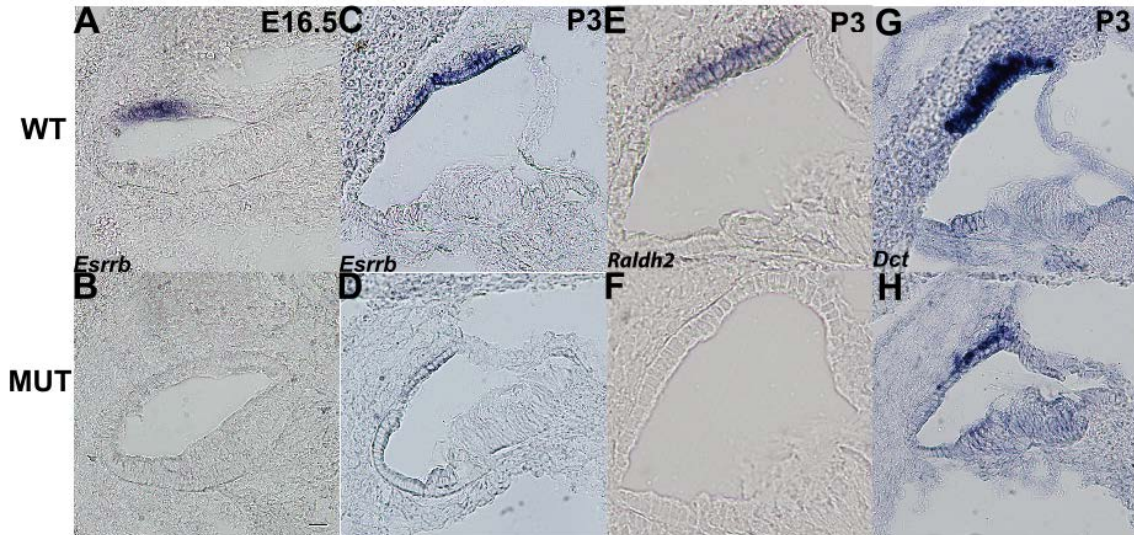


Figure 3.7 Examination of *Esrrb*, *Raldh2*, and *Dct* expression in the *Tbx1^{wdml}* mice and wild type mice with in situ hybridization

Esrrb, *Dct*, and *Raldh2* expression is detected in the stria vascularis in the wild type mice (A, C, E, G). *Esrrb* and *Raldh2* expression is undetectable in the *Tbx1^{wdml}* mice (B, D, F), while reduced *Dct* expression is observed in the *Tbx1^{wdml}* mice (H). Scale bar = 20 μ m.

3.4 Discussion

The *wdml* mutation carries a missense mutation that changes the amino acid aspartic acid to glycine. The aspartic acid altered by the *Tbx1^{wdml}* missense mutation is evolutionarily highly conserved, and both the PolyPhen 2 (<http://genetics.bwh.harvard.edu/pph2/>) and SIFT (<http://sift.jcvi.org/>) computer programs predict that the p.D212G substitution is probably damaging to protein function. The *wdml* mutation occurs in the T-box domain, which is highly conserved in all members of the T-box family. The T-box includes the DNA binding region of the protein but also contains sites of protein interactions. TBX1 localization is not affected by the *Tbx1^{wdml}* mutation (Figure 3.5), indicating that the mutant protein is stable and properly localized. This hypomorphic nature of the mutation can explain the less severe phenotype of *Tbx1^{wdml}* mutant mice compared to that of *Tbx1* knockout mice. The hypomorphic *Tbx1^{wdml}* mutation may affect protein conformation or interactions with co-regulatory proteins that affect particular aspects of TBX1 function.

In contrast to the undeveloped inner ear of *Tbx1* knockout mice, the inner ear of B6-*Tbx1^{w^{dm1}}* mutant mice is fully developed but with abnormalities very similar to those of *Esrrb^{-/-}* [103], *Kcne1^{-/-}* [80, 82], and *Kcnq1^{-/-}* [104] mice; all exhibit reduced endolymph volume and collapsed Reissner's membrane at early postnatal stages and hearing impairment and vestibular dysfunction at adult age. Potassium channel proteins KCNE1 and KCNQ1 are coexpressed in the apical membrane of both marginal cells and dark cells, and release K⁺ to the endolymph [80, 105]. ESRRB, an estrogen-related nuclear receptor, controls the expression of multiple ion channel and transporter genes in stria marginal cells and vestibular dark cells [103]. Chen and colleagues [103] reported that *Kcne1*, *Kcnq1*, and *Dct* are down regulated in *Esrrb^{-/-}* mice. They proposed that *Esrrb* is important for cell fate determination, as there is a cell fate change of marginal cells toward intermediate cells in *Esrrb^{-/-}* mice [103]. Our results (Figure 3.7) show an absence of *Esrrb* expression in the stria vascularis of *Tbx1^{w^{dm1}}* mutant mice as early as E16.5, indicating that *Tbx1* is a direct or indirect upstream regulator of *Esrrb* expression. Previous to this discovery, *Esrrb* was the only gene known to control development of the endolymph-producing epithelial cells of the inner ear.

Previous studies have not examined TBX1 expression beyond E18.5, Our results show that TBX1 is expressed in the marginal cells of the stria vascularis and the dark cells of the crista ampullaris in both mutant and control mice at P3. Interestingly, expression in these cells disappears between P3 and P15 (Figure 3.5), suggesting a transient function of TBX1 in the early postnatal stage. The cochlear marginal cells and vestibular dark cells are responsible for K⁺ transport to the endolymph of the inner ear and possess many similarities. Consistent with the marginal cell localization of TBX1, there was a lack of expression of the marginal cell marker KCNQ1 in *Tbx1^{w^{dm1}}* mutants and reduced expression of intermediate and basal cell markers, which are probably secondary effects of the marginal cell defect. Together, these data support an important role for *Tbx1* in marginal cell maturation and stria vascularis development and in the maturation and function of vestibular dark cells. We also found TBX1 expression

in the hair cells and supporting cells of the crista ampullaris at both P3 and P15 (Figure 3.5). Our TBX1 protein localization results agree with results deduced from reporter gene β -gal activity in *Tbx1*^{+lacZ} mice, where expression also was detected during late development of the ear (E18.5) in marginal cells of the stria vascularis and in hair cells and adjacent nonsensory dark cells of the crista ampullaris [106]. Lineage analysis of the late otocyst stage of mouse inner ears indicates that vestibular hair cells and supporting cells in the posterior crista are clonally related [107]. In addition, the lineage-tracing data raise the possibility that nonsensory epithelial cells bordering the crista may be clonally related to the vestibular sensory epithelium. These results may be related to our finding that TBX1 is expressed in sensory hair cells and supporting cells and also in the adjacent nonsensory dark cells of the crista in P3 mice, followed by a loss of the nonsensory dark cell expression by P15 (Figure 3.5).

Paintfills of the membranous labyrinths of E14.5 inner ears of B6-*Tbx1*^{wdml/wdml} mice revealed nonresorption of the fusion plate of the posterior semicircular canal, a vestibular phenotype similar to that observed in *Foxg1*^{-/-} mice [108]. Although *Tbx1*^{wdml} mutant mice have a normal looking cochlea, *Foxg1*^{-/-} mutant mice have a shortened cochlea, possibly because *Foxg1* acts upstream of the *Tbx1* gene. At the beginning of semicircular canal formation, fusion plates are formed through attachment of apposing lateral and medial epithelial extrusions of the dorsal otic vesicle. Epithelial cells at the fusion plate intercalate to form a single sheet and disappear through a process of resorption, either through apoptosis or retraction of the cells to the remaining canal pouch epithelium at the outer rim, to form the fluid-filled canal. Bone morphogenetic protein 4 (BMP4) marks the incipient posterior crista by E11.5, followed shortly thereafter by BMP4 delineation of the anterior and lateral cristae, which may share a common origin as evidenced by the single BMP4-positive area in the anterior portion of the otocyst that is later seen as two distinct domains[109]. The crista has been hypothesized to induce the formation of the associated semicircular canal structure [108]. Reduced function of TBX1 in the posterior crista of *Tbx1*^{vtx} mutants, therefore, may possibly be the underlying cause for the incomplete formation of the

posterior canal and ampulla during otic development.

To elucidate the molecular mechanisms underlying the *Tbx1^{wdml}* mutant phenotype, we performed RNA-seq with inner ears from mutant and control E16.5 embryos, the age at which stria vascularis development begins. We identified a number of genes that are expressed in the stria vascularis and are involved in stria development and function (Table 3.2). The RNA-seq results showed down regulation of *Esrrb*, which has a very similar expression pattern in the inner ear as *Tbx1*. Our *in situ* RNA hybridization results also showed a down regulation of *Esrrb* (Figure 3.7), supporting the reliability of the RNA-Seq data. We observed drastic reductions in *Kcne1* and *Kcne2* expression, which is not surprising because KCNE1 and KCNQ1 form a potassium channel complex and are important for K⁺ secretion into the inner ear endolymph. *Bsnd* and *Dct*, markers for stria vascularis basal cell and intermediate cells, respectively, are also down regulated in the *Tbx1^{wdml}* mutant mice as is *Dlx3*, a member of the distalless homeobox family of transcription factors, which are known to play important roles in the developing vestibular system of the inner ear [110]. Surprisingly more genes were up regulated than down regulated by the *Tbx1^{wdml}* mutation, suggesting that TBX1 inhibits expression of more genes than it enhances in the E16.5 inner ear.

We hypothesize that *Tbx1* is important for marginal cell fate determination. *Esrrb* is down regulated in *Tbx1^{wdml}* mutant mice, as shown from our *in situ* RNA hybridization and RNA-seq results, and therefore acts as a direct or indirect downstream target of *Tbx1*. Chen and colleagues showed a change of marginal cell fate toward intermediate cell in *Esrrb^{-/-}* mice [103]. If *Tbx1* regulates *Esrrb* expression and ESRRB regulates marginal cell fate determination, we can predict that marginal cell differentiation cannot be achieved in the *Tbx1^{wdml}* mutant mice, leading to failed marginal cell maturation and interdigitation and subsequent failure of stria vascularis development. Another possible but less likely explanation for the undeveloped stria vascularis of mutant mice is that *Tbx1* is required for cell proliferation and survival rather than cell fate determination.

TBX1 has been shown to regulate retinoic acid (RA) metabolic genes during cochlear morphogenesis [111], and *Aldh1a2* (*Raldh2*), which encodes the RA-synthesizing enzyme retinaldehyde dehydrogenase 2, was found to be expressed in the stria vascularis, Reissner's membrane and dark cells of the inner ear [112-114]. Our in situ RNA hybridization analysis showed that *Raldh2* expression is down regulated in the stria vascularis of *Tbx1^{w^{dml}}* mutant mice (Figure 3.7), consistent with previous studies of RALDH2 localization, and suggesting that RA may be specifically synthesized in this part of the cochlea [112]. RA secreted by the marginal cells may be required for vascularization in the stria vascularis and establishment of the inner ear blood-labyrinth barrier, as supported by a study showing that RA contributes to blood-brain barrier maturation [115]. Radial glial cells in fetal human brain tissue express high levels of *Raldh2* and tightly associate with the developing brain vasculature that expresses the RA receptor β during embryogenesis [116]. *Raldh2* expression may play a similar role in stria vascularis vasculature maturation.

Studies of prostate cancer patients and animal models have identified associations between *Tbx1* and *Raldh2* [117]. They showed that methylation of *Tbx1* regulates the RA signaling pathway through downregulation of *Raldh2*. *Raldh2* null mice are embryonic lethal [118], and a hypomorphic *Raldh2* mutation caused decreased RA synthesis and a DiGorge syndrome-like phenotype in the mice [119]. Expression of *Raldh2* (*Aldh1a2*) was reported to be down regulated in mice with an *Esrrb* loss of function mutation [103]. It is proposed that ESRRB heterodimerizes or directly cooperates with RAR at direct repeat hormone response element (HRE) motifs, facilitating stable binding events before and/or after RA signaling [120].

Our RNA-seq data showed downregulation of *Dlx3* in *Tbx1^{w^{dml}}* mutant E16.5 embryos. *Dlx3* is expressed in the dorsal region of the otic vesicle at E12.5, and its expression was lost in the developing semicircular canals of mesodermal *Tbx1* loss of function mutant mice [110]. A recent report using an oral squamous cell carcinoma line treated with all-trans retinoic acid suggests that *Dlx3* is negatively

regulated by RA [121]. Collectively, these data suggest that *Tbx1* may interact with the RA signaling pathway to regulate semicircular canal formation and stria vascularis maturation.

3.5 Summary

Tbx1 not only has a global effect on inner ear development evidenced by failed inner ear morphogenesis at the otocyst stage in the *Tbx1* homozygous knockout mice, but also plays possible specific roles for semicircular canal and stria vascularis development as suggested by *Tbx1* expression in the marginal cells of the stria vascularis and the dark cells of the crista ampullaris at later embryo stages. As no inner ear is formed in germline or conditional *Tbx1* knockout mice, *Tbx1^{wdml}* mice provide the first model that allow us to study *Tbx1* function during semicircular canal and stria vascularis development. The stria vascularis phenotype of the *Tbx1^{wdml}* mice at postnatal stages makes it a good model to examine the molecular network that regulates stria vascularis development and maturation. Various hearing disorders in human patients are associated with stria vascularis dysfunction; for example, mutation in the *KCNQ1* gene cause long QT syndrome, SESAME Syndrome is associated with mutations in the human *JCNJ10* gene, and Bartter syndrome is associated with mutations in the *BSND* gene. Investigation of the *Tbx1^{wdml}* mutation will provide us more knowledge of the molecular network that regulates stria vascularis development and function and opens a new avenue for developing therapeutic approaches to treat hearing disorders associated with its dysfunction.

3.6 Future directions

Posterior semicircular canal malformation is observed in the E14.5 mutant inner ear; however, it is unclear whether it is due to stopped or delayed development. To answer that question, two more ages of the *Tbx1^{wdml}* inner ear will be observed by paintfill analysis: E16.5 and P0. To further investigate the undeveloped stria vascularis observed in the *Tbx1^{wdml}* mice, we will apply transmission electron microscope (TEM) to observe the microstructure of the cell layers within the mutant stria vascularis. Failed development of the mutant stria vascularis is very likely because undifferentiated marginal cells

are not able to interdigitate with intermediate cells and the vasculature network. We hypothesize that interactions of TBX1 with other proteins that are important for inner ear development are disrupted by the *wdm1* mutation. We therefore propose to use an unbiased approach (yeast two hybridization) to screen for proteins that interact with TBX1 in E16.5 inner ears. We will localize the identified protein in the inner ear if no data is available, and confirm TBX1 interaction with these candidate proteins using co-immunoprecipitation or pull down assay. Lastly, we will detect whether the protein interactions between TBX1 and the candidate proteins are disrupted by the *wdm1* mutation.

CHAPTER 4 THESIS SUMMARY

Three new mouse mutations: *Enpp1^{asj}*, *Atp6v1b1^{vtx}*, and *Tbx1^{wdm1}*, are reported in this dissertation. All three mutations lead to severe hearing loss/deafness in the mutant mice, but are due to different underlying pathologies.

Chapter 1: The *Enpp1^{asj}* mutation causes middle ear inflammation that is associated with abnormal mineralization and calcification in the *asj* mutant mice. Inflammation causes transdifferentiation of ciliary epithelial cells into goblet cells, which leads to excessive mucus secretion in the middle ear cavity. Reduction of ciliary epithelial cells impair the clearance function of the ciliary epithelia. Both factors combined lead to accumulation of mucus in the middle ear cavity that causes progressive conductive hearing loss in the *asj* mutant mice. Another factor that contributes to the conductive hearing loss in the *asj* mice is tympanosclerosis, a subtype of otosclerosis, which is a common middle ear condition characterized by abnormal bone remodeling in the middle ear. Calcification of middle ear soft tissues, such as tympanic membrane, and mineralization of middle ear ossicles, are observed in patients with tympanosclerosis in addition to abnormal middle ear bone remodeling.

Chapter 2: The *Atp6v1b1^{vtx}* mutation leads to an enlargement of the endolymphatic duct and sac of the inner ear, which results in drastically reduced endolymphatic potential (EP), deafness and vestibular dysfunction in homozygous mutant mice. The *vtx* mutation arose on the MRL-MpJ background, which has a strong deleterious effect on its auditory phenotype, as opposed to a previously reported *Atp6v1b1* KO mouse on a B6 background that has normal hearing. MRL-*Atp6v1b1^{vtx}* mutant mice provide a new genetic model for some clinical cases of nonsyndromic deafness with enlarged vestibular aqueducts. We attempted to map the loci that contribute to hearing loss phenotype in the MRL-*vtx* mice, and found that the modifier effects on hearing loss are derived from multiple loci rather than a single locus with large effect. Genome-wide linkage analysis revealed a region on chromosome 13

that contains over 400 genes. Two candidate genes, *Slc9a3* and *Slc12a7*, were picked based on their expression pattern in the inner ear and the association with inner ear ion homeostasis. We did not detect either DNA sequence or mRNA expression differences in these genes between MRL and B6 mice, indicating that they are not likely the modifiers. Besides the large candidate gene pool, complete sequence of the MRL strain is not available, making the effort to narrow down the candidate region and identify the modifiers more challenging.

Chapter 3: The *Tbx1*^{w^{dml}} mutation leads to semicircular canal malformation and undeveloped stria vascularis in the inner ears of mutant mice, which contribute to the circling and deafness phenotype of these mice. In contrast to *Atp6v1b1*^{vtx} mice (Chapter 2), which have dramatically increased endolymph volume, *Tbx1*^{w^{dml}} mice have greatly reduced endolymph volume, due to lack of stria vascularis function. Initial efforts showed that the *w^{dml}* mutation does not affect the stability and localization of TBX1 protein in the mouse inner ear, and that TBX1 is only expressed in the stria vascularis and vestibular dark cells at the early postnatal stage. Reduced expression of the orphan nuclear receptor *Esrrb* in the *Tbx1*^{w^{dml}} mutant mice suggest that *Tbx1* is an upstream regulator of the gene network that regulates stria vascularis development.

We used a forward genetics approach to identify these new mouse mutations that affect ear development and function. This approach relies on the abundant mutant mouse resources available from the Jackson Laboratory. Besides the three genes reported in this dissertation, other genes such as *Clic5*, *Tmhs*, and *Duox2*, were identified using this strategy. These new mouse mutations were identified either by their vestibular phenotype, which is usually associated with hearing loss (though there are exceptions), or by hearing screen with auditory brainstem response measurement. Causative mutations were identified by linkage association analysis with either intercross or backcross mice.

One of the advantages of the forward genetics approach is that it can identify new alleles that can reveal a particular protein's role in a specific process in a way that deletion of the protein cannot.

Hypomorphic alleles that affect certain aspects of protein function or alter protein structure can lead to less severe phenotypes than KO alleles and therefore allow us to study specific functions of these genes. Take the *Tbx1^{wdml}* mutation as an example. The association of *TBX1* with human DiGeorge syndrome drove the creation of *Tbx1* KO and conditional KO mice. However, these mice could only tell us that *TBX1* is crucial for inner ear morphogenesis as the inner ear does not develop past the E10 otocyst stage in these mutant mice. Does *TBX1* have other functions during inner ear development? This question cannot be addressed with the KO mutant mice because they do not have a fully developed inner ear. Furthermore, studies showed that *TBX1* is expressed in the stria vascularis and vestibular dark cells during late embryo stage, suggesting potential involvement of *TBX1* in the development and/or function of these structures. The *wdml* point mutation in the *Tbx1* gene causes circling behavior and deafness in the mutant mice. Inner ears of *Tbx1^{wdml}* mutant mice fully develop but show pathologies in the stria vascularis and vestibule that correspond to their expression patterns. This mutation allows us to study *Tbx1* function during inner ear development and identify proteins that interact with *TBX1* and regulate the genetic network that regulates inner ear development.

Another advantage of the forward genetics approach is that it allows us to investigate strain background effects on the mutant phenotype.. Most engineered mutations are on the B6 background, which limits discovery of genetic background effects on mutant phenotypes. For example, mutations in the *ATP6V1B1* gene were reported in human patients with distal renal tubular acidosis with hearing loss, but a mouse KO of *Atp6v1b1* on the B6 background did not exhibit any renal or auditory deficits. The *vtx* mutation in the *Atp6v1b1* gene on a MRL background, in contrast, recapitulates the hearing loss phenotype observed in patients with distal renal tubular acidosis, indicating that the MRL background has a profound effect on the auditory phenotype associated with *Atp6v1b1* mutation in mice, and helps to explain the phenotype variability associated with human *ATP6V1B1* mutations.

In summary, the three mutations reported here provide valuable models to study common middle ear condition (otitis media), sensorineural hearing loss associated with enlarged vestibular aqueduct, and hearing loss associated with human DiGeorge syndrome. These missense mutations identified with a forward genetics approach suggest that despite of the emerging of new technique like CRISPR, it is still a valuable method to identify new genes that cause hearing loss phenotype. Previous studies predicted that hundreds of genes related to inner ear development are waiting to be discovered, and these discoveries can be aided by the forward genetics approach. These mouse models are also valuable tools for testing gene therapies. For example, the same amino acid change was reported in human patients as was discovered in the *Tbx1*^{w^{dm1}} mice. This missense mutation provides an easy target for gene therapy and will be very informative for future clinical trials. Another good model is the *Atp6v1b1*^{v^{tx}} mice and its modifier genes, which can provide new insight into genetic background effects underlying the phenotypic variability in human patients and the underlying mechanisms and pave a new avenue for therapeutic approaches.

BIBLIOGRAPHY

1. Rye, M.S., et al., *Unraveling the genetics of otitis media: from mouse to human and back again*. Mamm Genome, 2011. **22**(1-2): p. 66-82.
2. Zheng, Q.Y., R. Hardisty-Hughes, and S.D. Brown, *Mouse models as a tool to unravel the genetic basis for human otitis media*. Brain Res, 2006. **1091**(1): p. 9-15.
3. Yang, B., et al., *Sh3pxd2b mice are a model for craniofacial dysmorphology and otitis media*. PLoS One, 2011. **6**(7): p. e22622.
4. Noben-Trauth, K. and J.R. Latoche, *Ectopic mineralization in the middle ear and chronic otitis media with effusion caused by RPL38 deficiency in the Tail-short (Ts) mouse*. J Biol Chem, 2011. **286**(4): p. 3079-93.
5. Hilton, J.M., et al., *Exome sequencing identifies a missense mutation in Isl1 associated with low penetrance otitis media in dearisch mice*. Genome Biol, 2011. **12**(9): p. R90.
6. Tian, C., et al., *Otitis media in a new mouse model for CHARGE syndrome with a deletion in the Chd7 gene*. PLoS One, 2012. **7**(4): p. e34944.
7. Zhang, Y., et al., *Pathological features in the LmnaDhe/+ mutant mouse provide a novel model of human otitis media and laminopathies*. Am J Pathol, 2012. **181**(3): p. 761-74.
8. Han, F., et al., *Mutation in Phex gene predisposes BALB/c-Phex(Hyp-Duk)/Y mice to otitis media*. PLoS One, 2012. **7**(9): p. e43010.
9. Kerschner, J.E., et al., *A novel model of spontaneous otitis media with effusion (OME) in the Oxgr1 knock-out mouse*. Int J Pediatr Otorhinolaryngol, 2013. **77**(1): p. 79-84.
10. Tateossian, H., et al., *Otitis media in the Tgif knockout mouse implicates TGFbeta signalling in chronic middle ear inflammatory disease*. Hum Mol Genet, 2013. **22**(13): p. 2553-65.
11. Chen, J., et al., *Mcph1-deficient mice reveal a role for MCPH1 in otitis media*. PLoS One, 2013. **8**(3): p. e58156.
12. Harris BS, W.J., Ward-Bailey PF, Yu H, Bergstrom DE, Bronson RT, Donahue LR, *Ages with stiffened joints, A new mutation in Enpp1*. <http://mousemutant.jax.org/articles/mmrmutantasj.html>, 2012.
13. Li, Q., et al., *Mutant Enpp1asj mice as a model for generalized arterial calcification of infancy*. Dis Model Mech, 2013. **6**(5): p. 1227-35.
14. Okawa, A., et al., *Mutation in Npps in a mouse model of ossification of the posterior longitudinal ligament of the spine*. Nat Genet, 1998. **19**(3): p. 271-3.
15. Babij, P., et al., *New variants in the Enpp1 and Ptpn6 genes cause low BMD, crystal-related arthropathy, and vascular calcification*. J Bone Miner Res, 2009. **24**(9): p. 1552-64.

16. Mackenzie, N.C., et al., *Altered bone development and an increase in FGF-23 expression in Enpp1(-/-) mice*. PLoS One, 2012. **7**(2): p. e32177.
17. Nitschke, Y., et al., *Generalized arterial calcification of infancy and pseudoxanthoma elasticum can be caused by mutations in either ENPP1 or ABCC6*. Am J Hum Genet, 2012. **90**(1): p. 25-39.
18. Brachet, C., et al., *Hearing loss is part of the clinical picture of ENPP1 loss of function mutation*. Horm Res Paediatr, 2014. **81**(1): p. 63-6.
19. Zheng, Q.Y., K.R. Johnson, and L.C. Erway, *Assessment of hearing in 80 inbred strains of mice by ABR threshold analyses*. Hear Res, 1999. **130**(1-2): p. 94-107.
20. Johnson, K.R., et al., *Mouse models of USH1C and DFNB18: phenotypic and molecular analyses of two new spontaneous mutations of the Ush1c gene*. Hum Mol Genet, 2003. **12**(23): p. 3075-86.
21. Li, Q., et al., *Spontaneous asj-2J mutant mouse as a model for generalized arterial calcification of infancy: a large deletion/insertion mutation in the Enpp1 gene*. PLoS One, 2014. **9**(12): p. e113542.
22. Han, F., et al., *Otitis media in a mouse model for Down syndrome*. Int J Exp Pathol, 2009. **90**(5): p. 480-8.
23. Tian, C., et al., *Ush1c gene expression levels in the ear and eye suggest different roles for Ush1c in neurosensory organs in a new Ush1c knockout mouse*. Brain Res, 2010. **1328**: p. 57-70.
24. Lin, J., et al., *Mucin production and mucous cell metaplasia in otitis media*. Int J Otolaryngol, 2012. **2012**: p. 745325.
25. Linden, S.K., et al., *Mucins in the mucosal barrier to infection*. Mucosal Immunol, 2008. **1**(3): p. 183-97.
26. Mata, M., et al., *Gene mutations in primary ciliary dyskinesia related to otitis media*. Curr Allergy Asthma Rep, 2014. **14**(3): p. 420.
27. Terkeltaub, R.A., *Inorganic pyrophosphate generation and disposition in pathophysiology*. Am J Physiol Cell Physiol, 2001. **281**(1): p. C1-C11.
28. Yamada, S., et al., *Phosphate overload directly induces systemic inflammation and malnutrition as well as vascular calcification in uremia*. Am J Physiol Renal Physiol, 2014. **306**(12): p. F1418-28.
29. Hofmann Bowman, M.A. and E.M. McNally, *Genetic pathways of vascular calcification*. Trends Cardiovasc Med, 2012. **22**(4): p. 93-8.
30. Gurley, K.A., R.J. Reimer, and D.M. Kingsley, *Biochemical and genetic analysis of ANK in arthritis and bone disease*. Am J Hum Genet, 2006. **79**(6): p. 1017-29.

31. Morava, E., et al., *Autosomal recessive mental retardation, deafness, ankylosis, and mild hypophosphatemia associated with a novel ANKH mutation in a consanguineous family*. J Clin Endocrinol Metab, 2011. **96**(1): p. E189-98.
32. Davies, M., R. Kane, and J. Valentine, *Impaired hearing in X-linked hypophosphataemic (vitamin-D-resistant) osteomalacia*. Ann Intern Med, 1984. **100**(2): p. 230-2.
33. O'Malley, S.P., et al., *The petrous temporal bone and deafness in X-linked hypophosphataemic osteomalacia*. Clin Radiol, 1988. **39**(5): p. 528-30.
34. Weir, N., *Sensorineural deafness associated with recessive hypophosphataemic rickets*. J Laryngol Otol, 1977. **91**(8): p. 717-22.
35. Lorenz-Depiereux, B., et al., *New intragenic deletions in the PheX gene clarify X-linked hypophosphatemia-related abnormalities in mice*. Mamm Genome, 2004. **15**(3): p. 151-61.
36. Lysaght, A.C., et al., *FGF23 Deficiency Leads to Mixed Hearing Loss and Middle Ear Malformation in Mice*. PLoS One, 2014. **9**(9): p. e107681.
37. Lorenz-Depiereux, B., et al., *Loss-of-function ENPP1 mutations cause both generalized arterial calcification of infancy and autosomal-recessive hypophosphatemic rickets*. Am J Hum Genet, 2010. **86**(2): p. 267-72.
38. Diamond, M.K., *Coarctation of the stapedia artery: an unusual adaptive response to competing functional demands in the middle ear of some eutherians*. J Morphol, 1989. **200**(1): p. 71-86.
39. Thys, M. and G. Van Camp, *Genetics of otosclerosis*. Otol Neurotol, 2009. **30**(8): p. 1021-32.
40. Goycoolea, M.V. and L. Lundman, *Round window membrane. Structure function and permeability: a review*. Microsc Res Tech, 1997. **36**(3): p. 201-11.
41. Lang, F., et al., *Functional significance of channels and transporters expressed in the inner ear and kidney*. Am J Physiol Cell Physiol, 2007. **293**(4): p. C1187-208.
42. Karet, F.E., et al., *Mutations in the gene encoding B1 subunit of H⁺-ATPase cause renal tubular acidosis with sensorineural deafness*. Nat Genet, 1999. **21**(1): p. 84-90.
43. Stover, E.H., et al., *Novel ATP6V1B1 and ATP6VOA4 mutations in autosomal recessive distal renal tubular acidosis with new evidence for hearing loss*. J Med Genet, 2002. **39**(11): p. 796-803.
44. Vargas-Poussou, R., et al., *Genetic investigation of autosomal recessive distal renal tubular acidosis: evidence for early sensorineural hearing loss associated with mutations in the ATP6VOA4 gene*. J Am Soc Nephrol, 2006. **17**(5): p. 1437-43.
45. Batlle, D. and S.K. Haque, *Genetic causes and mechanisms of distal renal tubular acidosis*. Nephrology, Dialysis, Transplantation, 2012. **27**(10): p. 3691-704.

46. Lorente-Canovas, B., et al., *Mice deficient in the H⁺-ATPase α 4 subunit have severe hearing impairment associated with enlarged endolymphatic compartments within the inner ear*. *Dis Model Mech*, 2012.
47. Norgett, E.E., et al., *Atp6v0a4 knockout mouse is a model of distal renal tubular acidosis with hearing loss, with additional extrarenal phenotype*. *Proc Natl Acad Sci U S A*, 2012. **109**(34): p. 13775-80.
48. Finberg, K.E., et al., *The B1-subunit of the H(+) ATPase is required for maximal urinary acidification*. *Proc Natl Acad Sci U S A*, 2005. **102**(38): p. 13616-21.
49. Dou, H., et al., *Mice lacking the B1 subunit of H⁺ -ATPase have normal hearing*. *Hear Res*, 2003. **180**(1-2): p. 76-84.
50. Paunescu, T.G., et al., *Compensatory membrane expression of the V-ATPase B2 subunit isoform in renal medullary intercalated cells of B1-deficient mice*. *Am J Physiol Renal Physiol*, 2007. **293**(6): p. F1915-26.
51. Johnson, K.R., C.M. Longo-Guess, and L.H. Gagnon, *Mutations of the mouse ELMO domain containing 1 gene (Elmod1) link small GTPase signaling to actin cytoskeleton dynamics in hair cell stereocilia*. *PLoS One*, 2012. **7**(4): p. e36074.
52. Zheng, Q.Y., K.R. Johnson, and L.C. Erway, *Assessment of hearing in 80 inbred strains of mice by ABR threshold analyses*. *Hear Res*, 1999. **130**: p. 94-107.
53. Manly, K.F., R.H. Cudmore, Jr., and J.M. Meier, *Map Manager QTX, cross-platform software for genetic mapping*. *Mamm Genome*, 2001. **12**(12): p. 930-2.
54. Bond, B.R., L.L. Ng, and B.A. Schulte, *Identification of mRNA transcripts and immunohistochemical localization of Na/H exchanger isoforms in gerbil inner ear*. *Hear Res*, 1998. **123**(1-2): p. 1-9.
55. Miyazaki, H., P. Wangemann, and D.C. Marcus, *The gastric H,K-ATPase in stria vascularis contributes to pH regulation of cochlear endolymph but not to K secretion*. *BMC Physiol*, 2016. **17**(1): p. 1.
56. Boettger, T., et al., *Deafness and renal tubular acidosis in mice lacking the K-Cl co-transporter Kcc4*. *Nature*, 2002. **416**(6883): p. 874-8.
57. Subasioglu Uzak, A., et al., *ATP6V1B1 mutations in distal renal tubular acidosis and sensorineural hearing loss: clinical and genetic spectrum of five families*. *Renal Failure*, 2013. **35**(9): p. 1281-4.
58. Yang, Q., et al., *Vacuolar H⁺ -ATPase B1 subunit mutations that cause inherited distal renal tubular acidosis affect proton pump assembly and trafficking in inner medullary collecting duct cells*. *Journal of the American Society of Nephrology*, 2006. **17**(7): p. 1858-66.
59. Hulander, M., et al., *Lack of pendrin expression leads to deafness and expansion of the endolymphatic compartment in inner ears of Foxi1 null mutant mice*. *Development*, 2003. **130**(9): p. 2013-25.

60. Everett, L.A., et al., *Targeted disruption of mouse Pds provides insight about the inner-ear defects encountered in Pendred syndrome*. Hum Mol Genet, 2001. **10**(2): p. 153-161.
61. Vidarsson, H., et al., *The forkhead transcription factor Foxi1 is a master regulator of vacuolar H-ATPase proton pump subunits in the inner ear, kidney and epididymis*. PLoS One, 2009. **4**(2): p. e4471.
62. Kim, H.M. and P. Wangemann, *Failure of fluid absorption in the endolymphatic sac initiates cochlear enlargement that leads to deafness in mice lacking pendrin expression*. PLoS One, 2010. **5**(11): p. e14041.
63. Li, X., et al., *SLC26A4 targeted to the endolymphatic sac rescues hearing and balance in Slc26a4 mutant mice*. PLoS Genet, 2013. **9**(7): p. e1003641.
64. Alexander, R.T., et al., *Acidosis and Urinary Calcium Excretion: Insights from Genetic Disorders*. J Am Soc Nephrol, 2016. **27**(12): p. 3511-3520.
65. Andreucci, E., et al., *Inner ear abnormalities in four patients with dRTA and SNHL: clinical and genetic heterogeneity*. Pediatric Nephrology, 2009. **24**(11): p. 2147-53.
66. Joshua, B., et al., *Audiometric and imaging characteristics of distal renal tubular acidosis and deafness*. J Laryngol Otol, 2008. **122**(2): p. 193-8.
67. Pryor, S.P., et al., *SLC26A4/PDS genotype-phenotype correlation in hearing loss with enlargement of the vestibular aqueduct (EVA): evidence that Pendred syndrome and non-syndromic EVA are distinct clinical and genetic entities*. J Med Genet, 2005. **42**(2): p. 159-65.
68. Rehman, A.U., T.B. Friedman, and A.J. Griffith, *Unresolved questions regarding human hereditary deafness*. Oral Dis, 2016.
69. Yang, T., et al., *Mutations of KCNJ10 together with mutations of SLC26A4 cause digenic nonsyndromic hearing loss associated with enlarged vestibular aqueduct syndrome*. Am J Hum Genet, 2009. **84**(5): p. 651-7.
70. Yang, T., et al., *Transcriptional control of SLC26A4 is involved in Pendred syndrome and nonsyndromic enlargement of vestibular aqueduct (DFNB4)*. Am J Hum Genet, 2007. **80**(6): p. 1055-63.
71. Landa, P., et al., *Lack of significant association between mutations of KCNJ10 or FOXI1 and SLC26A4 mutations in Pendred syndrome/enlarged vestibular aqueducts*. BMC Med Genet, 2013. **14**: p. 85.
72. Zhao, J., et al., *KCNJ10 may not be a contributor to nonsyndromic enlargement of vestibular aqueduct (NSEVA) in Chinese subjects*. PLoS One, 2014. **9**(11): p. e108134.
73. Chen, K., et al., *Screening of SLC26A4, FOXI1, KCNJ10, and GJB2 in bilateral deafness patients with inner ear malformation*. Otolaryngol Head Neck Surg, 2012. **146**(6): p. 972-8.

74. Barald, K.F. and M.W. Kelley, *From placode to polarization: new tunes in inner ear development*. Development, 2004. **131**(17): p. 4119-30.
75. Zampini, V., et al., *Eps8 regulates hair bundle length and functional maturation of Mammalian auditory hair cells*. PLoS Biol, 2011. **9**(4): p. e1001048.
76. Steel, K.P. and C. Barkway, *Another role for melanocytes: their importance for normal stria vascularis development in the mammalian inner ear*. Development, 1989. **107**(3): p. 453-63.
77. Marcus, D.C., et al., *KCNJ10 (Kir4.1) potassium channel knockout abolishes endocochlear potential*. Am J Physiol Cell Physiol, 2002. **282**(2): p. C403-7.
78. Flagella, M., et al., *Mice lacking the basolateral Na-K-2Cl cotransporter have impaired epithelial chloride secretion and are profoundly deaf*. J Biol Chem, 1999. **274**(38): p. 26946-55.
79. Casimiro, M.C., et al., *Targeted disruption of the Kcnq1 gene produces a mouse model of Jervell and Lange-Nielsen Syndrome*. Proc Natl Acad Sci U S A, 2001. **98**(5): p. 2526-2531.
80. Nicolas, M., et al., *KCNQ1/KCNE1 potassium channels in mammalian vestibular dark cells*. Hear Res, 2001. **153**(1-2): p. 132-45.
81. Knipper, M., et al., *Deafness in LIMP2-deficient mice due to early loss of the potassium channel KCNQ1/KCNE1 in marginal cells of the stria vascularis*. J Physiol, 2006. **576**(Pt 1): p. 73-86.
82. Letts, V.A., et al., *A new spontaneous mouse mutation in the Kcne1 gene*. Mamm Genome, 2000. **11**(10): p. 831-835.
83. Schulze-Bahr, E., et al., *KCNE1 mutations cause jervell and Lange-Nielsen syndrome [letter]*. Nat Genet, 1997. **17**(3): p. 267-8.
84. Birkenhager, R., et al., *Mutation of BSND causes Bartter syndrome with sensorineural deafness and kidney failure*. Nat Genet, 2001. **29**(3): p. 310-4.
85. Rickheit, G., et al., *Endocochlear potential depends on Cl⁻ channels: mechanism underlying deafness in Bartter syndrome IV*. Embo J, 2008. **27**(21): p. 2907-17.
86. Delpire, E., et al., *Deafness and imbalance associated with inactivation of the secretory Na- K-2Cl co-transporter*. Nat Genet, 1999. **22**(2): p. 192-5.
87. Dixon, M.J., et al., *Mutation of the Na-K-Cl co-transporter gene Slc12a2 results in deafness in mice*. Hum Mol Genet, 1999. **8**(8): p. 1579-84.
88. Xu, H., et al., *Tbx1 has a dual role in the morphogenesis of the cardiac outflow tract*. Development, 2004. **131**(13): p. 3217-27.
89. Vitelli, F., et al., *Tbx1 mutation causes multiple cardiovascular defects and disrupts neural crest and cranial nerve migratory pathways*. Human Molecular Genetics, 2002. **11**(8): p. 915-922.

90. Jackson, A., et al., *Endoderm-Specific Deletion of Tbx1 Reveals an FGF-Independent Role for Tbx1 in Pharyngeal Apparatus Morphogenesis*. *Developmental Dynamics*, 2014. **243**(9): p. 1143-1151.
91. Choe, C.P. and J.G. Crump, *Tbx1 controls the morphogenesis of pharyngeal pouch epithelia through mesodermal Wnt11r and Fgf8a*. *Development*, 2014. **141**(18): p. 3583-3593.
92. Vitelli, F., et al., *Fgf8 expression in the Tbx1 domain causes skeletal abnormalities and modifies the aortic arch but not the outflow tract phenotype of Tbx1 mutants*. *Dev Biol*, 2006. **295**(2): p. 559-70.
93. Funato, N., et al., *Loss of Tbx1 induces bone phenotypes similar to cleidocranial dysplasia*. *Hum Mol Genet*, 2015. **24**(2): p. 424-35.
94. Ogata, T., et al., *TBX1 Mutation Identified by Exome Sequencing in a Japanese Family with 22q11.2 Deletion Syndrome-Like Craniofacial Features and Hypocalcemia*. *Plos One*, 2014. **9**(3).
95. Paylor, R., et al., *Tbx1 haploinsufficiency is linked to behavioral disorders in mice and humans: Implications for 22q11 deletion syndrome*. *Proceedings of the National Academy of Sciences of the United States of America*, 2006. **103**(20): p. 7729-7734.
96. Vitelli, F., et al., *TBX1 is required for inner ear morphogenesis*. *Human Molecular Genetics*, 2003. **12**(16): p. 2041-2048.
97. Arnold, J.S., et al., *Tissue-specific roles of Tbx1 in the development of the outer, middle and inner ear, defective in 22q11DS patients*. *Human Molecular Genetics*, 2006. **15**(10): p. 1629-1639.
98. Raft, S., et al., *Suppression of neural fate and control of inner ear morphogenesis by Tbx1*. *Development*, 2004. **131**(8): p. 1801-1812.
99. Xu, H., et al., *Tbx1 regulates population, proliferation and cell fate determination of otic epithelial cells*. *Dev Biol*, 2007. **302**(2): p. 670-82.
100. Xu, H.S., L. Chen, and A. Baldini, *In vivo genetic ablation of the periotic mesoderm affects cell proliferation survival and differentiation in the cochlea*. *Developmental Biology*, 2007. **310**(2): p. 329-340.
101. Moraes, F., et al., *Tbx1 is required for proper neural crest migration and to stabilize spatial patterns during middle and inner ear development*. *Mech Dev*, 2005. **122**(2): p. 199-212.
102. Niederreither, K., et al., *Restricted expression and retinoic acid-induced downregulation of the retinaldehyde dehydrogenase type 2 (RALDH-2) gene during mouse development*. *Mech Dev*, 1997. **62**(1): p. 67-78.
103. Chen, J. and J. Nathans, *Estrogen-related receptor beta/NR3B2 controls epithelial cell fate and endolymph production by the stria vascularis*. *Dev Cell*, 2007. **13**(3): p. 325-37.
104. Lee, M.P., et al., *Targeted disruption of the kvlqt1 gene causes deafness and gastric hyperplasia in mice*. *J Clin Invest*, 2000. **106**(12): p. 1447-55.

105. Jespersen, T., M. Grunnet, and S.P. Olesen, *The KCNQ1 potassium channel: from gene to physiological function*. Physiology (Bethesda), 2005. **20**: p. 408-16.
106. Xu, H., L. Chen, and A. Baldini, *In vivo genetic ablation of the periotic mesoderm affects cell proliferation survival and differentiation in the cochlea*. Dev Biol, 2007. **310**(2): p. 329-40.
107. Jiang, H., et al., *Lineage analysis of the late otocyst stage mouse inner ear by transuterine microinjection of a retroviral vector encoding alkaline phosphatase and an oligonucleotide library*. PLoS One, 2013. **8**(7): p. e69314.
108. Hwang, C.H., et al., *Foxg1 is required for proper separation and formation of sensory cristae during inner ear development*. Dev Dyn, 2009. **238**(11): p. 2725-34.
109. Morsli, H., et al., *Development of the mouse inner ear and origin of its sensory organs*. J Neurosci, 1998. **18**(9): p. 3327-35.
110. Monks, D.C. and B.E. Morrow, *Identification of putative retinoic acid target genes downstream of mesenchymal Tbx1 during inner ear development*. Developmental Dynamics, 2012. **241**(3): p. 563-573.
111. Braunstein, E.M., et al., *Tbx1 and Brn4 regulate retinoic acid metabolic genes during cochlear morphogenesis*. BMC Dev Biol, 2009. **9**: p. 31.
112. Romand, R., et al., *Specific expression of the retinoic acid-synthesizing enzyme RALDH2 during mouse inner ear development*. Mech Dev, 2001. **106**(1-2): p. 185-9.
113. Romand, R., et al., *Dynamic expression of retinoic acid-synthesizing and -metabolizing enzymes in the developing mouse inner ear*. J Comp Neurol, 2006. **496**(5): p. 643-54.
114. Romand, R., et al., *Complementary expression patterns of retinoid acid-synthesizing and -metabolizing enzymes in pre-natal mouse inner ear structures*. Gene Expr Patterns, 2004. **4**(2): p. 123-33.
115. Lippmann, E.S., et al., *A retinoic acid-enhanced, multicellular human blood-brain barrier model derived from stem cell sources*. Sci Rep, 2014. **4**: p. 4160.
116. Mizee, M.R., et al., *Retinoic acid induces blood-brain barrier development*. J Neurosci, 2013. **33**(4): p. 1660-71.
117. Lin, P.C., et al., *Epigenomic alterations in localized and advanced prostate cancer*. Neoplasia, 2013. **15**(4): p. 373-83.
118. Niederreither, K., et al., *Retinoic acid synthesis and hindbrain patterning in the mouse embryo*. Development, 2000. **127**(1): p. 75-85.
119. Vermot, J., et al., *Decreased embryonic retinoic acid synthesis results in a DiGeorge syndrome phenotype in newborn mice*. Proc Natl Acad Sci U S A, 2003. **100**(4): p. 1763-8.

120. Mahony, S., et al., *Ligand-dependent dynamics of retinoic acid receptor binding during early neurogenesis*. *Genome Biol*, 2011. **12**(1): p. R2.
121. Acquafreda, T., et al., *Expression of homeobox genes in oral squamous cell carcinoma cell lines treated with all-trans retinoic acid*. *J Cell Biochem*, 2010. **111**(6): p. 1437-44.

SCIENTIFIC REPORTS

OPEN

Effects of *Cdh23* single nucleotide substitutions on age-related hearing loss in C57BL/6 and 129S1/Sv mice and comparisons with congenic strains

Received: 01 November 2016

Accepted: 08 February 2017

Published: 13 March 2017

Kenneth R. Johnson¹, Cong Tian¹, Leona H. Gagnon¹, Haiyan Jiang², Dalian Ding² & Richard Salvè²

A single nucleotide variant (SNV) of the cadherin 23 gene (*Cdh23*^{c.753A}), common to many inbred mouse strains, accelerates age-related hearing loss (AHL) and can worsen auditory phenotypes of other mutations. We used homologous recombination in C57BL/6NJ (B6N) and 129S1/SvImJ (129S1) embryonic stem cells to engineer mouse strains with reciprocal single base pair substitutions (B6-*Cdh23*^{c.753A>G} and 129S1-*Cdh23*^{c.753G>A}). We compared ABR thresholds and cochlear pathologies of these SNV mice with those of congenic (B6.129S1-*Cdh23*^{AH+} and 129S1.B6-*Cdh23*^{ahI}) and parental (B6N and 129S1) strain mice. Results verified the protective effect of the *Cdh23*^{c.753G} allele, which prevented high frequency hearing loss in B6 mice to at least 18 months of age, and the AHL-inducing effect of the *Cdh23*^{c.753A} allele, which worsened hearing loss in 129S1 mice. ABR thresholds differed between 129S1-*Cdh23*^{c.753A} SNV and 129S1.B6-*Cdh23*^{ahI} congenic mice, and a linkage backcross involving these strains localized a Chr 10 QTL contributing to the difference. These results illustrate the large effects that strain background and congenic regions have on the hearing loss associated with *Cdh23*^{c.753} alleles. Importantly, the B6-*Cdh23*^{c.753G} strain can be used to eliminate the confounding influence of the *Cdh23*^{c.753A} variant in hearing studies of B6 mice and mutant mice on the B6 background.

Age-related hearing loss (AHL) is the most prevalent sensory impairment in elderly individuals and is becoming a major health concern with world population aging¹. AHL has been shown to have a significant genetic component^{2,3}; however because of its complex nature and late onset, causative gene variants influencing AHL susceptibility have been difficult to identify in human populations⁴. Mice serve as valuable model systems for studying human hearing loss because their auditory system is similar to that of humans and because genetic and environmental variation can be manipulated and controlled in mice⁵⁻⁷. Genetically homogeneous inbred strains of mice vary widely in onset times and progression of hearing loss⁸ making them highly amenable to genetic studies of AHL. The C57BL/6 (B6) strain, widely used in many research fields, has long been studied as a model for AHL⁹⁻¹¹.

A major genetic factor contributing to AHL in B6 mice was mapped to a locus (named *ahl*) on Chr 10¹² and later shown to be a common variant in many other inbred strains¹³. The coincident map position of *ahl* with cadherin 23 (*Cdh23*) and the correspondence of specific *Cdh23* alleles with hearing loss severity in multiple inbred strains provided evidence that a single nucleotide variant (SNV) of *Cdh23* underlies the *ahl* phenotype¹⁴. This SNV corresponds to SNP rs257098870 and is at the 753rd nucleotide position from the ATG translation start site of *Cdh23* cDNA (c.753), which corresponds to the last nucleotide of exon 7 in GenBank sequence AF308939 and to the last nucleotide of exon 9 in Ref Seqs NM_023370 and NM_001252635. A G nucleotide at this site (*Cdh23*^{c.753G}) results in normal exon splicing, whereas an A nucleotide (*Cdh23*^{c.753A}) disrupts the canonical donor splice site sequence and causes in-frame exon skipping¹⁴. The *Cdh23*^{c.753G} allele is associated with resistance to AHL and is dominant to the recessive *Cdh23*^{c.753A} allele, which is associated with AHL susceptibility.

¹The Jackson Laboratory, Bar Harbor, Maine 04609, USA. ²Center for Hearing and Deafness, University at Buffalo, Buffalo, NY 14214, USA. Correspondence and requests for materials should be addressed to K.R.J. (email: ken.johnson@jax.org)

N-acetyl-cysteine prevents age-related hearing loss and the progressive loss of inner hair cells in γ -glutamyl transferase 1 deficient mice

Dalian Ding¹, Haiyan Jiang¹, Guang-Di Chen¹, Chantal Longo-Guess², Vijaya Prakash Krishnan Muthaiah¹, Cong Tian², Adam Sheppard¹, Richard Salvi¹, and Kenneth R. Johnson²

¹Center for Hearing and Deafness, University at Buffalo, Buffalo, NY 14214, USA

²The Jackson Laboratory, Bar Harbor, ME 04609, USA

Key words: Inner hair cell loss, dwarf grey $Ggt1^{dwg/dwg}$, otoacoustic emission, compound action potential, vestibular dysfunction, auditory brainstem response, glutathione, N-acetyl-L-cysteine

Received: 01/03/16; Accepted: 02/18/16; Published: 03/14/16

Correspondence to: Richard Salvi, PhD; E-mail: salvi@buffalo.edu

Copyright: Ding et al. This is an open-access article distributed under the terms of the Creative Commons Attribution License, which permits unrestricted use, distribution, and reproduction in any medium, provided the original author and source are credited

Abstract: Genetic factors combined with oxidative stress are major determinants of age-related hearing loss (ARHL), one of the most prevalent disorders of the elderly. Dwarf grey mice, $Ggt1^{dwg/dwg}$, are homozygous for a loss of function mutation of the γ -glutamyl transferase 1 gene, which encodes an important antioxidant enzyme critical for the resynthesis of glutathione (GSH). Since GSH reduces oxidative damage, we hypothesized that $Ggt1^{dwg/dwg}$ mice would be susceptible to ARHL. Surprisingly, otoacoustic emissions and cochlear microphonic potentials, which reflect cochlear outer hair cell (OHC) function, were largely unaffected in mutant mice, whereas auditory brainstem responses and the compound action potential were grossly abnormal. These functional deficits were associated with an unusual and selective loss of inner hair cells (IHC), but retention of OHC and auditory nerve fibers. Remarkably, hearing deficits and IHC loss were completely prevented by N-acetyl-L-cysteine, which induces *de novo* synthesis of GSH; however, hearing deficits and IHC loss reappeared when treatment was discontinued. $Ggt1^{dwg/dwg}$ mice represent an important new model for investigating ARHL, therapeutic interventions, and understanding the perceptual and electrophysiological consequences of sensory deprivation caused by the loss of sensory input exclusively from IHC.

INTRODUCTION

Age-related hearing loss (ARHL) is one of the most prevalent disorders of the elderly. Nearly 25% of Americans 65-74 years of age have disabling hearing loss; this figure rises to 50% among those 75 or older (<http://www.nidcd.nih.gov/health/statistics/Pages/quick.aspx>). Severe hearing loss is a debilitating condition that can lead to communication difficulties, social isolation, depression and cognitive decline [1, 2]. Not surprisingly, susceptibility to ARHL is a complex, multifactorial disorder involving genetic, environmental, health and nutritional factors [3-6]. At the molecular level, the most overarching and widespread theory of aging involves

oxidative stress arising from reactive oxygen or nitrogen species [7, 8]. Human heritability studies suggest that 25-75% of the variance in ARHL has a genetic basis [9, 10]. Allelic variations and mutations in human oxidative stress genes, such as glutathione S-transferase and N-acetyltransferase, appear to contribute to ARHL susceptibility [11, 12]; however, others have failed to find such an association [13] possibly due to heterogeneity of the sample population. Animal studies of ARHL conducted with inbred mice circumvent many of the problems associated with genetically heterogeneous human samples. Murine models have proved highly effective in isolating genes that regulate the progression of ARHL [14-17] and have also proved

BIOGRAPHY OF THE AUTHOR

Cong Tian, was born in Zoucheng, China, in 1983. Cong attended the Ocean University of China (Qingdao, China), where he worked as a research assistant in the College of Environmental Science and Engineering, and earned a Bachelor of Science in Environmental Science in 2004. He worked at an Environment Protection Agency (Zoucheng, China) from 2004 to 2005. In 2006, Cong received research training in the National Research Council of Italy (Bari, Italy). Cong worked at the Agricultural Laboratory in Zoucheng, China from 2006 to 2007. In Late 2007, Cong joined the lab of Dr. Qing Yin Zheng at Case Western Reserve University (Cleveland, Ohio) and worked as a research associate, where he studied ear development and diseases using mouse models. In 2011, Cong left Cleveland to begin his graduate work at the University of Maine's Graduate School of Biomedical Science and Engineering, where he continued to study genes and pathways that are involved in ear development and diseases in Dr. Kenneth Johnson's laboratory (Bar Harbor, Maine), and the work done have culminated and been summarized in this current dissertation. Cong is the primary author of two peer-reviewed research articles: "Ectopic Mineralization and Conductive Hearing Loss in *Enpp1^{asj}* Mutant Mice, a New Model for Otitis Media and Tympanosclerosis," in the journal PLOS ONE, published 2016, and "Hearing loss without overt metabolic acidosis in *Atp6v1b1* deficient MRL mice, a new genetic model for nonsyndromic deafness with enlarged vestibular aqueducts", accepted pending revision in the journal Human Molecular Genetics, and the co-author of four peer-reviewed scholarly articles. He also had the honor of serving as ad hoc reviewers for the following journals: The Laryngoscope, Otology & Neurotology, Otolaryngology - Head and Neck Surgery, Disease Models & Mechanisms. Cong is a member of the Association of Research in Otolaryngology (ARO). Cong is married to Ye Zheng, and they live in Hampden, ME with their two children Kelly and Bowen. Cong is a candidate for the Doctor of Philosophy degree in Biomedical Science at the University of Maine in August 2017.